USE OF LOW COST ADSORBENTS TO TREAT INDUSTRIAL WASTEWATER

Evans Tongesai Musapatika

A dissertation submitted to the Faculty of Engineering and the Built Environment, University of the Witwatersrand, in fulfillment of the requirements for the degree of Master of Science in Engineering.

Johannesburg, 2010

Declaration

I declare that this dissertation is my own unaided work. It is being submitted for the degree of Master of Science in Engineering to the University of the Witwatersrand, Johannesburg. It has not been submitted before for any degree or examination in any other University.

……..

Signature of E.T Musapatika

24th day of May 2010

Abstract

Advanced wastewater treatment techniques, such as adsorption, are economically and environmentally essential in the removal of non-biodegradable toxic compounds from industrial wastewater. The present study focuses on the use of low cost adsorbents prepared from pine sawdust, coal fly ash and sugarcane bagasse to adsorb recalcitrant compounds such as heavy metals, phenol and direct dyes from synthetic wastewater. Carbonization of the adsorbents was done using a muffle furnace whereas a fluidized bed reactor was used to prepare steam activated sawdust. Both batch and column tests were performed to investigate the use of these alternative adsorbents as potential replacements for the current costly commercial adsorbents. A 2^3 full-factorial design with four centre points and response surface methodology were used to study the interactive effect of the operating conditions on the adsorption capacity of sawdust and coal fly ash. In addition, the performance of the low cost adsorbents was compared with that of commercial activated carbon (CAC). The maximum adsorption capacities were determined and correlated with the physicochemical properties of the adsorbents.

Adsorption capacity was found to vary with initial concentration, adsorbent dose and pH. An increase in pH led to a significant increase in heavy metal removal suggesting the involvement of ion exchange mechanism. In column studies, breakthrough times increased with an increase in bed height and aspect ratio. Conversely, breakthrough times decreased with an increase in initial concentration. Overall, commercial activated carbon was found to be superior; however, sawdust and coal fly ash showed potential as alternative adsorbents for the removal of heavy metals and phenol from petrochemical wastewater. Additionally, the trend followed by the maximum monolayer adsorption capacities, q_{max} for the four adsorbents used to treat petrochemical wastewater was in agreement with the specific surface area of the adsorbents i.e adsorbents with high specific surface area had high q_{max} values with a few exceptions. Amongst the low cost adsorbent, steam activated sawdust (SAS) was superior and coal fly ash had the lowest adsorption capacities. Also, the highest

adsorbed contaminant by steam activated sawdust was Fe (15.385 mg/g). It has been shown that the performance of steam activated sawdust was comparable to that of commercial activated carbon in the removal of Pb and Ni. Nevertheless, sugarcane bagasse proved to be a better adsorbent than coal fly ash in the uptake of direct red dyes from textile wastewater. Direct red 80 (DR 80) was the highest adsorbed dye by both sugarcane bagasse (6.536 mg/g) and coal fly ash (1.560 mg/g).

Equilibrium data for metal removal conformed well to the Freundlich isotherm whereas phenol and direct dye removal complied with the Langmuir adsorption isotherm model. Kinetic data were fitted to Lagergren first-order, pseudo second-order and the intraparticle diffusion models. Thus, kinetic parameters, rate constants, equilibrium adsorption capacities and related correlation coefficients, for each kinetic model were calculated and discussed. Consequently, the adsorption of cobalt followed pseudo second order kinetics suggesting chemisorption for all the tested adsorbents. Also, results suggested that intraparticle diffusion was not the only step controlling the overall adsorption process of cobalt. Results presented here can help to design an appropriate environmental management strategy to minimize the adverse impacts caused by industrial wastewater.

Publications and conference presentations

- **Musapatika, E.T**., Onyango, M.S., Aoyi, O. (2009). Cobalt (II) removal from synthetic wastewater by adsorption on South African coal fly ash, (submitted to *South African Journal of Science* for review on 30 October 2009).

- Moodley, K., Singh, R., **Musapatika, E.T**., Onyango, M.S., Aoyi, O. (2009). Removal of nickel using an agricultural adsorbent, (submitted to *Water SA* for review on 26 October 2009).

- **Musapatika, E.T**., Moodley, K., Singh, R., Onyango, M.S., Aoyi, O. (2008). Removal of Iron (III) from aqueous solution using sawdust, South African Institute of Chemical Engineers (SAIChE) Postgraduate Student Symposium in Process Engineering, Johannesburg, South Africa, 29 September 2008 (abstract: oral presentation).

- Moodley, K., Singh, R., **Musapatika, E.T**., Onyango, M.S., Aoyi, O. (2009). Removal of nickel using an agricultural adsorbent, South African Chemical Engineering Congress (SACEC 2009), Somerset West, Capetown, South Africa, 20 – 23 September 2009 (paper: oral presentation).

- **Musapatika, E.T**., Onyango, M.S., Aoyi, O. (2009). Removal of cobalt (II) from synthetic wastewater using South African coal fly ash, Wits Postgraduate Cross Faculty Symposium, Johannesburg, 19 – 23 October 2008 (abstract: oral presentation).

Awards

- Second best postgraduate poster presentation for the School of Chemical and Metallurgical Engineering, University of the Witwatersrand. Presented at the School of Chemical and Metallurgical Engineering poster day, 16 October 2008. Title: Use of low cost adsorbents to treat industrial wastewater.

- Outstanding poster presentation for the Faculty of Engineering and the Built Environment, University of the Witwatersrand. Presented at the Postgraduate Cross Faculty Symposium, 7-8 November 2008. Title: Use of low cost adsorbents to treat industrial wastewater.

Dedications

In memory of my late parents: Mrs Brandina and Mr. Ezekiel Musapatika, and to the whole Musapatika family, in particular Mr. Joseph and his wife Dephine.

Acknowledgements

Firstly, I would like to express my gratitude to my supervisors: Prof. Ochieng Aoyi, Dr. Maurice S. Onyango and Prof Sunny E. Iyuke for their advice, support, guidance and encouragement throughout the course of this work. This work would not have been possible without their supervision. I am very much indebted to them more than they know.

My heartfelt gratitude is very much extended to Dr. Lizelle Van Dyk for her valuable advice and assistance especially during the preparation of activated carbon from sawdust. It would have been difficult indeed to have made such progress without her fluidized bed reactor and continuous support. Furthermore, I wish to acknowledge the School of Chemical and Metallurgical Engineering for providing research facilities.

Special thanks to Custom Kitchens for supplying the sawdust used in this research. It is also a pleasure to convey my gratitude to Ruella Singh and Krishnie Moodley for laying a very good foundation for this work. My deepest appreciation to Bruce Mothibedi, Doctor Mthunzi Mbense and all the technicians in the School of Chemical and Metallurgical Engineering for their assistance.

Many thanks go to my fellow postgraduate colleagues: Geoffrey S. Simate, Gwiranai Danha, Augustine T. Mamvura and Kudakwashe Jakata for their support. Furthermore, I would like to acknowledge my nephew Engineer Lawrence Buwerimwe and his wife Fungisai Taderera for being there for me all the times.

Finally, I would like to thank everybody who played a very important role towards the completion of this work, as well as expressing my apology that I could not mention all the names one by one.

Table of Contents

Contents	Page
Declaration	ii
Abstract	iii
Publications and conference presentations	v
Awards	vi
Dedications	vii
Acknowledgements	viii
Table of Contents	ix
List of figures	xiv
List of tables	xviii
Nomenclature	xxiv
List of abbreviations	xxvi
1 Introduction	1
1.1 General Introduction	1
1.2 Justification	2
1.3 Problem statement	3
1.4 Hypothesis	4
1.5 Objectives	4
2 Literature review	6
2.1 Wastewater characteristics	7

2.1.1 Biodegradable wastewater 7

2.1.2 Recalcitrant wastewater 8

2.2 Effects of wastewater contaminants..... 10

2.3 Tertiary/advanced wastewater treatment 11

2.3.1 Ion exchange 11

2.3.2 Chemical precipitation 12

2.3.3 Membrane separation techniques 12

2.3.4 Coagulation and flocculation 13

2.3.5 Oxidation processes 14

2.3.6 Electrochemical method 15

2.3.7 Adsorption..... 15

2.4 Commercial adsorbents 17

2.4.1 Zeolites..... 17

2.4.2 Silica gel 17

2.4.3 Activated alumina 18

2.4.4 Activated carbon 18

2.5 Low cost adsorbents 20

2.5.1 Agricultural wastes 20

2.5.2 Industrial by-products 22

2.6 Equilibrium isotherm models..... 23

2.6.1 Langmuir adsorption isotherm 23

2.6.2 Freundlich adsorption isotherm 24

2.7 Mass transfer mechanism 25

2.7.1 Adsorption kinetic models..... 27

2.7.2 Lagergren pseudo-first order kinetics 28

2.7.3 Ho pseudo second-order kinetics 28

2.7.4 Intraparticle diffusion model 29

2.8 Column adsorption 30

2.9 Trends in adsorption studies 31

3 Materials and methods 34

3.1 Materials 34

3.2 Equipment 35

3.3 Preparation and characterization of adsorbents 36

3.3.1 Sawdust modified with citric acid 36

3.3.2 Steam activated sawdust (SAS) 37

3.3.3 Sugarcane bagasse (SB400) 38

3.3.4 Coal fly ash (CFA) 39

3.3.5 Commercial activated carbon (CAC) 39

3.3.6 Characterization of adsorbents 40

3.4 Synthetic wastewater preparation 41

3.4.1 Petrochemical wastewater 41

3.4.2 Textile wastewater 41

3.5 Batch adsorption experiments 42

3.5.1 Optimum adsorbent mass 43

3.5.2 Equilibrium study 43

3.5.3 Kinetic study 44

3.5.4 Experimental design 44

3.6 Column dynamics 46

3.7 Quantitative chemical analysis 48

4 Results and discussion 49

4.1 Characterization of the adsorbents 49

4.1.1 Sawdust modified with citric acid (SD500) 49

4.1.2 Sugarcane bagasse (SB400) 53

4.1.3 Coal fly ash (CFA) 55

4.1.4 Steam activated sawdust (SAS) 58

4.1.5 Commercial activated carbon (CAC) 60

4.1.6 Surface area and porosity of the adsorbents 62

4.2 Optimum adsorbent mass 64

4.3 Kinetic studies 65

4.3.1 Textile wastewater 65

4.3.2 Petrochemical wastewater 66

4.4 Adsorption kinetic modeling 67

4.5 Equilibrium modeling 71

4.5.1 Textile wastewater 71

4.5.2 Petrochemical wastewater 75

4.6 Response surface methodology (RSM) and statistical analysis 80

4.6.1 Coal fly ash (CFA) 80

4.6.2 Steam activated sawdust (SAS) 93

4.7 Dynamic column studies 98

4.7.1 Effect of bed height 99

4.7.2 Effect of aspect ratio 102

4.7.3 Effect of initial concentration 103

4.7.4 Effect of type of adsorbent 107

5 Conclusions and recommendations 109

5.1 Conclusions 109

5.2 Recommendations for future work 112

6 References 115

APPENDIX A: Characterization data 134

APPENDIX B: Data for determining adsorbent optimum mass and contact time . 139

APPENDIX C: Adsorption kinetics data 146

APPENDIX D: Adsorption isotherm data 149

APPENDIX E: Response surface methodology data 161

APPENDIX F: Matlab programs for plotting response surfaces for coal fly ash... 167

APPENDIX G: Matlab programs for plotting response surfaces for SAS 174

APPENDIX H: Data for column studies 180

LIST OF FIGURES

Figure **Page**

Figure 2.1. Schematic of an adsorbent particle depicting the surrounding stagnant fluid film 26

Figure 3.1. Schematic diagram of the experimental set up for activated carbon preparation 38

Schema 3.1. Chemical structures of direct red 80, direct red 81 and direct red 23 ... 42

Figure 3.2. Schematic diagram of the experimental set up for a laboratory scale adsorption column used for fixed bed studies. 46

Figure 4.1. The X-ray diffraction profile (diffractogram) of SD500 50

Figure 4.2. FT-IR spectra of SD500 before and after adsorption of heavy metals and phenol. 51

Figure 4.3. SEM images of SD500 before and after adsorption at 140 times magnification. 53

Figure 4.4. The X-ray diffraction profile (diffractogram) of SB400. 54

Figure 4.5. SEM images of SB400 before and after adsorption of direct red dyes at 1200 times magnification.. 55

Figure 4.6. The X-ray diffraction profile (diffractogram) of CFA. 56

Figure 4.7. FT-IR spectra of CFA before and after adsorption of heavy metals and phenol. 57

Figure 4.8. SEM images of coal fly ash before and after adsorption of heavy metals and phenol at 400 times magnification. 58

Figure 4.9. FT-IR spectra of SAS before and after adsorption of heavy metals and phenol. 59

Figure 4.10. SEM images of SAS before adsorption at 140 and 1200 times magnification, respectively. 60

Figure 4.11. Surface characterization results for CAC: (a) X-ray diffraction pattern and (b) FT-IR spectra before and after adsorption of heavy metals and phenol. 61

Figure 4.12. SEM images of CAC before adsorption at 140 and 600 times magnification, respectively. 62

Figure 4.13. Removal of Co^{2+}, Ni^{2+}, Fe^{2+}, Pb^{2+} and phenol using coal fly ash 64

Figure 4.14. Removal of DR80, DR81 and DR23 using SB400 and CFA 66

Figure 4.15. Lagergren pseudo-first-order plots for cobalt adsorption on SD500, CFA, SAS and CAC 67

Figure 4.16. Pseudo-second-order plots for cobalt adsorption on SD500, CFA, SAS and CAC. 69

Figure 4.17. Weber and Morris intraparticle diffusion plots for cobalt adsorption on SD500, CFA, SAS and CAC. 70

Figure 4.18. Fitting of Langmuir and Freundlich isotherm models to experimental data for removal of DR 80 using SB400 and CFA 72

Figure 4.19. Linear regression analysis of DR80 and DR81 removal using CFA and SB400 for Freundlich isotherm. 73

Figure 4.20. Linear regression analysis of DR80 and DR81 removal using CFA and SB400 for Langmuir isotherm. 74

Figure 4.21. Fitting of Langmuir and Freundlich isotherm models to experimental data for removal of cobalt using SD500 and CAC 76

Figure 4.22. Freundlich isotherm for cobalt, iron, lead and phenol removal using CAC, SAS, SD500 and CFA. 77

Figure 4.23. Parity plot of the experimental adsorption capacity and adsorption capacity predicted by the quadratic model equation for cobalt removal…….84

Figure 4.24. Response surface plot showing effects of adsorbent dose and pH on adsorption capacity of cobalt ions at constant initial concentration. 85

Figure 4.25. Response surface plot showing effects of adsorbent dose and initial concentration on adsorption capacity of cobalt ions at constant pH. 88

Figure 4.26. Response surface plot showing effects of pH and initial concentration on adsorption capacity of cobalt ions at constant dose. 89

Figure 4.27. Adsorption capacity as a function of: (a) pH and dose at constant initial concentration and (b) initial concentration and pH at constant dose for phenol removal..... 93

Figure 4.28. Adsorption capacity as a function of: (a) pH and dose at constant initial concentration and (b) initial concentration and pH at constant dose for phenol removal..... 97

Figure 4.29. Effect of bed height on breakthrough curves of phenol removal by SD500 at 10 cm , 20 cm and 30 cm bed height 99

Figure 4.30. Effect of bed height on breakthrough curves of cobalt, nickel, iron and lead removal by SD500 at 10 cm, 20 cm and 30 cm bed height..... 101

Figure 4.31. Effect of aspect ratio on breakthrough time, t_B in the removal of cobalt, nickel, iron and lead using SD500. 102

Figure 4.32. Effect of initial concentration on breakthrough curves of phenol removal at 180 mg/l and 90 mg/l using SD500..... 103

Figure 4.33. Effect of initial concentration on breakthrough curves of cobalt removal at 50 mg/l and 25 mg/l using SD500..... 104

Figure 4.34. Breakthrough curves for removal of: (a) 90 mg/l phenol in the presence of 50 mg/l and 90 mg/l heavy metal ions, (b) 50 mg/l cobalt in the presence of 90 mg/l and 180 mg/l phenol at 10 cm bed height..... 106

Figure 4.35. Breakthrough curves for removal of: (a) phenol and (b) cobalt using SD500, SAS and CAC at 10 cm bed height..... 107

Figure A1. FT-IR spectrum of SD500 before use..... 134

Figure A2. FT-IR spectrum of SD500 after adsorption of metals and phenol..... 134

Figure A3. FT-IR spectra of SB400 before use. 135

Figure A4. FT-IR spectrum of CFA before use 135

Figure A5. FT-IR spectrum of CFA after adsorption of metals and phenol 136

Figure A6. The X-ray diffraction profile (diffractogram) of SAS. 136

Figure A7. FT-IR spectrum of SAS before use 137

Figure A8. FT-IR spectrum of SAS after adsorption of metals and phenol 137

Figure A9. FT-IR spectrum of CAC before use..... 138

Figure A10. FT-IR spectrum of CAC after adsorption of metals and phenol..... 138

Figure D1. Linear regression analysis of DR23 removal using CFA and SD500 for (a) Freundlich and (b) Langmuir isotherm. 149

Figure D2. Linear regression analysis of nickel removal using CAC, SAS, SD500 and CFA for (a) Freundlich and (b) Langmuir isotherm 149

Figure D3. Linear regression analysis of cobalt, iron, lead and phenol removal using CAC, SAS, SD500 and CFA for Langmuir isotherm 150

LIST OF TABLES

Table **Page**

Table 2.1: Composition of acidic petrochemical wastewater 9

Table 3.1: The experimental range and levels of the independent variables for CFA and SAS..... 45

Table 3.2: Wastewater composition and conditions for different experimental runs 48

Table 4.1: Interpretation of FT-IR spectra for SD500 before and after adsorption ... 52

Table 4.2: Surface characteristics and pore structure of the adsorbents 63

Table 4.3: Kinetic parameters for cobalt adsorption..... 68

Table 4.4: Intraparticle diffusion constants for cobalt adsorption 71

Table 4.5: Freundlich and Langmuir adsorption isotherm constants for textile wastewater..... 75

Table 4.6: Freundlich and Langmuir isotherm constants for petrochemical wastewater 79

Table 4.7: The 2^3 factorial design with centre points for the independent variables for CFA..... 81

Table 4.8: Analysis of variance (ANOVA) for a quadratic model for cobalt removal 83

Table 4.9: The 2^3 factorial design with centre points for the independent variables for SAS 94

Table 4.10: Breakthrough and exhaustion times for different bed heights..... 100

Table 4.11: Breakthrough capacity at different concentrations 105

Table 4.12: Breakthrough and exhaustion times for different adsorbents 108

Table B1: Data for determining the optimum CFA mass 139

Table B2: Data for determining the optimum SD500 mass..... 140

Table B3: Data for determining the optimum SAS mass..... 141

Table B4: Data for determining the optimum CAC mass..... 141

Table B5: Data for determining contact time for the removal of dyes using SB400 and CFA 142

Table B6: Data for determining contact time using CFA to treat petrochemical wastewater..... 143

Table B7: Data for determining contact time using SAS to treat petrochemical wastewater..... 144

Table B8: Data for determining contact time using CAC to treat petrochemical wastewater..... 144

Table B9: Data for determining contact time using SD500 to treat petrochemical wastewater..... 145

Table C1: Data for Lagergren pseudo-first-order kinetic model for cobalt..... 146

Table C2: Data for pseudo-second-order kinetic model for cobalt removal..... 147

Table C3: Data for the intraparticle diffusion model for cobalt adsorption..... 148

Table D1: Freundlich and Langmuir adsorption isotherm data for DR80 removal using SB400 151

Table D2: Freundlich and Langmuir adsorption isotherm data for DR80 removal using CFA 151

Table D3: Freundlich and Langmuir adsorption isotherm data for DR81 removal using SB400 152

Table D4: Freundlich and Langmuir adsorption isotherm data for DR81 removal using CFA 152

Table D5: Freundlich and Langmuir adsorption isotherm data for DR23 removal using SB400 153

Table D6: Freundlich and Langmuir adsorption isotherm data for DR23 removal using CFA 153

Table D7: Freundlich and Langmuir adsorption isotherm data for cobalt removal using SAS 154

Table D8: Freundlich and Langmuir adsorption isotherm data for nickel removal using SAS 154

Table D9: Freundlich and Langmuir adsorption isotherm data for iron removal using SAS 154

Table D10: Freundlich and Langmuir adsorption isotherm data for lead removal using SAS 155

Table D11: Freundlich and Langmuir adsorption isotherm data for phenol removal using SAS 155

Table D12: Freundlich and Langmuir adsorption isotherm data for cobalt removal using SD500 155

Table D13: Freundlich and Langmuir adsorption isotherm data for nickel removal using SD500 156

Table D14: Freundlich and Langmuir adsorption isotherm data for iron removal using SD500 156

Table D15: Freundlich and Langmuir adsorption isotherm data for lead removal using SD500 156

Table D16: Freundlich and Langmuir adsorption isotherm data for phenol removal using SD500 157

Table D17: Freundlich and Langmuir adsorption isotherm data for cobalt removal using CFA 157

Table D18: Freundlich and Langmuir adsorption isotherm data for nickel removal using CFA 157

Table D19: Freundlich and Langmuir adsorption isotherm data for iron removal using CFA 158

Table D20: Freundlich and Langmuir adsorption isotherm data for lead removal using CFA 158

Table D21: Freundlich and Langmuir adsorption isotherm data for phenol removal using CFA 158

Table D22: Freundlich and Langmuir adsorption isotherm data for cobalt removal using CAC 159

Table D23: Freundlich and Langmuir adsorption isotherm data for nickel removal using CAC 159

Table D24: Freundlich and Langmuir adsorption isotherm data for iron removal using CAC 159

Table D25: Freundlich and Langmuir adsorption isotherm data for lead removal using CAC 160

Table D26: Freundlich and Langmuir adsorption isotherm data for phenol removal using CAC 160

Table E1: Experimental and predicted adsorption capacities for cobalt using CFA and SAS 161

Table E2: Experimental and predicted adsorption capacities for nickel using CFA and SAS 162

Table E3: Experimental and predicted adsorption capacities for iron using CFA and SAS 162

Table E4: Experimental and predicted adsorption capacities for lead using CFA and SAS 163

Table E5: Experimental and predicted adsorption capacities for phenol using CFA and SAS..... 163

Table E6: ANOVA for a quadratic model for nickel removal using CFA 164

Table E7: ANOVA for a quadratic model for iron removal using CFA..... 164

Table E8: ANOVA for a quadratic model for lead removal using CFA 164

Table E9: ANOVA for a quadratic model for phenol removal using CFA 165

Table E10: ANOVA for a quadratic model for cobalt removal using SAS..... 165

Table E11: ANOVA for a quadratic model for nickel removal using SAS..... 165

Table E12: ANOVA for a quadratic model for iron removal using SAS 166

Table E13: ANOVA for a quadratic model for lead removal using SAS..... 166

Table E14: ANOVA for a quadratic model for phenol removal using SAS..... 166

Table F1: Confirmatory experiments for cobalt removal using CFA 173

Table H1: Data for design calculation using SD500 as the adsorbent..... 180

Table H2: Data for metal (90 mg/l) breakthrough curves using SD500 at 10 cm bed height..... 181

Table H3: Data for heavy metal (90 mg/l) breakthrough curves using SD500 at 20 cm bed height..... 181

Table H4: Data for heavy metal (90 mg/l) breakthrough curves using SD500 at 30 cm bed height..... 182

Table H5: Data for phenol (90 mg/l) breakthrough curves using SD500 at varying bed height..... 183

NOMENCLATURE

Symbol	Description	Units
A	constant of the boundary layer thickness	(mg/g)
β_i	Regression coefficient	(dimensionless)
C_e	Equilibrium liquid phase solute concentration	(mg/l)
C_o	Initial liquid phase solute concentration	(mg/l)
C_t	Liquid-phase solute concentration at time, t	(mg/l)
D	Column diameter (internal)	(cm)
h	Initial sorption rate	($mgg^{-1}min^{-1}$)
i	= 0,1,2,…..,k	(dimensionless)
k	Number of independent variables	(dimensionless)
k_{ad}	Pseudo-first-order rate constant	(min^{-1})
K_F	Freundlich constant related with adsorption capacity	(mg/g)
k_{id}	Intraparticle diffusion rate constant	($mg/gmin^{1/2}$)
K_L	Langmuir affinity constant	(l/mg)
k_2	Pseudo-second-order rate constant	($gmg^{-1}min^{-1}$)
m	Mass of dry adsorbent	(g)
n	Adsorption intensity	(dimensionless)
P_b	Percentage burn-off	(%)
pH_{ppt}	pH point of precipitation	(dimensionless)
pH_{pzc}	pH point of zero charge	(dimensionless)
P_r	Percentage removal	(%)
q_{Co}	Predicted adsorption capacity for cobalt	(mg/g)
q_e	Equilibrium adsorption capacity	(mg/g)
q_{Fe}	Predicted adsorption capacity for iron	(mg/g)
q_{max}	Maximum monolayer adsorption capacity	(mg/g)
q_{Ni}	Predicted adsorption capacity for nickel	(mg/g)
q_{Phe}	Predicted adsorption capacity for phenol	(mg/g)
q_{Pb}	Predicted adsorption capacity for lead	(mg/g)
q_t	Amount of solute adsorbed at time, t	(mg/g)

Q_B	Breakthrough adsorption capacity	(mg/g)
Q_w	Volumetric flow rate of wastewater	(ml/min)
R^2	Correlation coefficient	(dimensionless)
S_{BET}	BET surface area	(m^2/g)
S_{mi}	micropore specific area	(m^2/g)
t	Time	(min)
t_B	Breakthrough time at desired concentration	(h)
t_E	Exhaustion time at desired concentration	(h)
V	Volume of solution	(l)
V_{me}	mesopore volume	(cm^3/g)
V_{mi}	micropore volume	(cm^3/g)
V_t	total pore volume	(cm^3/g)
W_f	final weight of the product	(g)
W_o	initial weight of the raw material	(g)
x_i	coded variable for X_i	(dimensionless)
X_i	independent variable real value	
X_o	independent variable real value on the centre point	
ΔX	step change value	
Z	Bed height	(cm)
λ_{max}	Maximum wavelength	(nm)

LIST OF ABBREVIATIONS

Analysis of Variance	ANOVA
Atomic Absorption Spectrometer	AAS
Brunauer-Emmett-Teller	BET
Biochemical Oxygen Demand	BOD
Chemical Oxygen Demand	COD
Coefficient of Variation	CV
Central Composite Design	CCD
Coal Fly Ash	CFA
Commercial Activated Carbon	CAC
Department of Environmental Affairs and Tourism	DEAT
Direct Red 23	DR23
Direct Red 80	DR80
Direct Red 81	DR81
European Union	EU
Fluidized Bed Reactor	FBR
Fourier Transform Infrared	FT-IR
International Union of Pure and Applied Chemistry	IUPAC
Response Surface Methodology	RSM
Sawdust carbonized at 250	SD250
Sawdust carbonized at 400	SD400
Sawdust carbonized at 500	SD500
Steam Activated Sawdust	SAS
Sugarcane Bagasse carbonized at 400	SB400
Scanning Electron Microscope	SEM
Ultraviolet-Visible	UV-VIS
Total Kjeldhal Nitrogen	TKN
Total Suspended Solids	TSS
X-ray Diffraction	XRD

CHAPTER 1

1 Introduction

1.1 General Introduction

Fast population growth, industrial expansion, rapid urbanization, use of energy and generation of wastes from domestic and industrial sources have rendered many water sources unwholesome and hazardous to man and the environment in most countries including South Africa. Wastewater is characterized in terms of its chemical, physical and biological composition. In South Africa, typical industries which produce significant volumes of wastewater include textile, steel mills, mineral processing, paper and fibre plants, chemical and fertilizer plants, breweries, refining and petrochemical operations, poultry processors and meat packers, fruit and vegetable packing operations and many more. Wastewater treatment can be done using three methods: primary, secondary and tertiary/advanced processes. Primary treatment separates suspended solids and greases from water and a secondary treatment such as biodegradation process is used in the removal of biodegradable compounds whilst tertiary/advanced treatment methods are largely used to remove non-biodegradable wastes.

Non-biodegradable contaminants pose a serious health and environmental hazard and removal of these wastes cannot be achieved using secondary methods. Hence, tertiary/advanced wastewater treatment methods such as ion exchange, precipitation, membrane separation, electrolysis and adsorption can be used to remove these recalcitrant wastes. However, most of these methods are costly and require high level of expertise, hence they are not applied by many end-users. For these reasons, adsorption technology has gained a wider application due to its inherent low cost, simplicity, versatility and robustness. The success of an adsorption process starts with the choice of an adsorbent. Several adsorbents can be used to treat industrial wastewater. A few of such adsorbent materials are commercial activated carbon,

zeolites, silica gel and activated alumina. Unfortunately, most of these adsorption media are very costly (Panday *et al*., 1985). Thus, the use of low cost adsorbents derived from agricultural and industrial solid wastes for wastewater treatment has attracted a vast amount of attention in recent years. These waste materials are underutilized and hence they are readily available. Consequently, the use of these low cost adsorbents forms the main focus of this study.

1.2 Justification

Much work on the use of sawdust, sugarcane bagasse, and coal fly ash for wastewater treatment has been reported by several researchers. However, no work has been reported on the co-adsorption of Co^{2+}, Ni^{2+}, Fe^{2+}, Pb^{2+} and phenol from synthetic petrochemical wastewater using the aforementioned adsorbents in both batch and continuous modes of adsorption. In addition, there has been limited research on the effects of initial metal concentration on phenol sorption and vice versa. Also, many researchers concentrate on batch adsorption mode using these alternative adsorbents. Although sorption capacity parameters obtained from batch experiments are useful in providing information about effectiveness of the adsorbate-adsorbent system, the data is not applicable to most treatment systems. Adsorption on continuous flow fixed bed columns is often preferred since it can be scaled-up from a laboratory process. Hence, there is a definite need to perform both batch and continuous flow experiments in a fixed bed.

Most researchers study adsorption processes by changing one factor and maintaining others constant (one-factor-at-a-time method). This method is extremely time consuming and expensive for a large number of process variables. In addition, the one-factor-at-a-time technique does not include interactive effects among the variables and, eventually, it does not depict the complete effects of the parameters on the process. Therefore, it is desirable and imperative to eliminate these limitations and establish how the process parameters interact with each other using response surface methodology (RSM).

1.3 Problem statement

Agricultural by-products and industrial solid wastes are currently underutilized and in recent years have become a serious environmental problem due to enactments of more stringent federal and state legislation regulating their disposal. Similarly, industrial wastewater streams containing some recalcitrant organic compounds like phenol and also heavy metals are a serious health and environmental threat. Phenol imparts a carbolic odour to rivers and is also toxic to fish and human beings whereas heavy metals are known to be detrimental to the living beings. On the other hand, most dyes used in textile industries are stable to light and are not biologically degradable. Industrial effluents containing dyes reduce light penetration, preventing the photosynthesis of aqueous flora. Some dyes may cause allergy, skin irritation and cancer to humans. In order to minimize the risk of pollution problems from such effluents, it is necessary to accurately treat them before discharging to the environment (Ardejani *et al*., 2007).

Conventional advanced wastewater treatment technologies such as ion exchange, membrane separation and electrolysis are costly and hence the driving force for search of creative, low cost and environmentally sound ways of treating wastewater as environmental laws become stringent. Most conventional methods require high capital investment and are high in operational costs and create sludge disposal problems. Although adsorption technique is relatively cheap, there is pressing need to replace commercial adsorbents like activated carbon, zeolite, activated alumina and silica gel with the low cost adsorbents. The method of adsorption using commercial activated carbon is costly especially for developing countries such as South Africa. Thus, single use adsorbent materials are desired considering the difficulties faced during commercial activated carbon regeneration and the disposal problems posed by regeneration solutions. This calls for research efforts to develop an industrially viable, cost effective and environmentally compatible adsorbent for wastewater treatment.

In an attempt to address the cost problems associated with commercial adsorbents; the use of abundant, locally available, low cost adsorbents derived from agricultural wastes and industrial solid wastes are proposed in this study. These adsorbents are cheaper and readily available. Also, these low cost adsorbents are proposed as single use materials to avoid regeneration problems. After use, the loaded adsorbent could be easily disposed off by landfilling or incineration and the metal residues could be recovered by subsequent treatment of the post-combustion ash (leaching). On the other hand, the problem associated with the low cost adsorbents is the performance. Therefore, performance evaluation of several low cost adsorbents is proposed and the best adsorbent will be selected.

1.4 Hypothesis

Low cost adsorbents derived from agricultural by-products and industrial solid wastes could be used to remove recalcitrant wastes from synthetic wastewater. These low cost adsorbents are expected to exhibit similar performance features as commercial activated carbon if they have similar physicochemical properties on which adsorption performance mainly depends. In addition, the presence of heavy metals may affect the removal of phenol and vice versa if they are both attracted to the same active sites. It is expected that the performance of the low cost adsorbents is comparable to that of commercial adsorbents.

1.5 Objectives

The main objective is to evaluate the adsorption performance of low cost adsorbents in the removal of non-biodegradable wastes from synthetic petrochemical (phenol and heavy metals) and textile wastewater (direct dyes). The specific objectives are to:

(a) Prepare and employ low cost adsorbents from agricultural wastes (sawdust and sugarcane bagasse) and an industrial solid waste (coal fly ash) to treat wastewater.

(b) Determine the physicochemical properties of the low cost adsorbents and compare with those of commercial activated carbon.

(c) Quantify the adsorption capacities of the low cost adsorbents and commercial activated carbon with respect to recalcitrant waste removal.

(d) To compare the performance of all the adsorbents in the removal of recalcitrant wastes

(e) Determine the effects of operating conditions such as solution pH, adsorbent dose and initial adsorbate concentration on the adsorption capacities in batch adsorption.

(f) Identify the applicable adsorption isotherms and kinetic models for each adsorbent.

(g) Analyze the effects of bed height (Z), aspect ratio (Z/D) and initial adsorbate concentration (C_o) on breakthrough in a continuous adsorption process.

CHAPTER 2

2 Literature review

The surge of industrial activities has intensified more environmental problems as seen for example in the deterioration of several ecosystems due to the accumulation of dangerous pollutants. Apart from the environmental damage, human health is likely to be affected as the presence of toxic wastes beyond a certain limit brings serious hazards to living organisms (Febrianto *et al*., 2009). For instance, petrochemical and chemical industries are concentrated in the South Durban area in South Africa where there is extreme contamination of ground and surface water and members of the community have consistently complained of high levels of cancer (Butler and Hallowes, 2002).

Adsorption is gaining interest as one of the most effective processes for treatment of industrial effluent containing toxic materials. The occurrence of non-biodegradable wastes in streams and lakes threatens the use of water resources and various treatment methods have been used for the removal of these wastes. Among these methods, adsorption using commercial activated carbon has proven to be efficient, however it is highly expensive. Hence in recent years there has been a continuous search for locally available and cheaper adsorbent.

The adsorption phenomenon is influenced by the nature of solution in which the contaminant is dispersed, molecular size and polarity of the contaminant and the type of adsorbent. Therefore, it is necessary to do a comprehensive literature review on different sources and characteristics of industrial wastewater. Furthermore, a complete assessment of various tertiary wastewater treatment techniques used to remove recalcitrant wastes from industrial wastewater is also important. The present literature review clearly establishes that wastewater treatment using low cost adsorbents prepared from agricultural waste and industrial solids is a technically

feasible process. Consequently, the results from the present study, literature and pilot plant tests can serve as the basis for industrial scale design.

2.1 Wastewater characteristics

An understanding of the nature of wastewater is essential in the design and operation of collection, treatment, and disposal facilities and in the engineering management of environmental quality. Thus, in this section, information on the physical and chemical characteristics of wastewater from different sources is given. However, special emphasis is on wastewater streams that contain non-biodegradable organic compounds and heavy metals. Various wastewater treatment techniques have been used to treat petrochemical, pharmaceutical, brewery, molasses, pulp and paper and textile wastewater. Considering the fact that South Africa is an agricultural and industrial country, it will be much logical and cost effective to use the abundant agricultural and industrial wastes as adsorbents since they are already posing disposal problems (DEAT, 2004)

2.1.1 Biodegradable wastewater

Food processing wastewater often contains multiple types of contaminants that are generally biodegradable**.** There are various types of wastewater discharged from the food processing industry due to the fact that the number of raw materials, processes and types of products involved in the industry are enormous. Nevertheless, most types of food processing wastewater require biological oxygen demand (BOD) reduction since they contain organic matter represented by starch, sugars and proteins. However, in some cases, suspended solids and oils are also contained in food processing wastewater. A typical example is brewery wastewater which is readily biodegradable and this is attributed to the fact that it contains nutrients that support microbial growth (Ochieng *et al*., 2002) and contain less aromatic hydrocarbons.

2.1.2 Recalcitrant wastewater

Rapidly changing technologies, industrial products and practices generate wastewater that is difficult to manage. For example wastewater from textile industries is not easy to biodegrade due to the fact that it contains dyes which are by design, highly stable molecules, made to resist degradation by light, chemical, biological and other exposures. Furthermore, textile wastewater contains many other materials such as particulates, processing assistants, salts, surfactants, acids and alkalis which makes it more complex (El-Qada *et al*., 2007). Pharmaceutical wastewater also contains various antibiotics, bactericidal–type compounds and other pharmaceuticals that have a toxic (inhibitory) impact upon various biological treatment methods. In addition, considerable amounts of total Kjeldhal nitrogen (TKN) still remain in the effluent even after undergoing a high level of conventional biological treatment. Total Kjeldhal nitrogen is defined as the sum of organic nitrogen and ammonia in a water sample measured in milligrams per litre (mg/l). Pharmaceutical wastes such as nitroanilines, phenol and toluene are quite resistant to biodegradation (Wang *et al*., 2004). On the other hand, molasses wastewater is not easily biodegradable as well since it is characterized by a COD:BOD ratio of 2.0, low pH, strong odor, high total suspended solids (TSS) and a dark brown color due to non-biodegradable hydrocarbons which can be removed by techniques such as adsorption (Satyawali, 2008).

Table 2.1 shows the composition of a particular acidic petrochemical wastewater sample reported by Patel and Madamwar, (2002). Petrochemical wastewater often contains high concentration of biodegradable compounds (Ting *et al*., 2007). However, it also contains both metals and recalcitrant organic compounds such as phenol which is considered a priority pollutant (Abdelwahad *et al*., 2009). The present study focuses on the use of the adsorption technology in the removal of these non-biodegradable wastes. The metal ions may originate from the catalysts used in the refinery process. Thus, the composition of the metals ions varies with the type of raw material and catalysts employed. Besides the example given in Table 2.1,

petrochemical wastewater may contain suspended solids as high as 400 mg/l, benzene levels of up to 100 mg/l and heavy metals in the range 0.1–100 mg/l may be present (Pollution Prevention and Abatement Handbook, 1998; Lenntech, 2008). The discharge of recalcitrant wastes poses a serious health and environmental hazard.

Table 2.1

Composition of acidic petrochemical wastewater (Patel and Madamwar, 2002)

Components	Concentration/value
Formic acid	46 600 mg/l
Acetic acid	46 600 mg/l
Cyclohexanol	300 mg/l
Cyclohexane	500 mg/l
Cyclohexanone	300 mg/l
Phenol	360 mg/l
Total nitrogen (as N_2)	50 – 212 mg/l
Total phosphate (as P)	102 – 227 mg/l
Total sulphate (as SO_4)	150 – 242 mg/l
Chlorides	2 – 3 mg/l
Iron	0.05–0.8 mg/l
Heavy metals (Co, Ni, Mo, Cr)	0.15–0.20 mg/l
Oil and grease	12–13 mg/l
COD	55 000 – 60 000 mg/l
BOD	30 000 – 32 000 mg/l
COD:BOD	1.85
Volatile fatty acids	93 000 – 95 000 mg/l
Total solids	20 – 300 mg/l
Total acidity	45 000 – 46 000 mg/l
pH	2.5 – 2.7

2.2 Effects of wastewater contaminants

A tremendous increase in the use of heavy metals over the past few decades has inevitably resulted in an increased flux of metallic substances in the aquatic environment. Heavy metals get distinguished from other toxic pollutants due to their non-biodegradability. Consequently, increased concentration of heavy metals in the aquatic environment can cause phyto-toxicity, bio-concentration and bio-magnification by organisms (Ayyappan *et al*., 2005). Furthermore, heavy metals can cause severe physiological or neurological damage to the human body (Wong *et al*., 2003) and a good example is the Minamata mercury-poisoning tragedy which occurred in Japan.

Similarly, the discharge of wastewater/effluent containing recalcitrant organic compounds such as phenol into natural surface water pose serious risk to aquatic organisms and human beings besides imparting a carbolic odor to receiving water. The health effects following repeated exposure to low levels of phenol in water include liver damage, diarrhea, mouth ulcer, dark urine and hemolytic anemia (Singh *et al*., 2008). Thus, phenol has been registered as a priority pollutant by the United States Environmental Agency (US EPA, 1985).

The discharge of coloured waste is not only damaging the aesthetic nature of receiving streams, but it may also be toxic to aquatic life. In addition, colour interferes with the transmission of sunlight into a stream and therefore reduces photosynthetic action (Kadirvelu *et al*., 2000). Furthermore, the expanded use of azo dyes, which contain one or more azo bonds (–N=N–) have shown that some of them and their reaction products such as aromatic amines are highly mutagenic and carcinogenic (Malik, 2004; Mahmoodi *et al*., 2005). Also, the release of these coloured wastewaters into the ecosystem is a dramatic source of eutrophication and perturbation of aquatic life. Hence, in view of the toxicity and in order to meet regulatory safe discharge standards, it is essential to remove toxic contaminants from wastewater/effluent before it is released into the environment.

2.3 Tertiary/advanced wastewater treatment

Advanced wastewater treatment is defined as: any process designed to produce an effluent of higher quality than normally achieved by secondary treatment processes or containing unit operations not normally found in secondary treatment (Sonune and Ghate, 2004). The most commonly used methods for removal of metal ions from industrial effluents include: chemical precipitation, solvent extraction, dialysis/electrodialysis, electrolytic extraction, reverse osmosis, ion exchange, cementation, dilution, air stripping, steam stripping, chemical oxidation or reduction, flocculation, soil flushing/washing chelation, adsorption, etc.

2.3.1 Ion exchange

Ion exchange is a process in which there is exchange of ions between a liquid phase and a porous solid. In ion exchange systems, polymeric resins as well as zeolites are usually employed (Ali and El-Bishtawi, 1997). Cation exchange resins are typically used in homes and municipal water treatment plants to remove Ca^{2+} and Mg^{2+} ions in 'hard' water and by industries in the production of ultra-pure water (Sonune and Ghate, 2004). Zhang *et al*. (2006) reported that the commercially-available Amberlite XAD-4 resin is an ideal adsorbent for a wide variety of aromatic compounds especially for phenols. However, XAD-4 resin has hydrophobic surfaces and a low capacity for most organic chemicals compared to activated carbon, which limits its application in industrial wastewater treatment (Fontanals *et al*., 2007). In order to obtain larger adsorption capacity and better selectivity for a specific organic pollutant, chemical modification of ordinary polymeric resins is often adopted by grafting some special functional groups onto the matrix of the resins (Pan *et al*., 2007). Ion exchange can remove heavy metal ions effectively and selectively, but the cost of the resins is relatively high (Kim *et al*., 2006a). Another disadvantage is the high cost of disposing of regeneration solutions (Sonune and Ghate, 2004).

2.3.2 Chemical precipitation

Chemical precipitation is the most commonly used technology to remove dissolved metal ions from wastewater. The metals ions are converted to an insoluble form (particles) using precipitating agents such as calcium hydroxide, sodium hydroxide, ferric chloride or ferrous sulphate. The particles formed are removed from solution by settling and/or filtration (US. EPA, 2000). The unit operations typically required in this technology includes neutralization, precipitation, coagulation/flocculation, solids/liquid separation and dewatering. The precipitation method is simple and economical. However, the method may not be a viable option for certain end-users since it is not versatile (Onyango *et al*., 2004). Also, the main disadvantage of these techniques is the production of solid residues (sludge) containing toxic compounds whose disposal is in general landfilling (which is the last priority in terms of the EU policies) (Cavaco *et al*., 2007). Furthermore, the produced sludge also requires licensed disposal (Dash *et al*., 2009). Another drawback of the precipitation method is that the metal concentration of treated water cannot be reduced below the solubility of the precipitate (Kim *et al*., 2006a). Therefore, the use of other techniques such as adsorption is advisable in order to protect the environment.

2.3.3 Membrane separation techniques

Membrane processes operate on the basis of mechanisms such as: pressure driven, which includes reverse osmosis (RO), ultrafiltration (UF) and nanofiltration (NF); concentration driven, which includes diffusion dialysis; electrically driven, which includes electrodialysis and finally, temperature difference driven, which includes membrane distillation. Membrane filtration (UF, RO and NF) is used to simultaneously remove colour, COD, heavy metals and total dissolved solids (TDS) from wastewater. The possibility of obtaining solid free effluents is a very attractive feature of this process (Wang *et al*., 2006). Additionally, membrane separation processes offer various advantages e.g a compact system, easy control of operation and maintenance and low needs for chemicals.

However, in spite of the advantages, membrane separation has the drawbacks of poor removal of the low molecular weight (organic) materials (ultrafiltration) and high energy consumption (reverse osmosis) (Gambolas *et al*., 2004). Another limitation of membrane processes is the flux decline caused by membrane fouling, which may result from plugging of organic and inorganic materials in the membrane pores. This fouling of membranes lowers the economical efficiency of the membrane processes by reducing the rate of production of treated water and shortening the membrane life (Laslo and Hodur, 2007).

2.3.4 Coagulation and flocculation

Coagulation is always considered along with flocculation and is used to remove particles which cannot be removed by sedimentation or filtration alone. These particles are usually less than 1 μm in size and are termed colloids. They have poor settling characteristics and are responsible for the colour and turbidity of water. They include clays, metal oxides, proteins and micro-organisms and some organic compounds. The important property which they all have is that they carry a negative charge and this, along with the interaction between the colloidal particles and the water, prevents them from aggregating and settling in still water. The particles can be aggregated by adding either multi-valent ions or colloids having an opposite (positive) charge and these are added as chemical coagulants e.g aluminium and ferric salts which are present as the ions Al^{3+} and Fe^{3+} (Drinan, 2001; Amuda and Alade, 2006).

Coagulation is the destabilization of colloids by neutralizing the forces that keep them apart. Cationic coagulants provide positive electric charges to reduce the negative charge (zeta potential) of the colloids. As a result, the particles collide to form large particles (flocs). Flocculation is the action of polymers to form bridges between the flocs, and bind the particles into large agglomerates or clumps. Bridging occurs when segments of the polymer chain adsorb on different particles and help particles aggregate (Drinan, 2001). The coagulation/flocculation technique is used in treating

wastewater, both from industrial and treated sewage, from municipal wastewater treatment plants. However, the far most extensive application has been in the area of portable water treatment (Bratby, 2006). Amuda and Alade (2006) used the coagulation/flocculation process in the treatment of abattoir wastewater. Generally, coagulation seems to be an expensive step taking into account expenses of chemicals and sludge disposal. Thus, there is a need for development of low cost alternatives for wastewater treatment (Mohana *et al*., 2009).

2.3.5 Oxidation processes

Ozone is a powerful oxidant for water and wastewater treatment. Once dissolved in water, ozone reacts with a greater number of organic compounds in two different ways: by direct oxidation as molecular ozone or by indirect reaction through formation of secondary oxidants like free radical species, in particular the hydroxyl radicals. Both ozone and the hydroxyl radicals are strong oxidants and are capable of oxidizing a number of compounds (Bes-Pia *et al*., 2003). Ozonation can also be used for the removal of inorganic species as an aid to the coagulation-flocculation process (Laslo and Hodur, 2007).

Ozone has been applied for the treatment of dyes, phenolics, pesticides, etc (Pena *et al*., 2003). However, ozone only transforms the chromophore groups, but does not degrade the dark coloured polymeric compounds in effluent (Alfafara *et al*., 2000; Pena *et al*., 2003). Satyawali and Balakrishnan (2008) reported that decolourization through chemical treatment with ozone and chlorine leads to temporary colour reduction because of transformation of the chromophore groups so these are not preferred solutions. Ozone treatment can create undesirable by-products that can be harmful to health if they are not controlled (e.g formaldehyde and bromate). Also, ozone is not effective at removing dissolved minerals and salts (Johnson, 2005).

2.3.6 Electrochemical method

The electrochemical method of wastewater treatment came into existence by treating sewage generated from ship onboard by mixing sewage and sea water at a ratio 3:1 and subjecting them to electrolysis. Thereafter, the application of electrochemical treatment was widely received in treating industrial wastewaters like textile and olive mill, tannery, distillery and beef effluent (Vijayaraghavan *et al*., 2007). Electrolytic methods are expensive and require special equipments and maintenance. Thus, there is an urgent need for the development of an alternative treatment process (Dash *et al*., 2009).

Removal of heavy metals can also be accomplished through treatment options such as complexation, solvent extraction, foam flotation, electrodeposition and cementation (Peters *et al*., 1985; Wan *et al*., 2007), but they have short-comings like slow kinetics and inadequate selectivity. Among these, adsorption has evolved as the frontline of defense especially for those wastes which cannot be removed by other techniques (Mohan and Kunwar, 2002).

2.3.7 Adsorption

Adsorption is defined as the mass transfer of a substance (adsorbate) from liquid or gas phase onto the solid interface (adsorbent) and becomes attached by physical and/or chemical interactions (Kurniawan *et al*., 2006). Thus, adsorption can either be physical or chemical in nature, and frequently involves both (Cheremisinoff and Morresi, 1978). In chemisorption the transfer of electrons is significant and equivalent to the formation of a chemical bond between the sorbate and the solid surface. In physisorption the interactive forces are relatively weak (Sing *et al*., 1985). In addition, physisorption involves the attraction by electrical charge differences between the adsorbent and the adsorbate. Adsorption proceeds through the following steps:

(i) Mass transfer: adsorptive molecules transfer to the exterior of the adsorbent granules;

(ii) Intraparticle diffusion: molecules move into the adsorbent pores

(iii) Physical and/ or chemical adsorption

Adsorption capacity depends on the physical and chemical characteristics of both the adsorbent and adsorbate, concentration of the adsorbate in liquid solution, experimental conditions such as temperature and solution pH, and the amount of time the adsorbate is in contact with the adsorbent (residence time) (Cheremisinoff and Morresi, 1978).

With regards to its simplicity and high-efficiency characteristics, adsorption is looked upon as a better technology. Adsorption processes have been and actually are the most applied in industries, and consequently the most studied (Chiarle *et al*., 2000). Choice of an adsorbent is the starting point in the development of an adsorption unit. Several adsorbents can be used to treat industrial wastewater. Activated carbon is a well-known adsorbent and has proven to be useful for the removal of heavy metals. Nevertheless, the application of activated carbon for wastewater treatment is not feasible due to its high price and cost associated with the regeneration as a result of high-degree of losses in real process (Febrianto *et al*., 2009). Mckay (1984) and Carvalho *et al*. (2007) used activated carbon to adsorb contaminants from wastewater and other workers reported on the use of zeolites in wastewater treatment (Qiu and Zheng, 2007). In addition, the use of other adsorbents such as synthetic polymeric (Zabkova *et al*., 2006) and silica based adsorbents (Lam *et al*., 2006) has been reported.

2.4 Commercial adsorbents

2.4.1 Zeolites

Zeolites are aluminosilicate minerals containing exchangeable alkaline and alkaline earth metal cations (normally Na, K, Ca and Mg) as well as water in their structural framework. The physical structure is porous, enclosing interconnected cavities in which the metal ions and water molecules are contained. Zeolites have high ion-exchange and size selective adsorption capacities as well as thermal and mechanical stabilities (Wang *et al*., 2009). Also, zeolites can be either synthetic (Hui *et al*., 2006) or natural (Rubio, 2006). They have been used as water softeners (Ali and El-Bishtawi, 1997), chemical sieves and adsorbents (Hui *et al*., 2005) for a long time. However, zeolites become unstable at high pH (Basu, *et al*., 2006) and for this reason; chemicals are added to adjust the pH, which makes this process expensive. The process of regenerating zeolite packed beds dumps salt water into the environment. Furthermore, the use of zeolites does not reduce the level of most organic compounds (Johnson, 2005).

2.4.2 Silica gel

Silica gel is a non-toxic, inert and efficient support and is generated by decreasing the pH value of the alkali silicate solution to less than ten. The solubility of silica is then reduced to form the gel and as the silica begins to gel, cells in silica are trapped in a porous gel, which is a three-dimensional SiO_2 network (Chaiko *et al*., 1998). Porous silica gel is an inorganic synthetic polymeric matrix often used to entrap cells and its use for entrapment is called the sol-gel technique (Weller, 2000). Reactive sites of silica gel exist in large numbers, and therefore, the number of immobilized organic molecules is high, which results in good sorption capacity for metal ions (Rangsayatorn *et al*., 2004; Chaiko *et al*., 1998).

2.4.3 Activated alumina

Activated alumina is a filter media made by treating aluminium ore so that it becomes porous and highly adsorptive. It can also be described as a granulated form of aluminium oxide. Activated alumina removes a variety of contaminants that often co-exist with fluoride such as excessive arsenic and selenium (Farooqi *et al*., 2007). The medium requires periodic cleaning with an appropriate regenerant such as alum or acid in order to remain effective. Activated alumina has been used as an effective adsorbent especially for point of use applications (Ghorai and Pant, 2005; Bouguerra *et al*., 2007). The main disadvantage of activated alumina is that the adsorption efficiency is highest only at low pH and contaminants like arsenites must be pre-oxidized to arsenates before adsorption. In addition, the use of other treatment methods would be necessary to reduce levels of other contaminants of health concern (Johnson, 2005).

2.4.4 Activated carbon

The most widely used adsorbent for industrial applications is activated carbon (Ho, 2004). It is a well known adsorbent due to its extended surface area, microporous structure, high adsorption capacity and high degree of surface reactivity (Satyawali and Balakrishnan, 2008). The structure consists of a distorted three dimensional array of aromatic sheets and strips of primary hexagonal graphic crystallites (Stoeckli, 1990). This structure creates angular pores between the sheets of molecular dimensions which give rise to many of the useful adsorption properties of activated carbon (Stoeckli, 1990; Innes *et al*., 1989). Pore size ranges from 1 nm to 1000 nm, and the extensive porosity is responsible for the high surface area of the material usually 500 - 1500 m^2/g (Cooney, 1980). Any carbon material can be used to make activated carbon; however, commercial activated carbon is manufactured from only a few carbon sources; wood, peat, coal, oil products, nut shells and pits (Davidson *et al*., 1968). Wood products and low-grade coal have some original porosity and are easier to activate than dense materials such as anthracite (Sun *et al*., 1997).

Activated carbon manufacturing consists of a charring or carbonization step in which most of the non-carbon material is volatilized by pyrolysis (usually between 500 and 750°C). The weight loss is usually 60 to 70% and some CO_2 is volatilized (Sun *et al*., 1997; Diaz-Teran *et al*., 2001). The fine pore structure is formed in an activation process. In gas activation, an oxidizing agent such as CO_2 or steam is used at high temperature to erode pores into the char. In chemical activation, the char is impregnated with a chemical and then fired to high temperatures (usually 800 to 1000°C). The activating chemical corrodes the carbon to form the pore structure and they are usually strong acids, bases or corrosives (phosphoric acid, sulfuric acid, potassium hydroxide, zinc chloride, potassium sulfide, or potassium thiocyanate) (Mozammel *et al*., 2002). The final pore structure depends on the nature of the starting material and the activation process (Diaz-Teran *et al*., 2001). Materials with an original pore structure like wood take less processing than a denser and isotropic material like coal or tar. Impurity amounts are usually higher in the less carbon dense materials.

According to the IUPAC definitions the pore sizes of activated carbon can roughly be classified as micropores (< 2 nm), mesopores (2 - 50 nm) and macropores (> 50 nm) (Stoeckli *et al*., 2002). The macropores act as transport pathways, through which the adsorptive molecules travel to the mesopores, from where they finally enter the micropores. Thus, macro- and mesopores can generally be regarded as the highways into the carbon particle, and are crucial for kinetics. The micropores usually constitute the largest proportion of the internal surface of the activated carbon and contribute most to the total pore volume (Rodriguez-Reinoso and Linares-Solano, 1989).

Activated carbon has both chemical and physical effects on the substance where it is used as a treatment agent. Activity can be separated into adsorption, mechanical filtration, ion exchange and surface oxidation. Adsorption is the most studied of these properties in activated carbon (Cheremisinoff and Morresi, 1978). Heavy metal

removal by adsorption using commercial activated carbon has been widely used. However, high costs of activated carbon and 10-15% loss during regeneration makes its use prohibitive in the developing countries like South Africa (Vimal *et al*., 2006). Commercial activated carbon also requires complexing agents to improve its removal performance for heavy metals. Therefore this situation no longer makes it attractive to be widely used in small-scale industries because of cost inefficiency (Sandhya and Kurniawan, 2003). This has led to a search for cheaper carbonaceous substitutes. In order to overcome the problems associated with the activated carbon, low cost adsorbents derived from agricultural waste and industrial solids are proposed in the present work.

2.5 Low cost adsorbents

In a developing country like South Africa, materials which are locally available in large quantities such as agricultural wastes and industrial by-products can be utilized as low cost adsorbents. Conversion of these materials into adsorbents for wastewater treatment would help to reduce the cost of waste disposal and provide an alternative to commercial activated carbon (Kurniawan *et al*., 2006). The adsorption of toxic waste from industrial wastewater using agricultural waste and industrial by-products has been massively investigated (Basu *et al*., 2006; Wan and Hanafiah, 2007; Srivastava *et al*., 2006). Several reviews can be referred to that discuss low-cost adsorbents application for industrial wastewater treatment (Kurniawan *et al*., 2006; Babel and Kurniawan, 2003; Crini, 2005; Pollard *et al*., 1992).

2.5.1 Agricultural wastes

Production of activated carbon from agricultural wastes serves a double purpose by converting unwanted, surplus wastes to useful, valuable material and provides an efficient adsorbent material for the removal of pollutants from wastewater. It is highly anticipated that this work would abate the environmental nuisance if these waste materials are used for removal of different contaminants from industrial wastewaters.

Karnitz *et al*. (2007) reported the use of chemically modified sugarcane bagasse to adsorb heavy metal ions and Mukherjee *et al*. (2007) studied the adsorption of phenol using an adsorbent derived from sugarcane bagasse as well. This shows that agricultural wastes are versatile; they can be used for sorption of both inorganic and organic wastes. Although sugarcane bagasse is burned to produce energy for sugar mills in South Africa, leftovers are still significant. On the other hand, the area surrounding the Lataba Citrus farm in Limpopo Province, South Africa is highly forested and there is abundant sawdust available as a waste product which is mostly stock-piled (DEAT, 2004). In addition, there are seventy-seven sawmills in KwaZulu Natal and the waste they generate usually far exceeds waste supplied to the pulp and paper, and board industries. The excess waste, mostly sawdust and timber off-cuts is a major problem in the province (Norris and Volschenk, 2007).

More studies have been carried out on the feasibility of using agricultural adsorbents such as sawdust (Ismadji *et al*., 2005), peanut shells (Wafwayo *et al*., 1999), poultry litter (Kelleher *et al*., 2002), coffee husk (Kumar, 2006), rice husk (Kumar and Bandyopadhyay, 2006), cow dung (Das *et al*., 2000), soybean hull and almond hull (Marshall *et al*., 2000), among others. Argun *et al*. (2007) investigated the effects of the shaking speed, contact time, dose and pH by varying one parameter at a time, maintaining others constant during the adsorption of Cu, Ni and Cr from aqueous solution using sawdust whilst Bulut and Tez (2007) investigated the effects of contact time, initial concentration and temperature on the removal of Pb(II), Cd(II) and Ni(II) from aqueous solution using walnut sawdust. McSweeny *et al*. (2006) showed that reacting citric acid with corn fiber, ground corn cobs, starch, and cellulose fiber greatly increased sorption of Cu^{2+} ion by these materials. Soybean hulls, peanut shells, almond hulls and cotton seeds were similarly modified by 0.6 M citric acid for enhanced heavy metal sorption at pH 4.8 and adsorption capacities greater than 1.0 mg/g were obtained for all the metal ions studied by Marshall *et al*. (2000).

2.5.2 Industrial by-products

Many industrial wastes are high in carbon content and offer significant potential for conversion into carbonaceous chars which may then be further activated to yield porous adsorbents. Like agricultural waste, industrial by-products such as fly ash, used tyres, waste iron, metallic iron, hydrous titanium oxide, and blast furnace slag are inexpensive and abundantly available (Kurniawan *et al*., 2006). These materials can be chemically modified to enhance their removal performance. However, unlike those from agricultural waste, adsorbents from this source can be obtained from industrial processing only. In South Africa, several such wastes currently pose a variety of disposal problems due to bulk volume, auto reactivity or physical nature like oily wastes and scrap tyres. Thus, the controlled pyrolysis of these wastes combined with the reuse of porous products contributes to a minimisation of handling difficulties (Pollard *et al*., 1992). Some of these industrial by-products combine good adsorption capacities and buffering effect, which assure almost complete removal of heavy metal ions without preliminary correction of the initial pH being necessary.

Fly ash, an industrial solid waste of thermal power plants is one of the cheapest adsorbents having excellent removal capabilities for different wastes. South Africa produces approximately 28 million tons of coal fly ash per annum (Reynolds *et al*., 2002). Only 5% of the fly ash is used as a construction material while the rest is stored in ash damps, which in turn have to be rehabilitated increasing the cost of ash handling (Woolard *et al*., 2000). Sen and De (1987) carried out a study on the adsorption of mercury using coal fly ash and it was reported that the maximum adsorption capacity of 2.82 mg Hg^{2+}/g took place at a pH range of 3.5–4.5 and that adsorption followed the Freundlich model. In another work, a comparative adsorption study was carried out by Jain *et al*. (2001) using carbon slurry waste obtained from a fertilizer plant and blast furnace sludge, dust, and slag from steel plant wastes as adsorbents for the removal of dyes. It was found that carbonaceous adsorbent prepared from the fertilizer plant waste exhibited a good potential for the removal of dyes as compared to the other three adsorbents prepared.

Adsorption is influenced by the nature of solution in which the contaminant is dispersed, molecular size and polarity of the contaminant and the type of adsorbent. Hence, it is important to be able to relate the amount of contaminant adsorbed from the wastewater stream to the amount of adsorbent needed to reduce the contaminant to acceptable levels (Rowe and Abdel-Magid, 1995). The presentation of the amount of solute adsorbed per unit weight of the adsorbent as a function of the equilibrium concentration in bulk solution at constant temperature is termed the adsorption isotherm. Adsorption isotherm models can be regarded as benchmark for evaluating the characteristic performance of an adsorbent.

2.6 Equilibrium isotherm models

Analysis of the isotherm data is important to develop an equation which accurately represents the results and which could be used for design purposes and to optimize an operating procedure. The most common isotherms applied in solid/liquid systems are the theoretical equilibrium isotherm; Langmuir and Freundlich (two parameter models) (Ho, 2004; Basha *et al*., 2008). Simplicity and easy interpretability are some of the reasons for extensive use of these models. At the same time, linear regression has been frequently used to evaluate the model parameters (Basha *et al*., 2008). However, equilibrium isotherms such as the Temkin, two site Langmuir, Langmuir-Freundlich (Sips isotherm), Redlich-Peterson, Tóth, and Dubinin-Radushkevitch can also be used to model experimental data (Onyango *et al.,* 2004).

2.6.1 Langmuir adsorption isotherm

The Langmuir isotherm also called the ideal localized monolayer model was developed to represent chemisorption (Wang *et al*., 2009). Langmuir (1918) theoretically examined the adsorption of gases on solid surfaces, and considered sorption as a chemical phenomenon. The Langmuir equation relates the coverage of molecules on a solid surface to concentration of a medium above the solid surface at a fixed temperature. This isotherm is based on the assumption that; adsorption is limited to mono-layer coverage, all surface sites are alike and can only accommodate

one adsorbed molecule, the ability of a molecule to be adsorbed on a given site is independent of its neighbouring sites occupancy, adsorption is reversible and the adsorbed molecule cannot migrate across the surface or interact with neighbouring molecules (Febrianto *et al*., 2009; Sarkar and Acharya, 2006). By applying these assumptions and the kinetic principle (rate of adsorption and desorption from the surface is equal), the Langmuir equation can be written in the following hyperbolic form:

$$q_e = q_{\max} \frac{K_L C_e}{1 + K_L C_e} \tag{2.1}$$

This equation is often written in different linear forms (Febrianto *et al*., 2009):

$$\frac{1}{q_e} = \left(\frac{1}{K_L q_{\max}} \right) \frac{1}{Ce} + \frac{1}{q_{\max}} \tag{2.2}$$

$$\frac{C_e}{q_e} = \frac{1}{q_{\max}} C_e + \frac{1}{K_L q_{\max}} \tag{2.3}$$

where q_e is the adsorption capacity at equilibrium (mg/g), q_{max} is the theoretical maximum adsorption capacity of the adsorbent (mg/g) and, as such, can be thought of as the best criterion for comparing adsorptions (Ho *et al*., 1995), K_L is the Langmuir affinity constant (l/mg) and C_e is the supernatant equilibrium concentration of the system (mg/l). This isotherm equation has been most frequently applied in equilibrium study of adsorption, however, it should be realized that the Langmuir isotherm offers no insights into aspects of adsorption mechanism (Liu and Liu, 2008).

2.6.2 Freundlich adsorption isotherm

The Freundlich isotherm was originally of an empirical nature, but was later interpreted as sorption to heterogeneous surfaces or surfaces supporting sites of varied affinities. It is assumed that the stronger binding sites are occupied first and that the binding strength decreases with increasing degree of site occupation (Davis *et al*., 2003). The Freundlich isotherm can describe the adsorption of organic and

inorganic compounds on a wide variety of adsorbents (Febrianto *et al*., 2009). According to this model the adsorbed mass per mass of adsorbent can be expressed by a power law function of the solute concentration as (Freundlich, 1906):

$$q_e = K_F C_e^{1/n} \tag{2.4}$$

where K_F is the Freundlich constant related with adsorption capacity (mg/g), n is the heterogeneity coefficient (dimensionless). For linearization of the data, the Freundlich equation is written in logarithmic form:

$$\log q_e = \log K_F + (1/n) \log C_e \tag{2.5}$$

The plot of log q_e versus log C_e has a slope with the value of 1/n and an intercept magnitude of log K_F. On average, a favorable adsorption tends to have Freundlich constant n between 1 and 10. Larger value of n (smaller value of 1/n) implies stronger interaction between the adsorbent and the adsorbate while 1/n equal to 1 indicates linear adsorption leading to identical adsorption energies for all sites. Linear adsorption generally occurs at very low solute concentrations and low loading of the adsorbent (Site, 2001).

2.7 Mass transfer mechanism

Physical adsorption is an extremely rapid process so that in a porous adsorbent the overall rate of adsorption is almost controlled by mass or heat transfer resistance rather than by the intrinsic rate of sorption at the active surface. Diffusion controlled processes may exhibit many of the features commonly associated with the slow activated surface adsorption process. There are several distinct resistances to mass and heat transfer. Thus, there are essentially three consecutive mass transport steps associated with the adsorption of solutes by porous adsorbents. The first step, bulk transport of solute in the solution phase, is usually rapid due to mixing and convective flow. The second step, film transport, involves diffusion of the solute through a hypothetical "film" or hydrodynamic boundary layer. Except for a small

amount of adsorption that occurs on the exterior of the adsorbent, the solute then must diffuse within the pore volume of the adsorbent and/or along pore-wall surfaces to an active adsorption site (intraparticle transport) (Ruthven, 1984).

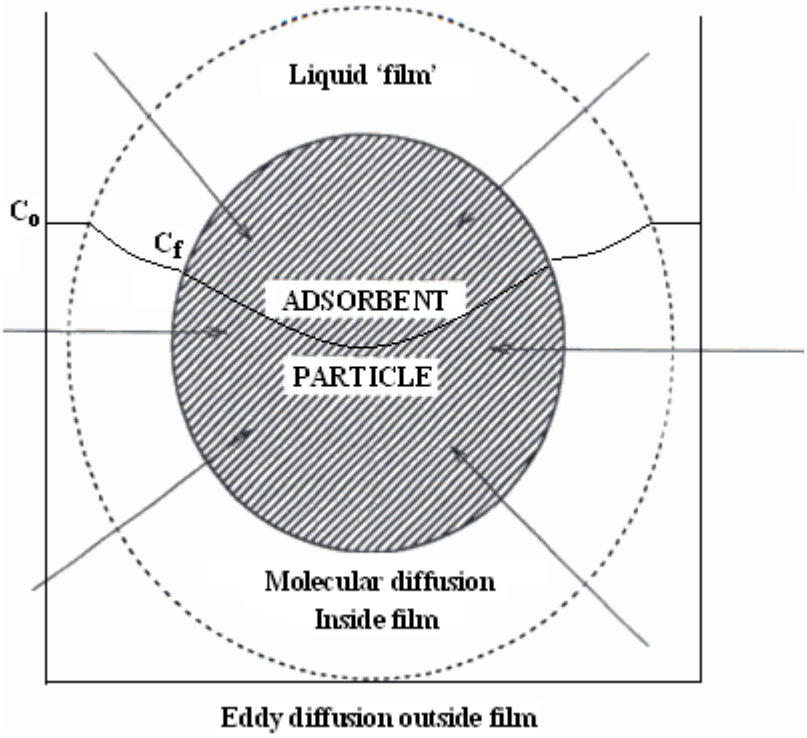

Figure 2.1. Schematic of an adsorbent particle depicting the surrounding stagnant fluid film (Cooney, 1998).

Figure 2.1 shows a particle of adsorbent, visualized as being perfectly spherical, with a smooth surface, even though most real adsorbent particles are only approximately spherical and often have quite rough surfaces. Assuming that the particle is initially free of solute, and that at time zero it is tossed into a relatively large volume of well-mixed liquid having an initial concentration, C_o, the adsorbent can be visualized as having a stagnant "film'' of liquid surrounding it. Film and intraparticle transports are thus the major factors controlling rates of adsorption by porous adsorbents. Transfer of solute across the film can only occur by molecular diffusion, an intrinsically slow process. If the intensity of mixing is increased, the film thickness

can be made smaller, and the mass transfer resistance reduced. There are only two regions: a stagnant region in which all the mass transfer resistance lies and a well-mixed region outside of that in which no mass transfer resistance exist (due to the fact that the concentration is uniform there). Of course, a very sizable mass transfer resistance exists in the particle itself. Once a solute molecule reaches the opening of a pore at the particle surface, it must diffuse through the liquid, which fills a typically tortuous network of interconnected pores, until it reaches a vacant adsorption site, where it can attach itself to the solid surface. As adsorption proceeds, successive solute molecules must travel longer into the particle in order to find vacant sites. Thus, the process of reaching all the surface sites in a particle is a slow one. Two major resistances to mass transfer then should be considered: the external resistance in the liquid phase and the internal resistance in the solid phase (Cooney, 1998).

2.7.1 Adsorption kinetic models

The contact time experimental results can be used to study the rate-limiting step in the adsorption process. The overall adsorption process may be controlled either by one or more steps like film or external diffusion, pore diffusion, surface diffusion and adsorption on the pore surface or a combination of more than one step. In batch adsorption, the diffusive mass transfer can be related by an apparent diffusion coefficient, which will fit the experimental sorption data (Srivastava *et al*., 2006). Several adsorption kinetic models have been established to understand the adsorption kinetics and rate-limiting step. These include pseudo-first and second-order rate model, Weber and Morris sorption kinetic model, Adam–Bohart–Thomas relation, first-order reversible reaction model, external mass transfer model, first-order equation of Bhattacharya and Venkobachar, Elovich's model and Ritchie's equation (Febrianto *et al*., 2009). Kavitha and Namasivayam (2008) used four kinetic models which are pseudo-first order, pseudo-second order, Bangham and intra-particle diffusion models to fit the experimental data obtained from the adsorption of acid brilliant blue onto activated coir pith carbon in a batch system.

2.7.2 Lagergren pseudo-first order kinetics

The pseudo-first order rate expression of Lagergren model is generally expressed as (Lagergren, 1898):

$$\frac{dq_t}{dt} = k_{ad}(q_e - q_t) \tag{2.6}$$

where q_e and q_t are the amount of adsorbed waste (mg/g) at equilibrium and at any instant of time t (min), respectively, and k_{ad} is the rate constant of pseudo first order adsorption operation (min^{-1}). The integrated rate law after application of the initial condition of $q_t = 0$ at $t = 0$, becomes a linear equation as given by:

$$\log(q_e - q_t) = \log q_e - \frac{k_{ad}}{2.303}t \tag{2.7}$$

The plot of log ($q_e - q_t$) versus t gives a straight line for the pseudo first-order adsorption kinetics, from which the adsorption rate constant, k_{ad}, is estimated.

Pseudo first-order kinetic equation differs from a true first-order equation in two ways: (i) the parameter, k_{ad} ($q_e - q_t$) does not represent the number of available sites, and (ii) the parameter, log (q_e) is an adjustable parameter and often it is found that it is not equal to the intercept of the plot of log ($q_e - q_t$) versus t, whereas in a true first-order model the value of log q_e should be equal to the intercept. Hence, pseudo first-order kinetic model (equation (2.6)) is used for estimating k_{ad} alone, which is considered as mass transfer coefficient in the design calculations (Gupta and Babu, 2009).

2.7.3 Ho pseudo second-order kinetics

As pseudo first-order kinetic model gives only k_{ad} and as q_e cannot be estimated using this model, applicability of the pseudo second-order kinetics has to be tested for the estimation of q_e with the rate equation given by Ho (1995):

$$\frac{dq_t}{dt} = k_2(q_e - q_t)^2 \tag{2.8}$$

where k_2 is the equilibrium rate constant of pseudo second-order adsorption ($gmg^{-1}min^{-1}$). From the boundary conditions, $t = 0$ to t and $q_t = 0$ to q_t, the integrated form of the equation (2.8) is:

$$\frac{1}{(q_e - q_t)} = \frac{1}{q_e} + k_2 t \tag{2.9}$$

Equation (2.9) can be re-arranged to obtain a linear form as:

$$\frac{t}{q_t} = \frac{1}{k_2 q_e^2} + \frac{1}{q_e} t \tag{2.10}$$

The plot of t/q_t versus t should give a linear relationship which allows the computation of a second-order rate constant, k_2 and q_e. The pseudo-second order model is based on the assumption that the rate limiting step may be chemical adsorption involving valence forces through sharing or exchange of electrons between the adsorbent and adsorbate (Ho and Mckay, 2000).

2.7.4 Intraparticle diffusion model

The intraparticle diffusion model is based on the theory proposed by Weber and Morris (1963). The Weber and Morris equation is:

$$q_t = k_{id} \sqrt{t} + A \tag{2.11}$$

where q_t is the adsorption capacity (mg/g) at time t (min), k_{id} is the diffusion rate constant ($mg/gmin^{1/2}$) and A (mg/g) is a constant that gives an indication of the thickness of the boundary layer, i.e. the higher the value of A, the greater the boundary layer effect. In a rapidly stirred batch adsorption process, the particles experience high turbulence of the bulk fluid during the adsorption period, it is probably reasonable to assume that the rate is not limited by mass transfer from the bulk liquid to the particle external surface. One might then postulate that the rate limiting step is intra-particle diffusion, and if this is the case a rate constant can be found from a plot of q_t against $t^{1/2}$ (Weber-Morris plot). If the postulated mechanism

is correct, then a linear plot passing through the origin is obtained. Additionally, the value of the rate constant for diffusion is obtained from the slope of the line. However, if the data exhibit multi-linear plots, then two or more steps influence the sorption process. In general, a mass transfer process is diffusion controlled if its rate is dependent upon the rate at which components diffuse towards one another. The intra-particle diffusion model has been applied in three different forms:

(i) The amount of adsorption at any time, q_t is plotted against $t^{1/2}$ to get a straight line that is forced to pass through the origin. This means that A is equal to zero which implies that the rate is not limited by mass transfer across the boundary layer. This occurs when a system is agitated and mixed to a sufficient extent (high turbulence);

(ii) multi-linearity in q_t versus $t^{1/2}$ plot is considered (that is, two or three steps are involved). In this form, the external surface adsorption or instantaneous adsorption occurs in the first step; the second step is the gradual adsorption step, where intra-particle diffusion is controlling; and the third step is the final equilibrium step, where the solute moves slowly from larger pores to micropores causing a slow adsorption rate. The time required for the second step usually depends on the variations of the system parameters such as solute concentration, temperature, and adsorbent particle size;

(iii) q_t is plotted against $t^{1/2}$ to obtain a straight line but does not necessarily pass through the origin; that is, there is an intercept (Wu *et al*., 2009). This implies that the rate is limited by mass transfer across the boundary layer. This occurs in a slowly stirred batch adsorption process.

2.8 Column adsorption

In the dynamic adsorption studies, the adsorbent is loaded in columns which form a bed through which the aqueous solution of the adsorbate is passed. During its passage through the bed, the solution continuously meets a fresh part of the adsorbent

and tends to establish a new equilibrium. However, as the time of contact with a given part of the adsorbent is limited, a true equilibrium is never attained. As the solution is passed continuously, the adsorption zone moves downwards, and at a certain time, t_B, the adsorption zone has just reached the bottom of the bed and concentration has suddenly risen to an appreciable value for the first time. In practice, system operation is interrupted when the effluent concentration reaches a certain level, called breakthrough concentration, above which it is not profitable to continue the operation (Gonzalo *et al*., 2006). Breakthrough time, t_b, is defined as the time it takes for the effluent concentration to reach the maximum allowable discharge limit.

When calculating the characteristic parameters of the system, the maximum allowable discharge limit is considered as the breakthrough concentration (Bhakat *et al*., 2007). The solute concentration in the effluent now rises rapidly as the adsorption zone passes through the bottom of the bed until it eventually reaches the initial concentration ($C_t/C_o = 1$). In the latter stages ($C_t/C_o \geq 0.9$) little or no adsorption takes place since the bed is for all practical purposes entirely in equilibrium with the feed solution. The shape and time of appearance of the breakthrough curve greatly influence the method of operating a fixed bed adsorbent. The curves generally have an S-shape, but they may be steep or relatively flat and in some cases considerably distorted (Attia *et al*., 2008).

2.9 Trends in adsorption studies

A vast amount of work on the use of low cost adsorbents for wastewater treatment has been reported by several researchers. However, the general observation is that most of the authors dealt with the adsorption of single-component aqueous solutions in batch systems. Conclusions drawn from such studies may not necessarily be valid when applying adsorption to a mixed/multi-component effluent system such as that containing a mixture of phenol, Ni^{2+}, Co^{2+}, Fe^{2+} and Pb^{2+} or the one containing a mixture of red dyes. In most practical adsorption processes, there is more than one

component to be adsorbed. Although sorption capacity parameters obtained from batch processes are useful in providing information about effectiveness of the adsorbate-adsorbent system, the data is not applicable to most treatment systems. Hence, for a sound engineering design of water treatment plants, both batch and column adsorption data is required.

Also, there has been limited research on the effects of initial metal ion concentration on phenol sorption and vice versa. Even less is known about the adsorption kinetics of multi-heavy metal ions and phenol by sawdust and coal fly ash. Knowledge on this subject could be useful in designing wastewater treatment systems using low cost adsorbent materials. On the other hand, most researchers study adsorption processes by changing one factor maintaining others constant (one-factor-at-a-time method). However, this method is extremely time consuming and expensive for a large number of process variables. Further, the one-factor-at-a-time technique does not include interactive effects among the variables and, eventually, it does not depict the complete effects of the parameters on the process.

The purpose of this study is to cover some of the gaps that exist in literature with regards to the use of low cost adsorbents. Thus, in this work, co-adsorption of Co^{2+}, Ni^{2+}, Fe^{2+}, Pb^{2+} and phenol from petrochemical wastewater using low cost adsorbents was investigated. Then the rate kinetics and equilibrium parameters were determined to understand the mechanism of adsorption. In addition, the co-adsorption of direct dyes from synthetic textile wastewater using coal fly ash and sugarcane bagasse was studied. Further, response surface methodology was used to assess the interactive effects of process parameters such as adsorbent dose, solution pH and initial concentration on the adsorption capacity of the low cost adsorbents. Also, the effects of bed depth, initial concentration and aspect ratio on breakthrough in fixed bed adsorption studies were explored. Similarly, the performance of the commercial activated carbon was tested for comparison purposes. It was also necessary to test the feasibility criteria, i.e, the most preferred adsorption isotherm. The present work

focuses on the use of South African low-cost adsorbents prepared from sawdust, sugarcane bagasse and coal fly ash to remove non-biodegradable toxic wastes from wastewater.

CHAPTER 3

3 Materials and methods

After a comprehensive literature review on the tertiary/advanced techniques used for wastewater purification, a final choice on the materials and experimental methods to be used was made. All the low cost adsorbents and commercial activated carbon were properly characterized and used in adsorption studies, both batch and column tests were carried out using synthetic wastewater. The wastewater selected in this study contains some recalcitrant contaminants. However, for practical reasons, it is impossible to synthesize wastewater containing all the relevant contaminants found in real wastewater. Therefore, the strategy proposed in this work was to select a representative subset of non-biodegradable wastes, i.e, for petrochemical wastewater; phenol (an organic compound) and four different heavy metal ions commonly found in real petrochemical wastewater were selected.

As for textile wastewater, three different recalcitrant dyes commonly found in real textile wastewater were chosen. Further, application of statistical experimental design provided a way to systematically and simultaneously alter a set of variables, thus ensuring that the whole experimental domain is covered. It was an efficient strategy of reducing the number of experiments when many factors were considered at the same time. When deriving response surface model equations for predicting the adsorption capacities, the factors considered were initial concentration, pH and adsorbent dose.

3.1 Materials

The low cost adsorbents used in this study were derived from pine sawdust, sugarcane bagasse and coal fly ash. These wastes were selected because of their availability and desirable physical characteristics. Citric acid monohydrate ($C_6H_8O_7{\cdot}H_2O$) was used to modify the surfaces of sawdust. In addition, nitrogen gas (N_2) supplied by African Oxygen Limited (South Africa) was used during the

preparation of activated carbon from sawdust. Additionally, all aqueous solutions were prepared in distilled water. Solutions containing Co(II), Ni(II), Fe(II), Pb(II) and phenol were prepared using analytical grade $Co(NO_3)_2 \cdot 6H_2O$, $NiSO_4 \cdot 6H_2O$, $FeSO_4 \cdot 7H_2O$, $Pb(NO_3)_2$ and C_6H_5OH, respectively, supplied by Merck Chemical Company (South Africa). Dilute HCl and NaOH were used for pH adjustments. Additionally, solutions containing direct red 23 (DR23), direct red 80 (DR 80) and direct red 81 (DR 81) were prepared using $C_{35}H_{28}N_7NaO_{10}S_2$ (30 % dye content), $C_{45}H_{26}N_{10}Na_6O_{21}S_6$ (25 % dye content) and $C_{29}H_{19}N_5Na_2O_8S_2$ (50 % dye content), respectively. These dyes were obtained from Sigma Aldrich (South Africa).

3.2 Equipment

An oven (EcoTherm) was used for drying purposes and for heating samples up to a maximum temperature of 250 °C, however, when higher temperatures were required, a muffle furnace (BRF 16/5-2416, Elite) was used. Preparation of the activated carbon from sawdust was done using a fluidized bed reactor (FBR) and a calibrated peristaltic pump (Vera Varistaltic pump plus, Manostat) was used to control water flow into the reactor. Also, a calibrated peristaltic pump (PERCOM-I, WATSON MARLOW) was used to supply the wastewater feed into the adsorption column. Further, the X-ray diffractometer (PANalytical, Philips PW 1710), Fourier Transform Infrared (Bruker, Tensor 27 TPR) system, Scanning Electron Microscope (SEM) (Jeol, JSM-840) and Micrometrics (TriStar 3000) Surface Area and Porosity Analyzer were used to characterize all the adsorbents used in this work. The pH measurements were done using a pH meter (LabX Direct-SevenMulti, Mettler Toledo). Furthermore, an incubator with a shaking platform (FSIM-SPO16, Labcon) was used to agitate the adsorbates-adsorbent mixtures during batch adsorption experiments. The concentrations of phenol and the direct red dyes were determined using the UV-VIS Double Beam Spectrophotometer (SQ-4802 UNICO) and all the changes in metal ion concentration were measured using the Atomic Absorption Spectrometer (SpectroAA 55 B, Varian).

3.3 Preparation and characterization of adsorbents

Sawdust was used as a raw material for the sawdust modified with citric acid sample (SD500) and steam activated sawdust sample (SAS). However, only one adsorbent was derived from sugarcane bagasse through heat treatment. Conversely, coal fly ash was used as such without any chemical or heat treatment. The commercial activated carbon used for comparison in this study was peat based Norit RO 0.8. Characterization of the adsorbents included the determination of phases, functional groups, surface morphology, specific surface area and pore structural parameters.

It is known that particle size affects the performance of an adsorbent, hence, for proper comparison; the particle size range was expected to be the same for the tested adsorbents. Thus, a particle size range of 53-180 µm was selected for all the adsorbents. This size was chosen due to the fact that most of the particles of the coal fly ash procured from Lethabo thermal power station were in the range 53-180 µm. Therefore, all the other adsorbents were crushed and screened to the same particle size range.

3.3.1 Sawdust modified with citric acid

Pine sawdust collected from a local timber company was ground and sieved to a particle size range of 53-180 µm using standard sieves. It was then placed in stainless steel trays and dried in an oven at 50°C for 24 h. A mass of 100 g was placed in a 1 L glass beaker and 660 mL of 0.6 M citric acid solution was added. The mixture was stirred using impellers for 30 min, and then separated by vacuum filtration. The wet sawdust was then spread in stainless steel trays and dried in an oven at 50°C for 24 h, after which, the temperature was raised to 120°C and maintained for 90 min. The sawdust was allowed to cool and washed five times using hot distilled water (60-80°C) and then dried at 50°C for 24 h (Wafwoyo *et al*., 1999). After that, the sawdust sample was split into three portions.

One portion was heated at 250°C for 1 h (SD250) in a muffle furnace, the second portion was heated at 400°C for 1 h (SD400) and the third portion was heated at 500°C for 1 h (SD500). Then, all the carbonized sawdust samples (SD250, SD400 and SD500) were tested for their performance in preliminary experiments using synthetic petrochemical wastewater and the best adsorbent (SD500) was chosen for further experiments. The highest carbonization temperature of 500°C was chosen on the basis of preliminary carbonization experiments which showed that sawdust was completely ashed at 600°C for 1 h. No leaching experiments were carried out to check for the presence of toxic soluble leachate which could possibly emanate from pine sawdust especially when its source (pine tree) has been previously treated with pesticides.

3.3.2 Steam activated sawdust (SAS)

The sawdust was repeatedly washed with distilled water in order to remove dust and other inorganic impurities and then oven dried at 120°C for 24 h to reduce the moisture content. It was pulverized and sieved to a particle size range of 53-180 µm. The activated carbon preparation experiments were conducted in two stages; the first stage was carbonization of the sawdust under nitrogen flow followed by activation with water vapour (steam). Carbonization of the raw material (sawdust) was done in a stainless steel fluidized bed reactor (FBR) which was installed inside a vertical electrically-heated furnace (Figure 3.1). A thermocouple was used to measure the temperature inside the reactor.

For the carbonization step, 150 g of sawdust was fed into the fluidized bed reactor which was preheated to 600°C and purged with nitrogen gas at a flow rate of 8 L/min. The sample was subjected to carbonization at 600°C for 1 h. After that, the resulting char was removed from the reactor and allowed to cool in a dessicator. The percentage burn-off, P_b of the resulting carbonized char was found to be 76.9%. The reactor temperature was then increased to 800°C under nitrogen flow, at this temperature; water was pumped into the reactor using a peristaltic pump to give a

steam flow rate of 5.41 g/min. The carbonized sawdust was fed into the reactor and activated at 800°C for 1 h. During carbonization and activation experiments, the volatile by-products were absorbed in acetone and some were evacuated by an extractor hood. Finally, the activated carbon was kept in a dessicator for further adsorption tests using synthetic petrochemical wastewater and this sample was designated as SAS (steam activated sawdust). The percentage burn-off of SAS was found to be 86.5%.

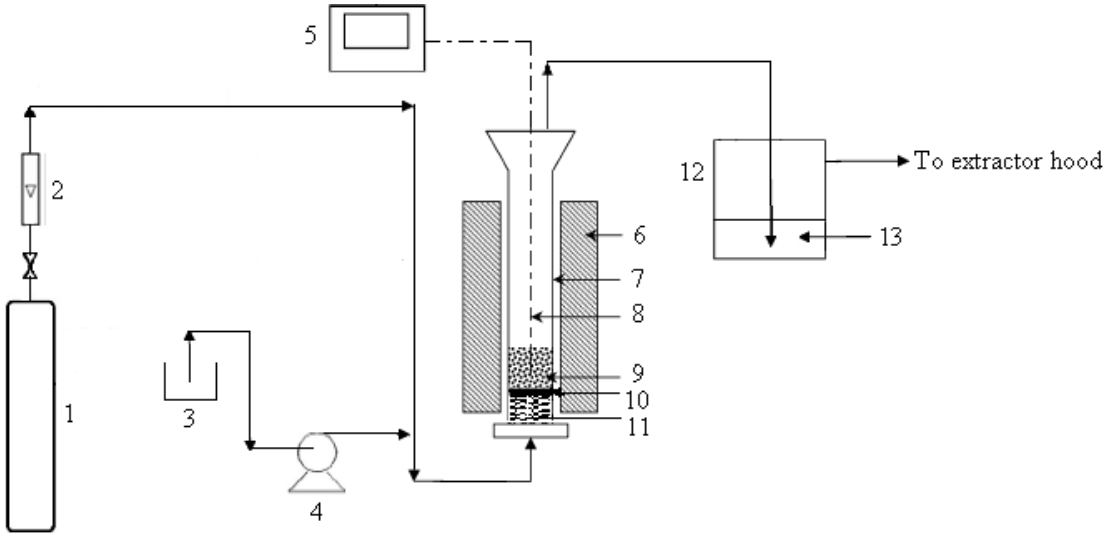

Figure 3.1. Schematic diagram of the experimental set up for activated carbon preparation: (1) N_2 gas cylinder; (2) Rotameter; (3) Beaker with distilled water; (4) Peristaltic pump; (5) Temperature controller; (6) Electric furnace; (7) Fluidized Bed Reactor; (8) Thermocouple; (9) Sawdust sample; (10) Stainless steel screen; (11) Ceramic beads; (12) Tank (liquid by-product collector); (13) Acetone.

3.3.3 Sugarcane bagasse (SB400)

Sugarcane bagasse collected from Tshikunda in Thohoyandou (South Africa) was washed several times with distilled water to remove the water soluble impurities and surface adhered particles. After that, it was dried at 50°C for 24 h in an oven to get rid of the moisture and other volatile impurities. Furthermore, the bagasse was

ground and sieved to a particle size range of 53 – 180 μm. The bagasse particles were placed in a stainless steel box with cover and heated for 1 h in a muffle furnace at 400°C and this carbonized bagasse sample was designated as SB400 (sugarcane bagasse carbonized at 400°C) which was then stored in a dessicator for further experiments using synthetic textile wastewater only. A carbonization temperature of 400°C was chosen on the basis of preliminary experiments which showed that a greater amount of sugarcane bagasse was ashed at a temperature of 500°C for 1 h, thus a slightly lower temperature had to be selected to avoid sample ashing. No activation experiments were carried out on the carbonized bagasse.

3.3.4 Coal fly ash (CFA)

The fly ash produced from the burning of pulverized coal in a coal-fired boiler is a fine-grained, powdery particulate material that is carried off in the flue gas and usually collected from the flue gas by means of electrostatic precipitators, baghouses, or mechanical collection devices such as cyclones. Coal fly ash used in this study was obtained from Lethabo power station situated in Viljoensdrift (South Africa). The raw coal fly ash was sieved to a particle size range of 53 to 180 μm and used as such without any pretreatment. This sample was designated as CFA (coal fly ash) which was then stored in a dessicator for further experiments using both synthetic textile and petrochemical wastewater.

3.3.5 Commercial activated carbon (CAC)

Extruded activated carbon pellets (Norit RO 0.8) obtained from Norit activated carbon company (USA) was used in this work for comparison purposes. Norit RO 0.8 is an acid washed extruded carbon which is made from peat by the conventional process of steam activation to produce a uniform product. According to the company, this type of activated carbon is suitable for a wide range of applications in the food, chemical and bulk pharmaceutical industries. Norit RO 0.8 (particle size range 53 to 180 μm) has a particle shape, which gives an extremely low hydrodynamic pressure drop in liquid phase applications and it is designated as CAC

(commercial activated carbon) in the present study. This sample was used to treat synthetic petrochemical wastewater and the results were compared with those for the low cost adsorbents.

3.3.6 Characterization of adsorbents

The X-ray diffraction spectra for SD500, SAS, SB400, CFA and CAC were obtained using an X-ray diffractometer with Cu Kα radiation at 40 kV and 50 mA to determine the phases present (armophous or crystalline). The spectra were recorded from 10 to 65° at a scan rate of 1.2°min^{-1}. Fourier Transform Infrared (FT-IR) spectra of the adsorbents were recorded in the range 500 – 4000 cm^{-1} on an FT-IR system to explore the number and positions of the functional groups available for the binding of adsorbates. The surface morphology of the adsorbents was visualized via a Scanning Electron Microscope (SEM) operated at the accelerating voltage of 20 keV.

The Brunauer-Emmett-Teller (BET) surface area (S_{BET}) and pore structural parameters of the adsorbents were determined from the adsorption-desorption isotherm of nitrogen at 77 K using the Micrometrics (TriStar 3000) Surface Area and Porosity Analyzer. All the samples were de-gassed at 200°C for 4 h, prior to adsorption-desorption experiments. The BET surface area was calculated by the Brunauer-Emmett-Teller (BET) equation, micropore volume (V_{mi}) and micropore specific area (S_{mi}) area were obtained using the *t*-plot. The total pore volume (V_t) was obtained by converting the nitrogen adsorption amount at a relative pressure (P/P_o) of 0.98 to the liquid nitrogen volume. The mesopore volume (V_{me}) was calculated by subtracting V_{mi} from V_t (Zhu *et al*., 2007). The burn-off weight percentage, P_b for SAS was determined and it measures the degree of activation process. It is defined as the ratio of percentage weight loss of the material during preparation to the original weight of the raw material. It is mathematically expressed as (Kumar *et al*., 2006):

$$P_b = \frac{W_0 - W_f}{W_0} \times 100 \qquad (3.1)$$

where W_o is the initial weight of the raw material (g) and W_f is the final weight of product (g).

3.4 Synthetic wastewater preparation

3.4.1 Petrochemical wastewater

Stock solutions (1000 mg/l) of Co(II), Ni(II), Fe(II), Pb(II) and phenol were prepared by dissolving 4.94, 4.48, 4.98, 1.60 and 1.00 g of $Co(NO_3)_2 \cdot 6H_2O$, $NiSO_4 \cdot 6H_2O$, $FeSO_4 \cdot 7H_2O$, $Pb(NO_3)_2$ and C_6H_5OH, respectively in 1 L of distilled water. The stock solutions were diluted with distilled water to obtain the desired initial concentrations. The composition of the synthetic aqueous solutions used in this study were based on literature data (Patel and Madamwar, 2002) and concentrations fall within the range of the typical petrochemical wastewater described in the Pollution Prevention and Abatement Handbook (1998) which specifies that phenol concentration range is (20-200 mg/l) and that for heavy metals is (0.1-100 mg/l). The pH of the solutions was adjusted using either 0.1 M HCl or 0.1 M NaOH. A maximum pH level of 6 which is below the pH point of precipitation (pH_{ppt}) for each of the metal ions was chosen to prevent possible metal hydroxide precipitation (Al-Degs *et al*., 2006; Habib-ur-Rehman *et al*., 2006).

3.4.2 Textile wastewater

Stock solutions of direct red 23 (DR 23), direct red 80 (DR 80) and direct red 81 (DR 81) were prepared (1000 mg/l) by dissolving 3.33, 4.00 and 2.00 g of $C_{35}H_{28}N_7NaO_{10}S_2$ (30% dye content), $C_{45}H_{26}N_{10}Na_6O_{21}S_6$ (25% dye content) and $C_{29}H_{19}N_5Na_2O_8S_2$ (50% dye content), respectively in 1 L of distilled water. The stock solutions were diluted with distilled water to obtain the desired initial concentrations. Dye solutions were prepared using distilled water to prevent and minimize possible interferences in this study although in actual cases, the textile wastewater will have a different ionic strength and organics present (Arami *et al*., 2006). The chemical structures of the dyes are shown in Schema 3.1. These azo dyes

were selected in this study due to the fact that they are among the most widely used synthetic dyes and normally become major pollutants in textile wastewaters. This can be attributed to the stability of their molecular structures which render them resistant to biological or even chemical degradation (Mahmoodi *et al*., 2005).

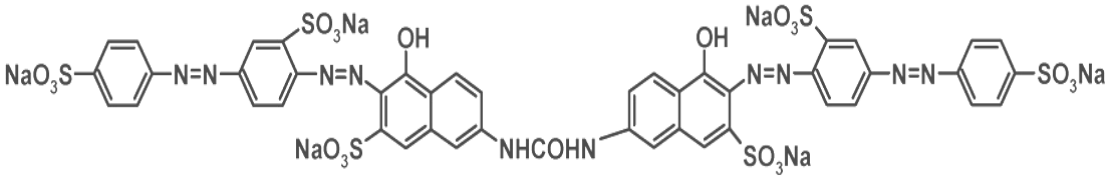

(a)

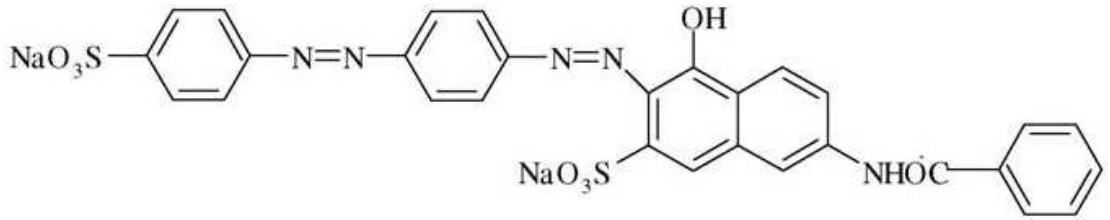

(b)

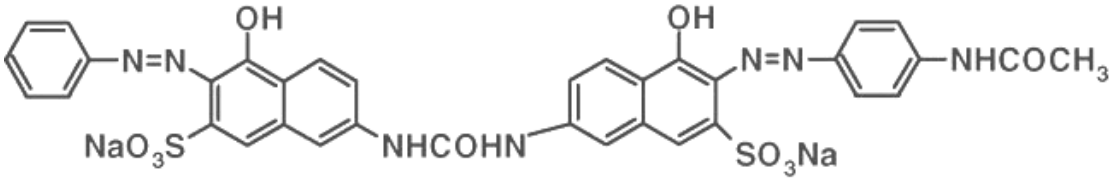

(c)

Schema 3.1. Chemical structure of (a) direct red 80, (b) direct red 81, (c) direct red 23

3.5 Batch adsorption experiments

Batch adsorption experiments were conducted in order to determine the optimum adsorbent mass and equilibrium time, to generate adsorption kinetics data, adsorption isotherm data and the data used to derive response surface model equations. Blank

solutions (solution without the adsorbent) were also included to check if there was any adsorption on the surface of the conical flask. Before the beginning of an adsorption experiment, the initial concentrations of all the adsorbates were determined. After equilibrium, the supernatant was separated by filtration. Final concentrations of the adsorbates were determined and the adsorption capacity, q_e, was calculated as:

$$q_e = \frac{(C_o - C_e)V}{m} \tag{3.2}$$

where C_o and C_e are the initial and equilibrium adsorbate concentrations in solution (mg/l), respectively, V is a known volume of synthetic wastewater (l), and m is a known mass of dry adsorbent (g).

3.5.1 Optimum adsorbent mass

The optimum masses for treating synthetic petrochemical wastewater using SD500, CFA, SAS and CAC were determined by varying the adsorbent mass from 0.2 to 6 g under the selected contact time (48 h) using wastewater made up of 50 mg/l heavy metal ions and 110 mg/l phenol at pH 4.0 which is the zero level composition (Table 3.1). The agitation speed (250 rpm) and temperature (25°C) were selected for the experiment. The same procedure was repeated using CFA and SB400 on synthetic textile wastewater made up of direct dyes at pH 6.0. All the percentage removals, P_r were computed by:

$$P_r = \frac{(C_0 - C_t)}{C_0} \times 100 \tag{3.3}$$

3.5.2 Equilibrium study

The equilibrium adsorption isotherm data was generated by contacting a fixed predetermined optimum mass of adsorbent (SD500, SAS, CFA and CAC) with 100 ml of synthetic petrochemical wastewater with the concentration of metal ions and phenol ranging from 20 to 90 mg/l at pH 4.0 in 250 ml Elernmeyer flasks. The

flasks were agitated at 250 rpm in an incubator with shaking platform at 25°C for a predetermined contact time. At the end of the experiment, the residual concentrations of the metal ions and phenol were measured. The equilibrium adsorption capacities, q_e, values were calculated using equation (3.2) and the results were fitted to the common adsorption isotherms. The same procedure was repeated using 4 g of CFA and also SB400 on synthetic textile wastewater made up of DR23, DR80 and DR81 with the initial concentration range of 5 - 100 mg/l at pH 6.0.

3.5.3 Kinetic study

For kinetic studies, a predetermined optimum mass of adsorbent was contacted with 100 ml of petrochemical wastewater consisting of 50 mg/l heavy metal ions and 110 mg/l phenol at pH 4.0 and shaken at 250 rpm at 25°C. At predetermined intervals of time, small quantities (0.5 ml) of solutions were withdrawn and analyzed for the final concentration. The percentage removals were computed using equation (3.3) and the adsorption capacity at time t, q_t (mg/g), was calculated as:

$$q_t = \frac{(C_0 - C_t)V}{m} \tag{3.4}$$

where C_t (mg/l) is the residual concentration at time t. In another experiment, 4 g of CFA was contacted with 100 ml of textile wastewater consisting of 50 mg/l of direct red dyes at pH 6.0 and shaken at 250 rpm. Samples were withdrawn and analyzed for the final concentration at predetermined time intervals and the percentage removals were calculated. The same procedure was repeated using 4 g of SB400.

3.5.4 Experimental design

The best agricultural adsorbent (SAS) and an industrial by-product (CFA) were tested on synthetic petrochemical wastewater. The adsorbent dose, pH and initial concentration were chosen as independent variables and the adsorption capacity, q_e, as the dependent output response variable. A 2^3 full-factorial design with four centre points leading to 12 experimental runs was performed. The center point replicates

were chosen to verify any change in the estimation procedure, as a measure of precision property (Ravikumar *et al.*, 2007). For statistical calculations, the variable X_i was coded as x_i according to the following relationship:

$$x_i = \frac{X_i - X_0}{\Delta X} \tag{3.5}$$

where x_i is the independent variable coded value; X_i, independent variable real value; X_o, independent variable real value on the centre point; and ΔX, step change value (Elibol, 2002). The range and the levels of the variables (low and high) investigated in this work are given in Tables 3.1 for CFA and SAS.

Table 3.1

The experimental range and levels of the independent variables for CFA and SAS

Factor	Symbols		Range and levels					
	Actual	Coded	CFA			SAS		
			-1	0	1	-1	0	1
Dose (g/l)	X_1	x_1	20	40	60	10	20	30
pH	X_2	x_2	2	4	6	2	4	6
$[\text{heavy metal}]_o$ (mg/l)	X_3	x_3	25	50	75	25	50	75
$[\text{Phenol}]_o$ (mg/l)	X_3	x_3	55	110	165	55	110	165

The quadratic model for predicting the adsorption capacities was expressed according to equation (3.6):

$$y = \beta_o + \beta_1 x_1 + \beta_2 x_2 + \beta_3 x_3 + \beta_{11} x_1^2 + \beta_{22} x_2^2 + \beta_{33} x_3^2 + \beta_{12} x_1 x_2 + \beta_{13} x_1 x_3 + \beta_{23} x_2 x_3 \tag{3.6}$$

where y is the response predicted by the model whilst x_1, x_2, x_3 are the coded forms of dose, pH and initial concentration, respectively. The term β_o is the offset term, β_1, β_2 and β_3 are linear terms, β_{11}, β_{22} and β_{33} are the quadratic terms whilst β_{12}, β_{13} and β_{23} are the interaction terms (Bhatia *et al*., 2009). The analysis of variance (ANOVA) for quadratic model was carried out to establish its statistical significance at 5% level of

significance (95% confidence level). Design Expert Version 6.0.6 (Stat Ease, Inc., Minneapolis, USA) and Matlab Version 7.0.1 softwares were used for regression and graphical analysis of the data obtained. The statistical significance of the regression coefficients was determined by the Student's *t*-test and *p*-values.

3.6 Column dynamics

Batch adsorption studies only may not be directly applied for field applications in the treatment of wastewater. Thus, batch equilibrium and kinetic tests are often complemented by dynamic column studies to determine system size requirements, contact time, etc, and these parameters can be obtained from the breakthrough curves. Therefore, fixed bed column experiments were conducted at room temperature using a laboratory scale pyrex glass column of 2.5 cm internal diameter and 45 cm length (Figure 3.2). Experiments were carried out in a down flow mode which ensures that the bed remains packed and steady during the entire operation, thereby resulting in

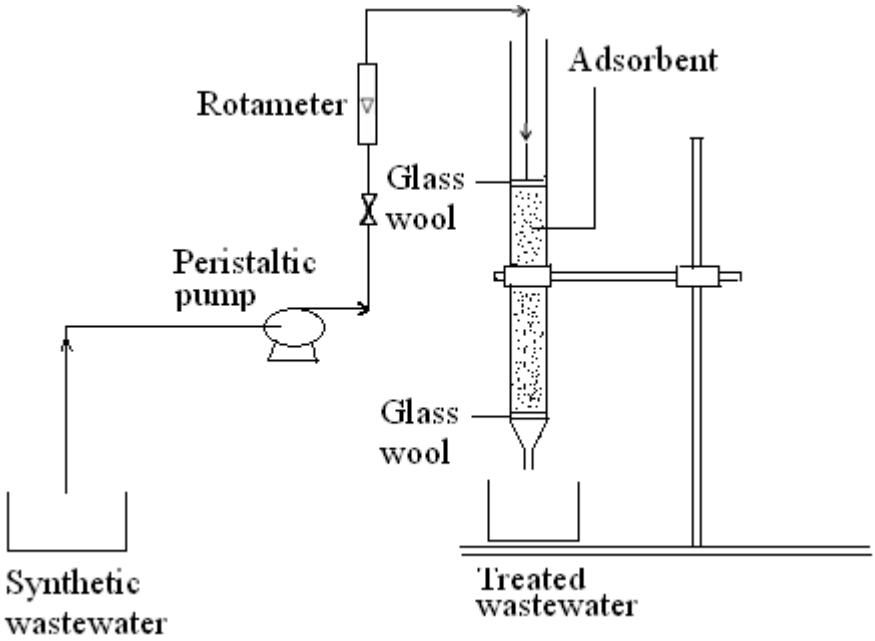

Figure 3.2. Schematic diagram of the experimental set up for a laboratory scale adsorption column used for fixed bed studies.

maximum contact between the adsorbent and the adsorbates in the influent wastewater. The column was packed with a known quantity of SD500 to obtain a particular bed depth (10 cm). A glass wool plug was provided at the bottom to support the SD500 bed and another glass wool plug was also provided on top of the bed to prevent floating up of the adsorbent particles.The presence of air pockets within the packed SD500 column would cause channeling of the influent wastewater and lower the adsorption efficiency of the bed (Ko *et al*., 2000). Thus, to ensure expulsions of the trapped air, the SD500 packed column was fully wetted by filling with distilled water for 5 h prior to starting of the experiments.

In each and every experimental run, influent wastewater feed at a particular volumetric flow rate (Q_w), pH and initial concentration as shown in Table 3.2 was supplied and maintained throughout the experiment by use of a calibrated peristaltic pump (PERCOM-I, WATSON MARLOW). The concentrations given in Table 3.2 fall within the range of typical petrochemical wastewater specified in the Pollution Prevention and Abatement Handbook (1998). A rotameter was incorporated in the feed line of the column to monitor the flow rate. Furthermore, the flow rate was cross checked at the exit of the column at regular intervals of 30 min by physically collecting samples of solution for a given time to prevent and minimize the flow rate fluctuations (Kumar and Chakraborty, 2009). The effluent samples were collected periodically and analyzed. Run 4 (Table 3.2) was repeated using 16.36 and 24.54 g of SD500 which corresponded to a bed depth of 20 and 30 cm, respectively. Further column tests were carried out with SAS (8.06 g) and also CAC (52.79 g) using wastewater of composition and conditions specified for Run 4 at 10 cm bed depth. All the column experiments were carried out to investigate the effects of bed depth, initial concentration and aspect ratio (Z/D) on the performance of the adsorbents under study.

Table 3.2

Wastewater composition and conditions for different experimental runs

Run no.	Conditions		Composition and initial concentration (mg/l)				
	pH	Q_w (ml/min)	Co^{2+}	Ni^{2+}	Pb^{2+}	Fe^{2+}	Phenol
1	2.6	5.0	25.0	25.0	25.0	25.0	180.0
2	2.6	5.0	50.0	50.0	50.0	50.0	180.0
3	2.6	5.0	50.0	50.0	50.0	50.0	90.0
4	2.6	5.0	90.0	90.0	90.0	90.0	90.0

3.7 Quantitative chemical analysis

The initial and final phenol concentrations for all the samples were measured by means of the UV-VIS Double Beam Spectrophotometer at a predetermined maximum wavelength, λ_{max} of 269.0 nm using the quartz cuvettes. The λ_{max} of 269.0 nm was initially determined by performing scanning spectrophotometry on the phenol standard solution with highest concentration. The phenol calibration curves (absorbance versus concentration) showed linear working ranges for all the phenol standards prepared. The same UV-VIS was used for the quantitative analysis of direct red 23, direct red 80 and direct red 81 at predetermined λ_{max} of 542.5, 559.0 and 534.0 nm, respectively. On the other hand, all heavy metal ion concentration changes were determined using the Atomic Absorption Spectrometer (AAS) with an air/acetylene flame. Standard solutions (20, 40, 60, 80 and 100 mg/l) of each metal ion were used to calibrate the AAS before analysis.

CHAPTER 4

4 Results and discussion

The performance of the studied adsorbents was compared and an attempt was made to link the physicochemical characteristics of the adsorbents to their performance. Additionally, adsorption results for the removal of direct red dyes from synthetic textile wastewater using CFA and SB400 were presented and fitted to the commonly used adsorption isotherm models. Similarly, results for the removal of heavy metals and phenol using SD500, CFA, SAS and CAC were given and explained in detail. As a result, the theoretical maximum monolayer adsorption capacity, q_{max}, values for all the adsorbents were calculated from the Langmuir isotherm model. Cobalt was selected to illustrate adsorption kinetic modeling for SD500, CFA, SAS and CAC. On the other hand, the CFA and SAS results for petrochemical wastewater treatment were analyzed using response surface methodology. Consequently, response surface model equations were developed and validated. Also, the adsorption behaviour of the SD500-column was studied in the treatment of petrochemical wastewater and column performance of SD500, SAS and CAC were compared.

4.1 Characterization of the adsorbents

4.1.1 Sawdust modified with citric acid (SD500)

Since adsorption is a surface phenomenon, the rate and extent of adsorption are functions of the specific surface area of the adsorbent used, i.e., the portion of the total surface area that is available for adsorption. In fact, the amount of adsorption per unit weight of an adsorbent depends on its composition, texture and porosity (Sarkar and Acharya, 2006). X-ray diffraction technique is a powerful tool to analyze the crystalline nature of the materials. If the material under investigation is crystalline, well-defined peaks are observed while non-crystalline or amorphous systems show a hollow instead of well-defined peak (Namasivana and Kavitha, 2006). The X-ray diffraction pattern of SD500 presented in Figure 4.1 shows two

very broad diffraction peaks. The absence of a sharp peak shows that the major part of SD500 is amorphous, which is an advantageous property for a good adsorbent (Madhava *et al*., 2008). The only two broad peaks at around 24.4 and 42.3° could be attributed to the presence of carbon and graphite (Bouchelta *et al*., 2008). The X-ray diffraction pattern of sawdust is very much similar to that of highly mesoporous spherical activated carbons reported by Zhu *et al*. (2007).

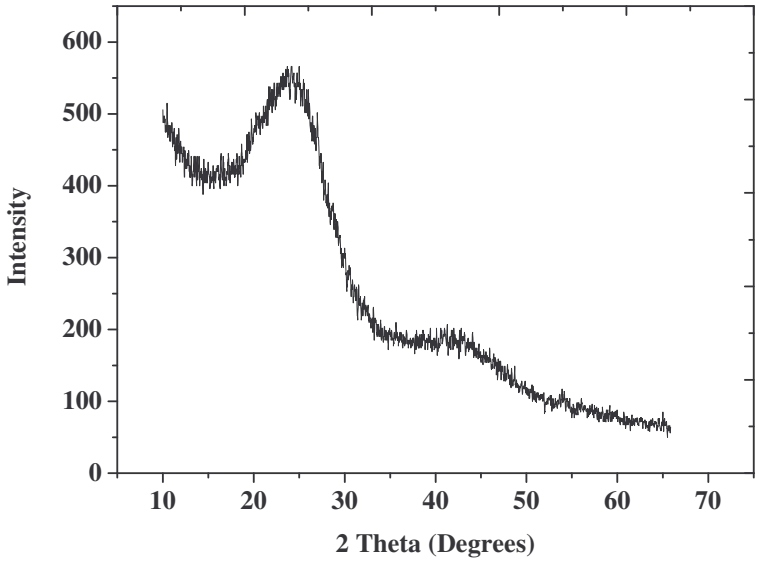

Figure 4.1. The X-ray diffraction profile (diffractogram) of SD500

The FT-IR spectra of SD500 before and after sorption of heavy metals and phenol were plotted to determine the vibration frequency changes in the functional groups of the adsorbent. The functional group is one of the keys to understand the mechanism of adsorbate binding on the adsorbent. The spectra shown in Figure 4.2 display a number of absorption peaks, indicating the complex nature of the surfaces of SD500. Table 4.1 presents the fundamental peaks of SD500 before and after use. The spectra with labeled peaks are shown in Figure A1 and A2 (Appendix). Assignment of absorption bands shows that the functional groups: alcohol, phenol, carboxylic acid, ketone, ester, lactone, ether, alkyne and aromatic are present in SD500 before

adsorption. The presence of cellulose, hemicelluloses and lignin is probably responsible for the appearance of these bands. Agricultural biomasses mainly consist of lignin, cellulose, hemicelluloses and some proteins which make them effective adsorbents for heavy metal cations (Garg *et al*., 2008).

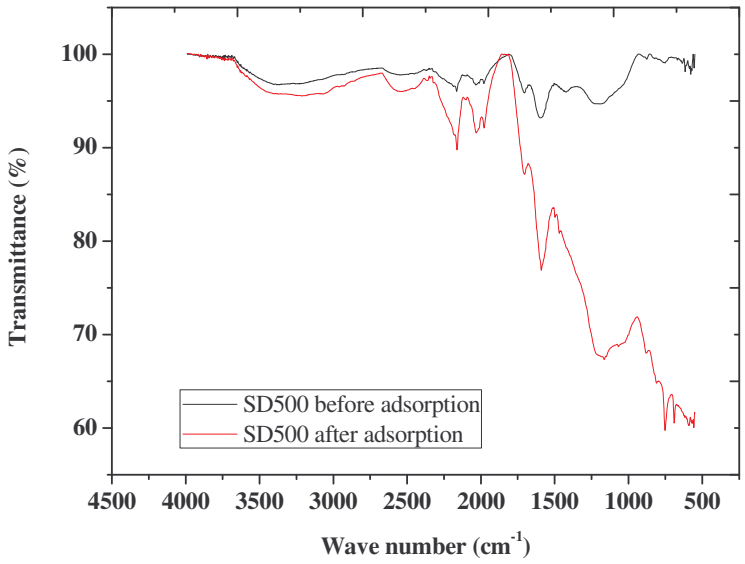

Figure 4.2. FT-IR spectra of SD500 before and after adsorption of heavy metals and phenol.

The peak at 3381.2 cm^{-1} before adsorption can be attributed to the hydrogen-bonded OH group of alcohols and phenols (Yang and Lua, 2003; Puziy *et al*., 2003) and it shifted to 3217.2 cm^{-1} after adsorption. Additionally, the peak (1184.3 cm^{-1}) for C—O stretching vibrations in SD500 before adsorption shifted to 1163.1 cm^{-1} after adsorption. These major shifts in band suggest that the alcohols/phenols and carboxylic acid groups were involved in metal binding. Assessing the nature of adsorption exclusively by the presence of specific functional groups is rather complex. However, previous researchers (Meena *et al*., 2008; Yasemin and Zeki, 2007) reported that the H^+ ions in the —OH and —COOH groups on sawdust particles can be exchanged for cations in solution. Therefore, it may be supposed that

ion exchange was the principal mechanism for the removal of heavy metal ions from petrochemical wastewater. Nevertheless, the sites responsible for the adsorption process might not be exclusively due to the —OH and —COOH groups, other sites on the adsorbent can also contribute to the adsorption process and even physical adsorption is also probable.

Table 4.1

Interpretation of FT-IR spectra for SD500 before and after adsorption

σ (cm^{-1})		Possible assignment and comments
Before	After	
3381.2	3217.2	(O—H) Stretching in hydroxyl groups in alcohols and phenols
2540.2	2542.1	(O—H) Stretching in carboxylic acids
2164.1	2164.1	(C Ξ C) Stretching in alkynes
1707.0	1710.8	(C = O) Stretching in aldehydes, ketones, esters and lactones
1597.0	1587.4	(C = C) Skeletal stretch in condensed aromatic system
1184.3	1163.1	(C—O) Stretching in alcohol, ether, carboxylic acids, esters
754.2	758.0	(C—H) Vibrations bending modes of an aromatic compound

σ is the wave number

The increase in intensity of the peak due to the C—O bond in esters after adsorption (1163.1 cm^{-1}) can be explained by the fact that phenol reacts with carboxylic groups on the surfaces of SD500, forming ester bonds. Carboxylic groups can react with phenol to form esters i.e chemisorption on the surface of the adsorbent. However, this chemisorption reaction will take place if the energetics of the process is more favourable than that of physisorption (Salamane and Bandosz, 2003). From the FT-IR spectra of SD500 before and after sorption, it can be seen that there was an increase in the intensity of the absorption band for C—O in esters confirming that more ester bonds were formed.

The SEM image analysis of SD500 (Figure 4.3) before and after adsorption of heavy metals and phenol revealed that surfaces of SD500 seems to be rough and protrusions can be seen throughout the micrographs. The surface roughness is indicative of maximum surface area (Habib-ur-Rehman *et al*., 2006). Surface coverage in the form of flakes indicates the presence of inorganic elements which could be heavy metals especially after adsorption. From the particle morphology, it is apparent that SD500 is suitable to be used as adsorbent.

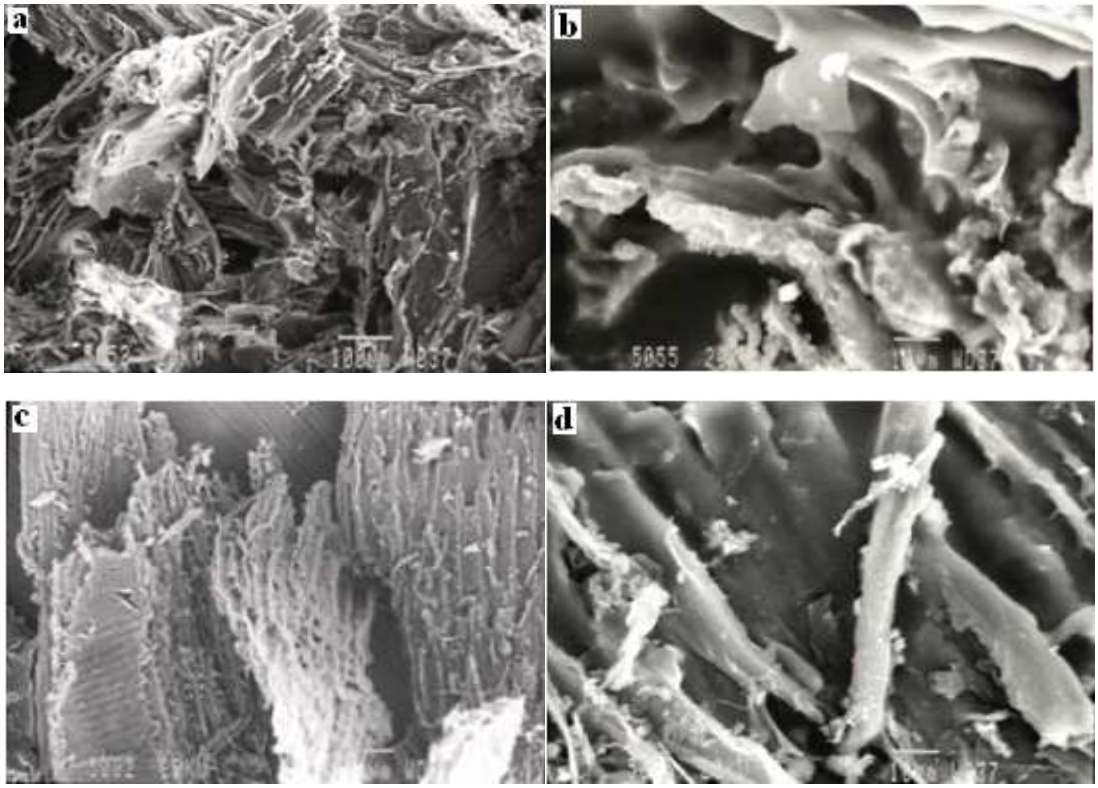

Figure 4.3. SEM images of SD500 before (a & b) and after (c & d) adsorption at 140 times magnification.

4.1.2 Sugarcane bagasse (SB400)

The major component identified in SB400 as shown in Figure 4.4 is mullite ($Al_6Si_2O_{13}$) and this confirms that SB400 is crystalline. The FT-IR spectrum of SB400 is shown in Figure A4 (Appendix). It can be seen that there are some peaks at

2546.0, 2363.9, 2161.9, 2036.0, 1977.5, 1582.6, 1422.9, 1104.0 and 616.4 cm^{-1}. Most of these bands have been reported by other investigators for different carbon materials (Bouchelta *et al*., 2008; Tsai *et al*., 2001; Ardejani *et al*., 2008). The most significant absorbance peak is at 1104.0 cm^{-1}. This can be associated with ether C-O symmetric and asymmetric stretching vibration (-C-O-C- ring) (Lapuente *et al*., 1998). The peak at 1582 cm^{-1} is characteristic of C=C skeletal stretch in condensed aromatic system.

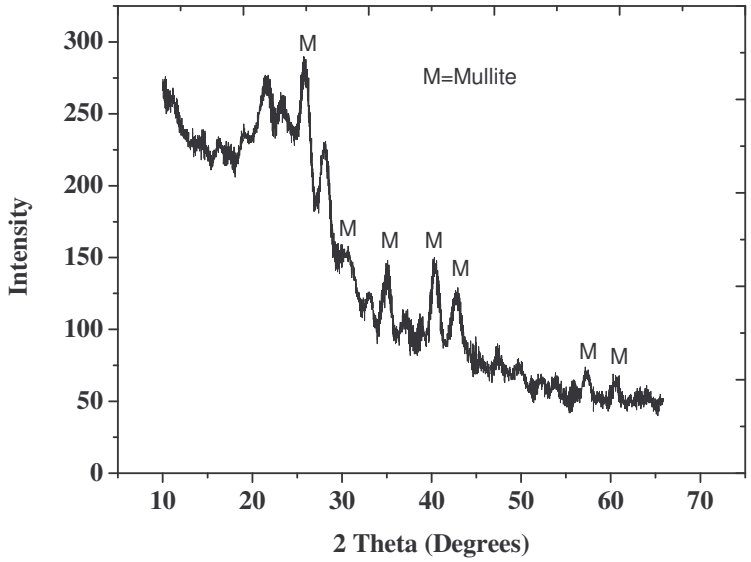

Figure 4.4. The X-ray diffraction profile (diffractogram) of SB400.

The SEM photograph of the SB400 before use (Figure 4.5 a) shows that SB400 has a rough surface with a skeletal structure. It is clear that SB400 has linear type of fibers with pores in them and it has considerable numbers of pore spaces where appropriate conditions exist for direct red dyes to be trapped and adsorbed into these pores. Figure 4.5 (b) illustrates that the direct red dyes are homogeneously adsorbed on the surfaces of SB400 causing a smoother surface.

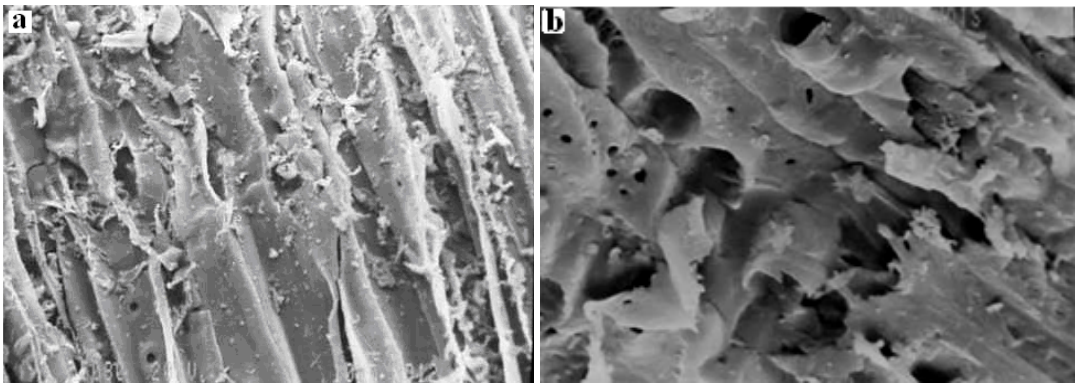

Figure 4.5. SEM images of SB400 before (a) and after (b) adsorption of direct red dyes at 1200 times magnification.

4.1.3 Coal fly ash (CFA)

It is readily apparent from Figure 4.6 that the crystalline phases (sharp peaks) present in the raw coal fly ash are quartz (SiO_2), mullite ($Al_6Si_2O_{13}$), low content of hematite (Fe_2O_3) and calcium oxide (CaO) also known as lime. Thus, coal fly ash is alkaline and can therefore neutralize wastewater and adsorb heavy metals. It appears that the quartz and mullite were produced from the thermal decomposition of clay minerals such as kaolinite during combustion (Mohan and Gandhimathi, 2009). These results were consistent with literature reports (Potgieter *et al*., 2009; Mohan and Gandhimathi, 2009). A broad peak indicating the presence of amorphous phase due to unburned carbon was observed around 24°. This peak was also observed by other researchers on coal fly ash (Papandreon *et al*., 2007; Wang and Zhu, 2007). Thus, coal fly ash has an amorphous aluminosilicate nature and its actual composition depends on the variety of coal used, the degree of burning and the method of collection (Sen and De, 1987).

The FT-IR spectrum (Figures 4.7) gives the functional groups or binding sites which are on the surfaces of coal fly ash. However, the availability of a particular functional group or binding site does not necessarily guarantee its accessibility as a sorption site

for a metal ion, due to steric, conformational or other types of barriers (Dakiky *et al*., 2002). The spectrum of CFA before adsorption displays a number of absorption

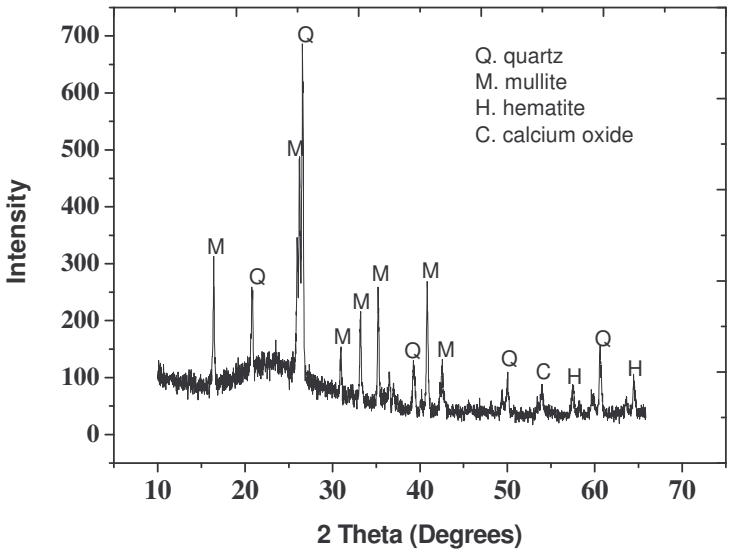

Figure 4.6. The X-ray diffraction profile (diffractogram) of CFA.

peaks, of which the band appearing at 1059.0 cm^{-1} is associated with X–O (X = Si, Al) asymmetric stretching vibrations. This peak was also observed by El-Naggar *et al*. (2008) on coal fly ash obtained from Shubra El-Khaima power station (Egypt). Also, the same peak at 1059.0 cm^{-1}could be attributed to C–O stretching (Pavia and Lampman, 1987). Peaks at 1975.7 cm^{-1} and 2363.7 cm^{-1} may be due to C=O and alkyl groups present in clay material of the coal fly ash, respectively. The band appearing at 555.86 cm^{-1} is associated with the octahedral aluminium present in mullite. Further, bands appearing between 800 and 600 cm^{-1} are associated with the tetrahedral vibrations formed by what are known as secondary building units (SBU) and fragments of the alumino silicate system. These bands are typical characteristic of the double or single rings (depending on the structure of the material) and/or the XO_4 (X = Si, Al) tetrahedral bonds (Jime´nez and Palomo, 2005). Thus, comparing the spectra before and after adsorption, it is clear that the bands at 2530.8, 2160.5, 2028.5, 1975.7 and 1059.0 cm^{-1} are shifted to 2600.0, 2175.7, 2036.8, 1965.4 and

1043.5 cm^{-1}, respectively. This indicates that all these functional groups were involved in the adsorption process, suggesting chemical interactions with the adsorbates.

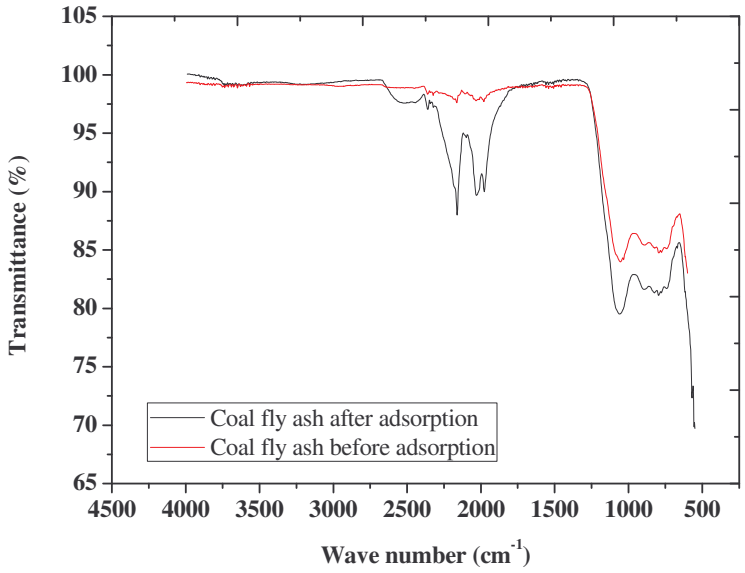

Figure 4.7. FT-IR spectra of CFA before and after adsorption of heavy metals and phenol.

Figure 4.8 shows the SEM pictures of coal fly ash before (a & b) and after adsorption (c & d). These images reveal that the raw coal fly ash mainly consist of well-developed, smooth, glassy spherical particles (cenospheres) and some irregular shaped particles which are interspersed with aggregates of crystalline compounds which may correspond to quartz and hematite. These results were comparable with those reported by El-Naggar *et al*. (2008) for coal fly ash. Lu *et al*. (2009) also described these spheres as hollow particles filled with micro-spheres which are linked with the inner part of the bigger spherical particles. The SEM images show less pore development in coal fly ash. Comparing raw coal fly ash (Figure 4.8a & b) and coal fly ash after adsorption (Figure 4.8c & d), it can be seen that there are morphological changes in the fly ash after sorption. The spheres of coal fly ash after adsorption are

covered with precipitates and complexes (chemisorption) formed by the heavy metal ions; and also phenol adsorbed forming a molecular cloud (Namasivana and Kavitha, 2006). Similar observations were made by Mohan and Gandhimathi (2009).

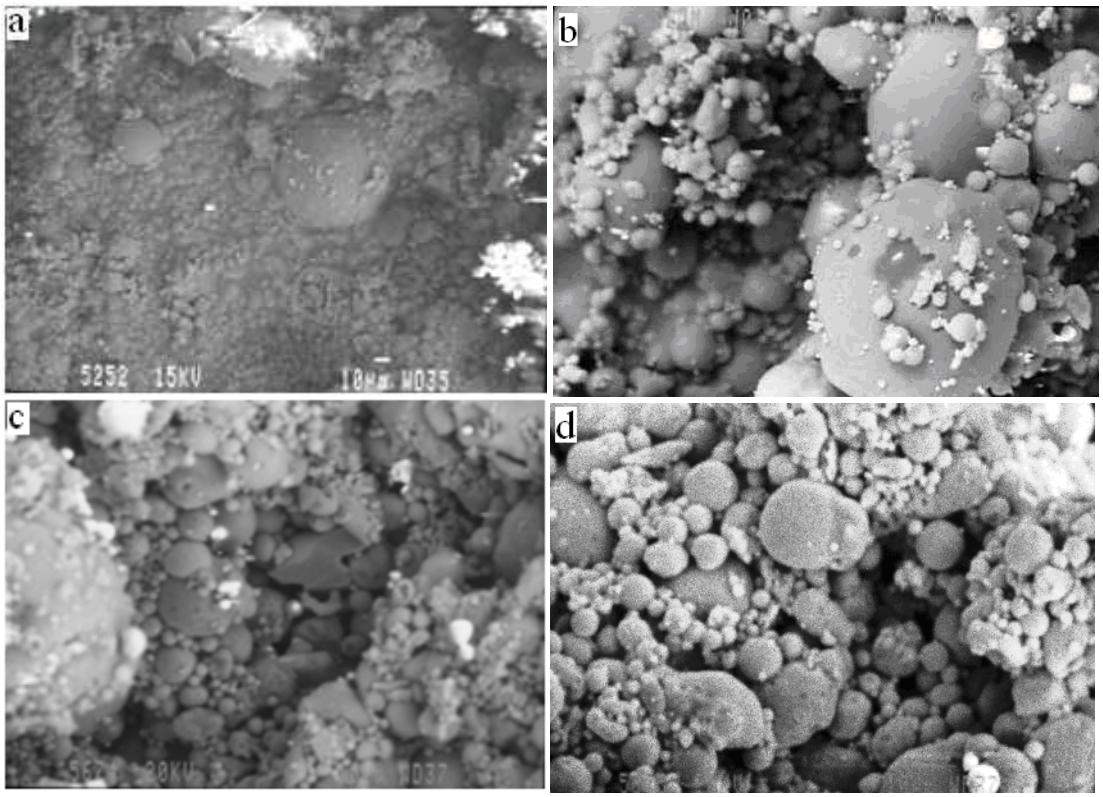

Figure 4.8. SEM images of coal fly ash before (a & b) and after (c & d) adsorption of heavy metals and phenol at 400 times magnification.

4.1.4 Steam activated sawdust (SAS)

The X-ray diffraction pattern of SAS shown in Figure A6 (Appendix) is similar to that of SD500 (Figure 4.1). This means that both SD500 and SAS are amorphous and they contain carbon and graphite. The FT-IR spectroscopic study of the steam activated carbon prepared from pine sawdust (SAS) is shown in Figure 4.9. In addition to that, the spectra with labeled peaks are shown in Figures A7 and A8 in Appendix. The peak positions showing major absorption bands were observed at 2655.9, 2088.9, 1996.3, 1842.0, 1560.4, 1215.1, 947.0 and 669.3 cm^{-1}. The band at

2669.4 cm^{-1} may represent the (O—H) stretching in carboxylic acids. Also, the band at 2088.9 cm^{-1} represents the CΞC stretching in alkynes and the peak at 1560.4 cm^{-1} should be the characteristic one of C=O in the quinone structure (Tsai *et al*., 2001). The band at 1215.1 cm^{-1} is due to C–H deformation vibration. Peak at 669.3 cm^{-1} can be assigned to the out-of-plane C-H bending modes of an aromatic compound (Al-Qodah and Shawabkah, 2009). After adsorption of heavy metals and phenol, bands at 2655.9, 2362.8, 1842.0, 1560.4, 947.0 and 669.3 shifted to 2899.0, 2603.9, 1749.4, 1521.8, 1016.5 and 628.8 cm^{-1}, respectively. All these findings suggest chemical attachment of heavy metals and phenol onto SAS.

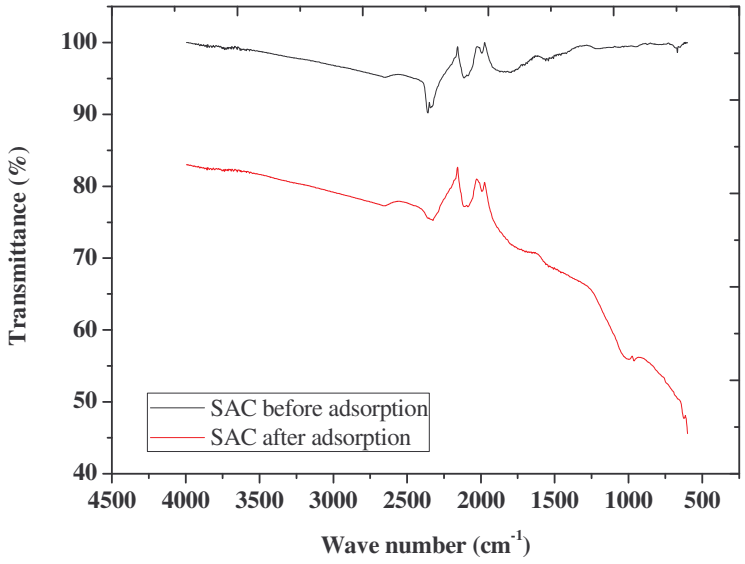

Figure 4.9. FT-IR spectra of SAS before and after adsorption of heavy metals and phenol.

Figure 4.10 shows the SEM photographs of SAS at different magnifications. Pores of different sizes and different shapes could be observed. It can be seen from the micrographs that the external surface of SAS is full of cavities which resulted from the evolution of volatile compounds during the carbonization stage. Similar images were reported by Mohanty *et al*. (2005) for activated carbon prepared from sawdust. The pores on SAS seem to be more than those on CFA, SD500 and SB400.

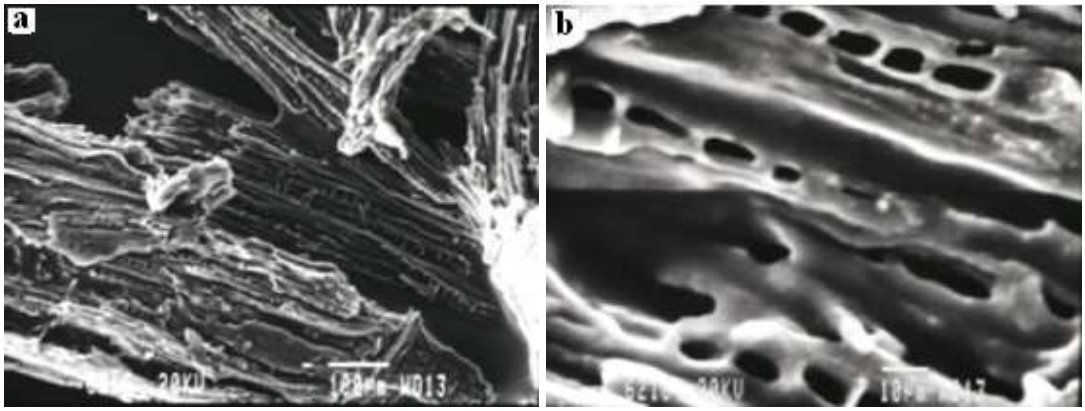

Figure 4.10. SEM images of SAS before adsorption at 140 (a) and 1200 (b) times magnification, respectively.

4.1.5 Commercial activated carbon (CAC)

Activated carbon is generally described as an amorphous form of graphite with a random structure of graphite plates; having highly porous structure with a range of cracks and crevices reaching molecular dimensions. The XRD pattern for CAC is presented in Figure 4.11(a). Comparison of the XRD pattern of CAC with the other adsorbents shows that the intensity of the peak around 42.3° which represents graphite follows the order: CAC > SD500 ≈ SAS > SB400 > CFA. Furthermore, the intensity of the peak around 24.4° (due to carbon) in all the adsorbents decreases in the order: SD500 > SAS > CAC > SB400 > CFA.

Figure 4.11 (b) shows the FT-IR spectra of commercial activated carbon before and after use. Comparison of the FT-IR spectra of CAC and SAS before adsorption indicates that these two adsorbents have common functional groups which are the C–H on aromatic and aliphatic compounds, carbonyl groups in aldehydes and ketones, C=O in the quinone structure, alkyl groups, C–O groups and the O–H groups in carboxylic acids. However, the intensity (proportional to concentration) of the peaks on the spectra for CAC was low as compared to SAS.

(a)

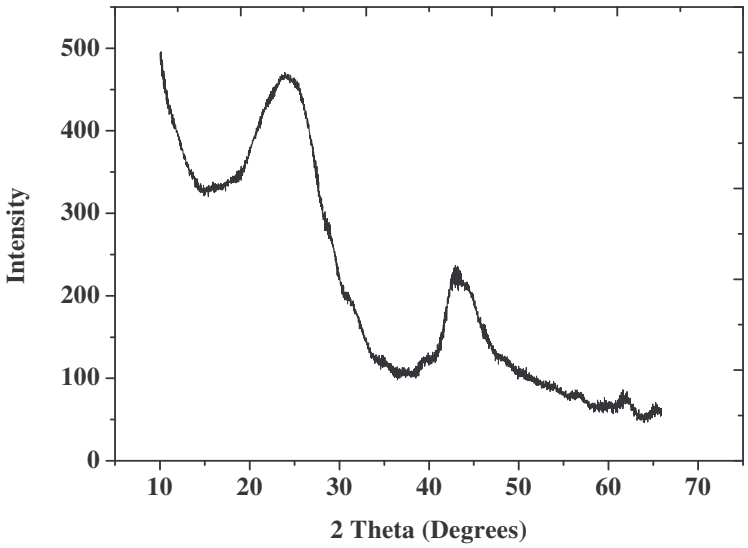

(b)

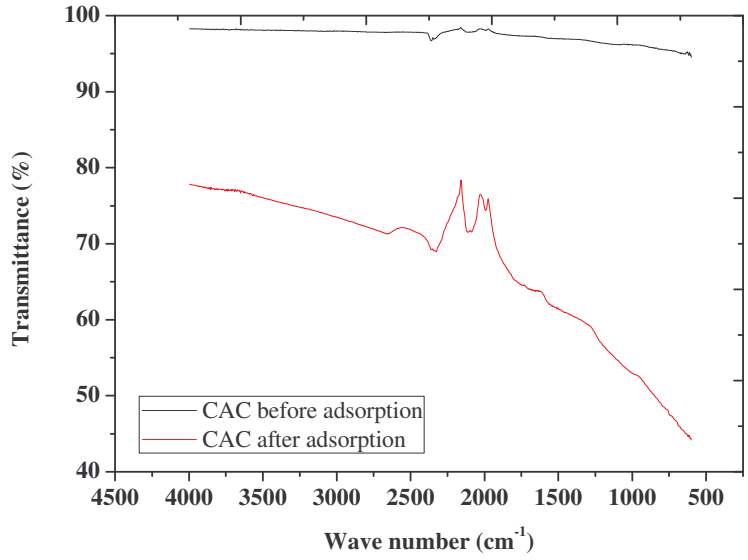

Figure 4.11. Surface characterization results for CAC: (a) X-ray diffraction pattern and (b) FT-IR spectra before and after adsorption of heavy metals and phenol.

The scanning electron microscopy examination of CAC, as presented in Figure 4.12, shows a heterogeneous phase material. It is clear that CAC has a honeycomb-like

structure which is highly porous. Also, the SEM images for CAC especially the one in Figures 4.12 (b) is very much comparable to that of SAS. From all the characterization results, it is seen that all the studied adsorbents have heterogeneous surfaces.

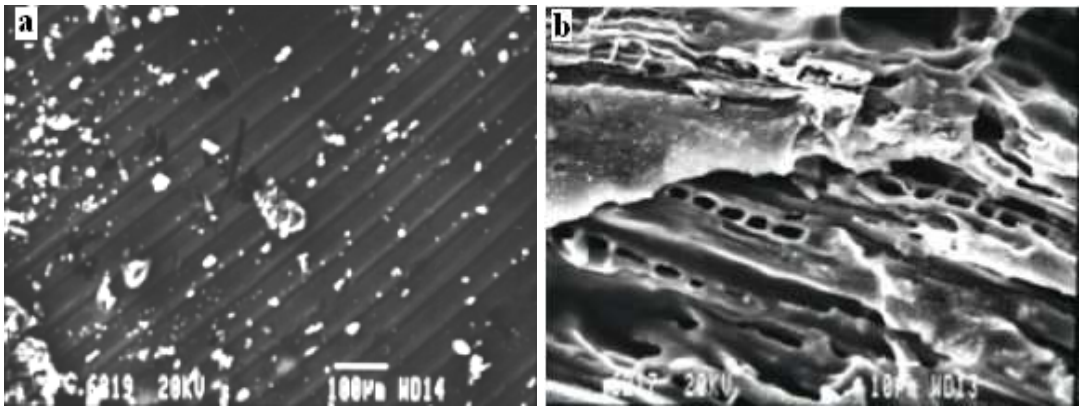

Figure 4.12. SEM images of CAC before adsorption at 140 (a) and 600 (b) times magnification, respectively.

4.1.6 Surface area and porosity of the adsorbents

The surface characteristics of all the adsorbents studied in this work are presented in Table 4.2. Comparing the surface characteristics of SD250, SD400 and SD500, it can be seen that increasing the carbonization temperature from 250 to 500°C results in an increase in the development of porosity and hence the S_{BET}, S_{mi}, V_t, V_{mi} and V_{me} gradually increase. This can be explained by the fact that increasing the carbonization temperature increases the amount of volatile matter released thereby resulting in the development of more pores (Zhu *et al*., 2007). Thus, amongst the adsorbents derived from sawdust, SD500 performed better than SD250 and SD400 towards synthetic petrochemical wastewater in preliminary experiments and this can be attributed to the difference in their surface area. Hence, SD500 was chosen for further experiments. Commercial activated carbon has the highest surface area followed by SAS and SD500. It is interesting to note that the surface area of SD500

and SAS falls within the range of commercial activated carbon (500—1500 m^2/g) (Cooney, 1980), hence, their performance is expected to be comparable to that of commercial activated carbon. Habib-ur-Rehman *et al*. (2006) reported a surface area of 143.125 m^2/g for sawdust treated with sodium hydroxide solution and this is lower than the surface area of the sawdust modified with citric acid and heat treated.

Table 4.2

Surface characteristics and pore structure of the adsorbents

Adsorbent	S_{BET} (m^2/g)	S_{mi} (m^2/g)	V_t (cm^3/g)	V_{mi} (cm^3/g)	V_{me} (cm^3/g)	V_{mi}/V_t
SB400	160.48	119.59	0.085	0.055	0.031	0.647
SD250	175.79	131.69	0.087	0.060	0.028	0.690
SD400	280.11	199.00	0.143	0.091	0.052	0.636
SD500	592.97	430.00	0.279	0.183	0.096	0.656
SAS	795.68	588.80	0.386	0.258	0.128	0.668
CAC	1057.04	785.68	0.584	0.387	0.197	0.663
CFA	1.73	1.31	$2.25x10^{-3}$	$1.52x10^{-3}$	$7.23x10^{-4}$	0.676

The surface area and total pore volume, V_t of South African coal fly ash used in this study were found to be 1.7287 m^2/g and 0.0023 cm^3/g, respectively. The low surface area of coal fly ash is consistent with the SEM images in Figure 4.8 which shows low pore development on coal fly ash. In a study conducted by Potgieter *et al*. (2009), the surface area of South African coal fly ash was 1.2790 m^2/g. In addition, Bayat (2002) analyzed two different Turkish fly ash samples and observed S_{BET} values less than 0.342 m^2/g which were even lower than that for South African coal fly ash. However, the adsorption performance of those two Turkish samples was good. On the other hand, Viraraghavan and Rao (1991) reported S_{BET} of 1.7000 m^2/g for Saskatchewan coal fly ash which is comparable to South African fly ash.

4.2 Optimum adsorbent mass

The results shown in Figure 4.13 indicate that the percentage removal of Co(II), Ni(II), Fe(II), Pb(II) and phenol increases with an increase in mass of coal fly ash. The increase in the percentage removal with the increasing adsorbent mass is due to the increase in the surface area consequent to the increase in the number of adsorbent particles with a larger number of active surface sites for the adsorption (Goel *et al*., 2006). It is observed that as the mass of the adsorbent increases, the amount of solute adsorbed increases and reaches a maximum value corresponding to a certain mass of

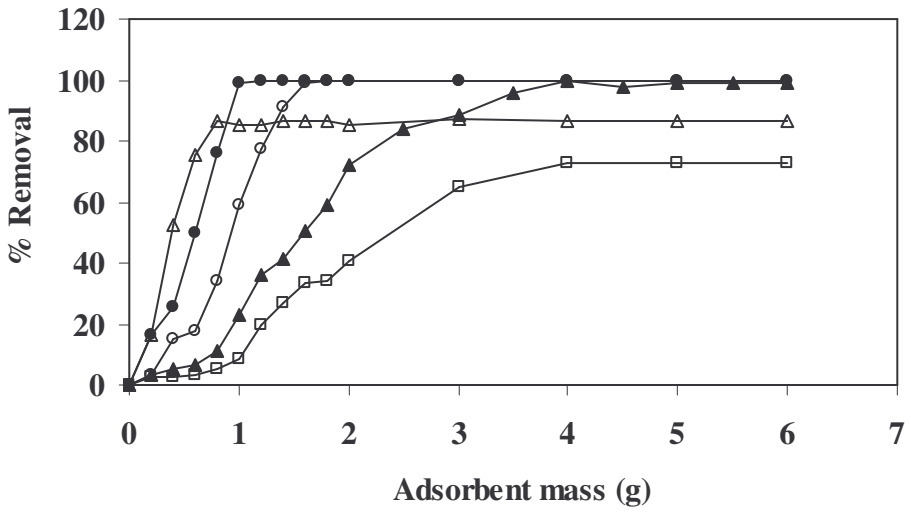

Figure 4.13. Removal of Co^{2+}(▲), Ni^{2+}(○), Fe^{2+}(●), Pb^{2+}(Δ) and phenol (□) using coal fly ash (pH = 4.0, contact time = 48 h, temperature = 25°C, shaking speed = 250 rpm, initial metal concentration = 50 mg/l, initial phenol concentration = 110 mg/l).

adsorbent. The minimum amount of adsorbent corresponding to the maximum adsorption is declared as the optimum mass. In this case, the highest percentage removals for Co(II), Ni(II), Fe(II), Pb(II) and phenol were observed at an optimum mass of 4.0, 1.8, 1.2, 0.8 and 4.0 g, respectively. Thus, 4.0 g was selected as the optimum mass for treating petrochemical wastewater using coal fly ash in subsequent experiments. Results for the other adsorbents are presented in Table B2 to B4 in

Appendix and it is also clear that the removal efficiency increases up to the optimum mass beyond which the removal efficiency remains constant. Consequently, the optimum masses selected were 4.0 g SD500, 2.0 g SAS and 1.6 g CAC per 100 ml of petrochemical wastewater. Similarly, the optimum masses for textile wastewater treatment were 4.0 g CFA and 4.0 g SB400 per 100 ml of the solution (Table B5 in Appendix). It is also important to point out that as the adsorbent mass increases, the adsorbate removal efficiency increases, however, the amount adsorbed per unit mass decreases due to the incomplete use of adsorption sites or particles interaction such as aggregation, as a result of a high adsorbent concentration. Such aggregation state may result in a decrease in the total surface area of the adsorbent (Shukla *et al*., 2002). In this study, no adsorption on the surface of conical flask was observed and hence all the adsorption recorded was due to the adsorbent.

4.3 Kinetic studies

4.3.1 Textile wastewater

Information on the kinetics of dye uptake is required for selecting the optimum operating conditions for further experiments. It can be noticed from Figure 4.14 that the contact time significantly affects the dye uptake: the dye sorption increases sharply in the first stages. This rapid stage was probably due to the abundant availability of active sites on the adsorbents, and with the gradual occupancy of these sites, the sorption became less efficient in the slower stage. Optimum contact time for removal of all the dyes was 8 h using SB400 and 9 h for CFA. The maximum percentage removals were in the order: DR80 > DR81 > DR 23 for both SB400 and CFA. However, percentage removals obtained for dye removal with SB400 were higher than those for CFA indicating that the dyes have more affinity for SB400 than CFA (Figure 4.14). This observation can be explained by the fact that there was more surface area available for dye adsorption on the surfaces of SB400 (160.48 m^2/g) as compared to CFA (1.73 m^2/g). Consequently, it can be inferred from this observation that physisorption took place during dye adsorption.

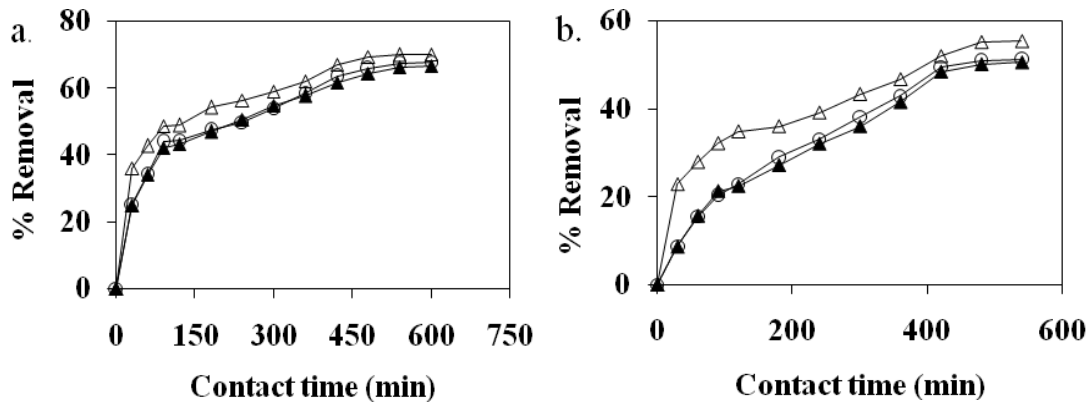

Figure 4.14. Removal of DR80 (Δ), DR81 (○) and DR23 (▲) using (a) SB400 and (b) CFA (pH = 6.0, temperature = 25°C, shaking speed = 250 rpm, initial dye concentration = 50 mg/l, dose = 40 g/l, volume = 100 ml).

4.3.2 Petrochemical wastewater

The experimental results on the effect of contact time on batch adsorption of heavy metals and phenol at 25°C and at initial pH value 4.0 are presented in Table B6 to B9 (Appendix) for all the adsorbents. The initial rapid adsorption gives way to a very slow approach to equilibrium. The removal of all the heavy metals using CFA reached equilibrium after 6 h; however, phenol removal from the same solution took 24 h. Thus, 24 h was selected as the contact time in further experiments using CFA to allow phenol equilibrium to be established. In the cases of SAS and CAC, the contact time was selected as 4 h whereas that for SD500 was 6 h. This means that the residence time required to treat the synthetic petrochemical wastewater followed the order: CFA > SD500 > SAS ≈ CAC. The nature of adsorbent and its available sorption sites affected the time needed to reach the equilibrium (Naiya *et al*., 2009). The observed order of residence time can be related to the specific surface area of the adsorbents. It should be noted that CFA has the least surface area followed by SD500 whereas CAC and SAS have the highest which explains why the time to reach equilibrium time was short for these two adsorbents. The rapid kinetics has significant practical importance as it will facilitate smaller reactor volumes, ensuring efficiency and economy (Basha *et al*., 2009).

4.4 Adsorption kinetic modeling

It is known that the adsorption process can be controlled by different kinds of mechanisms such as mass transfer and chemical reactions. In order to determine the adsorption mechanism, several adsorption models were applied to evaluate the experimental data. For this purpose, Lagergren's pseudo first-order kinetic model (Lagergren, 1898), pseudo second-order kinetic model (Ho, 1995), and intraparticle diffusion model (Weber and Morris, 1963) were considered and fitted to the experimental data. In this study, the adsorption kinetic modeling of cobalt removal was done as an example using four different adsorbents with the same particle size range (53–180 μm). This decision was based on the fact that there is limited literature on the kinetics of cobalt removal using low cost adsorbents derived from sawdust and coal fly ash. Figures 4.15 to 4.17 show the plots of the pseudo first-order (equation (2.6)), pseudo second-order (equation (2.8)) and intraparticle diffusion (equation (2.11)) models for adsorption of cobalt ions, respectively. The estimated equilibrium adsorption capacity, q_e values and coefficients related to the pseudo first-order and second-order kinetic plots are listed in Table 4.3.

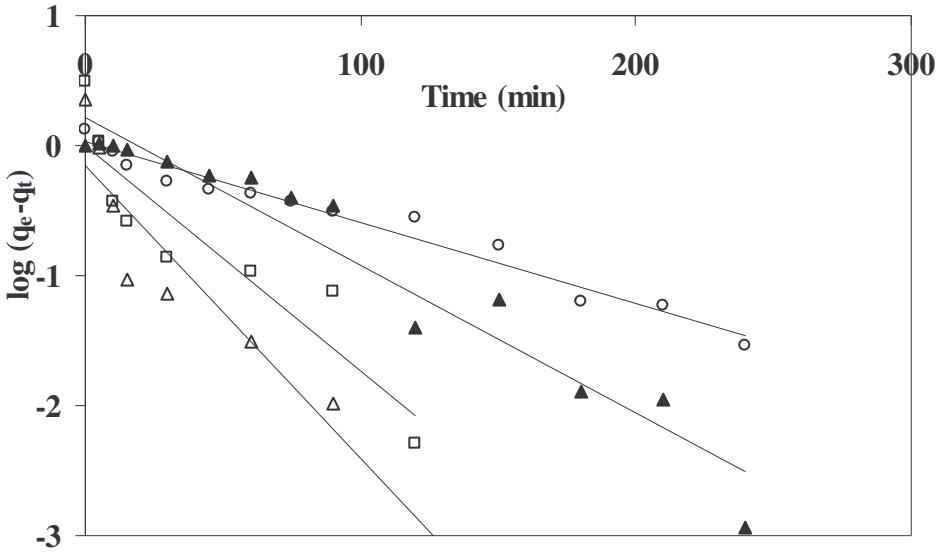

Figure 4.15. Lagergren pseudo-first-order plots for cobalt adsorption on SD500 (▲), CFA (○), SAS (Δ) and CAC (□).

The correlation coefficients (R^2) were in the range of 0.8170–0.9380 for pseudo-first-order. Additionally, the q_e values predicted by the pseudo-first-order model were not in agreement with the experimental values suggesting that cobalt adsorption did not fit the pseudo-first-order model. On the other hand, the R^2 values for pseudo-second order model were in the range 0.9690–0.9999 and the predicted q_e values agreed well with the experimental ones. Thus, higher correlation coefficients of pseudo-second-order equation and the predicted q_e values close to the experimental values indicated that the pseudo-second-order kinetic model might be suitable to describe the kinetics adsorption process of cobalt onto CFA, SD500, SAS and CAC better than the pseudo-first-order kinetic model. This suggests that during the adsorption of cobalt, there was chemisorption due to the sharing of electrons between the adsorbent surface and the *d* orbitals of Co (II) (Hanafiah *et al*., 2009). At the same time, the q_e values for cobalt followed the order: CAC > SAS >SD500 > CFA which is in accordance with the increase in specific surface area of the adsorbents described in section 4.1.6, suggesting that physisorption also took place. Therefore, it could be concluded that

Table 4.3

Kinetic parameters for cobalt adsorption

Model	CFA	SD500	SAS	CAC
Pseudo-first-order				
k_{ad} (min^{-1})	0.0184	0.0253	0.0507	0.0392
q_e (mg/g)	0.7031	0.9863	1.0544	1.6673
R^2	0.9100	0.9380	0.8170	0.8340
Experimental q_e (mg/g)	1.2575	1.2650	2.1650	3.0256
Pseudo-second-order				
k_2 ($gmg^{-1}min^{-1}$)	0.0131	0.0311	0.3126	0.1934
q_e (mg/g)	1.3477	1.3870	2.2883	3.1746
R^2	0.9890	0.9900	0.9999	0.9999

in the adsorption of cobalt by the tested adsorbents, both chemical and physical adsorption occurred.

If the Weber–Morris plot of q_t versus $t^{1/2}$ gives a straight line that passes through the origin, then the adsorption process is controlled by intra-particle diffusion only. However, if the data exhibit multi-linear plots, then two or more steps influence the sorption process (Srivastava *et al*., 2006). Figure 4.17 presents the multi-linear plots of the adsorbed cobalt ion mass per unit mass of adsorbent versus $t^{1/2}$ for CFA, SD500, SAS and CAC. The initial period is attributed to the diffusion of cobalt through the solution to the external surface of adsorbent or the boundary layer

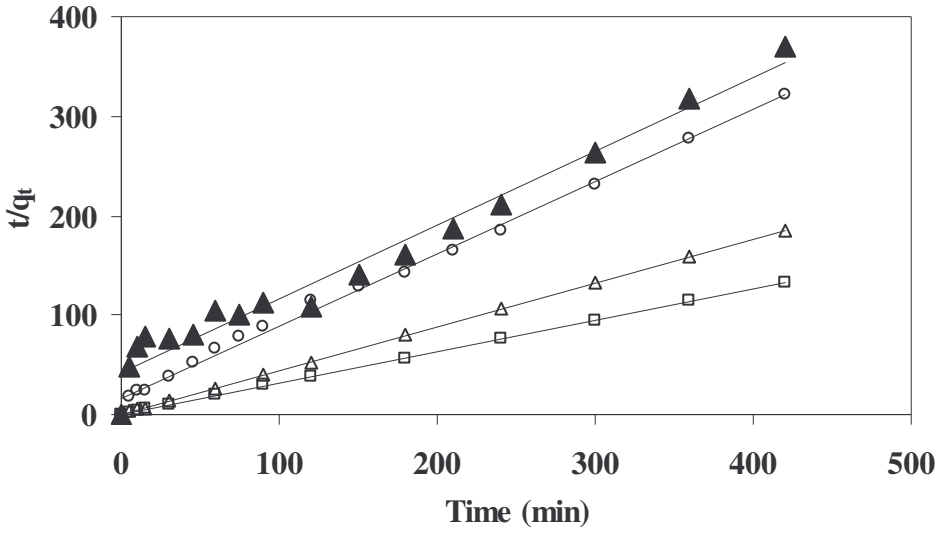

Figure 4.16. Pseudo-second-order plots for cobalt adsorption on SD500 (▲), CFA (○), SAS (Δ) and CAC (□).

diffusion of the cobalt ions. Then the first linear portion describes the gradual adsorption stage, where intraparticle diffusion is rate-limiting and the second linear portion is attributed to the final equilibrium stage where intraparticle diffusion starts to slow down due to low cobalt concentration left in solution (Alzaydien, 2009). The slope of the first linear portion characterizes the rate parameter corresponding to the

intraparticle diffusion, whereas the intercept of this portion is proportional to the boundary layer thickness. The intra-particle diffusion constants could be calculated using equation (2.11).

Table 4.4 summarizes the intraparticle diffusion constants (k_{id1}, k_{id2}) for the different stages of the adsorption process. From Table 4.4, it is clear that the adsorption rate was higher in the first stage (k_{id1}) than in the second (k_{id2}). At the beginning, cobalt was adsorbed by the external surface of the adsorbent particles so the sorption rate was very high. When the adsorption of the exterior surface reached saturation, the cobalt ions diffused into the adsorbent particles through the pores and were adsorbed by the interior surface of the particles.

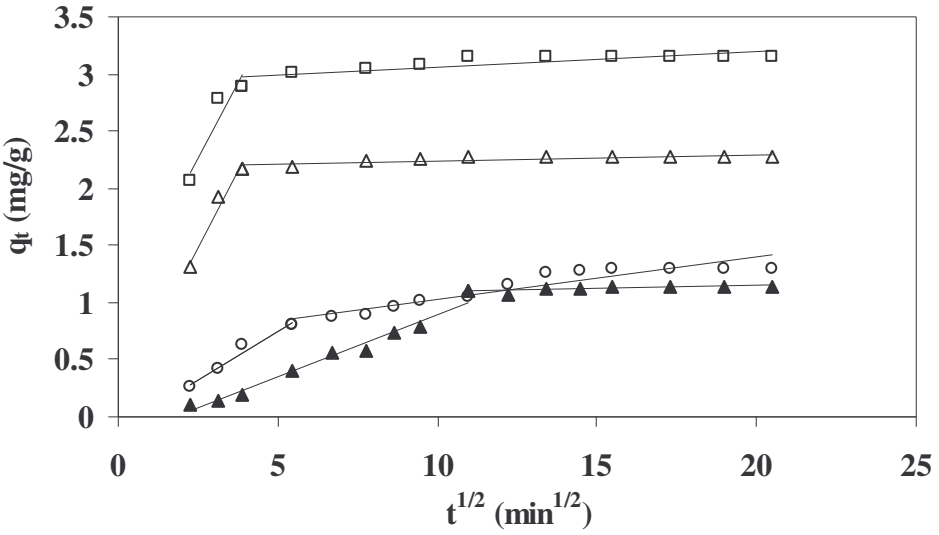

Figure 4.17. Weber and Morris intraparticle diffusion plots for cobalt adsorption on SD500 (▲), CFA (○), SAS (Δ) and CAC (□).

When the cobalt ions diffused in the pores of the adsorbent particles, the diffusion resistance increased, which caused the diffusion rate to decrease. Due to the decrease of the cobalt ion concentration in the solution, the diffusion rate became lower. Therefore the changes on k_{id1} and k_{id2} could be attributed to the adsorption stages of

the external and internal surfaces and equilibrium approach, respectively (Sun and Yang, 2003). Similar phenomena were reported by Valderrama *et al*. (2008) in the removal of acid red dye using activated carbon.

Table 4.4

Intraparticle diffusion constants for cobalt adsorption

Adsorbent	Parameter			
	k_{id1}(mg/gmin)	R_1^2	k_{id2} (mg/gmin)	R_2^2
CFA	0.150	0.979	0.047	0.958
SD500	0.099	0.958	0.005	0.571
SAS	0.575	0.995	0.008	0.815
CAC	0.886	0.998	0.020	0.842

4.5 Equilibrium modeling

Equilibrium data is important in evaluating the adsorption capacity of an adsorbent for a given adsorbate. Information derived from such data is important also in comparing different adsorption media (Eskandarpour *et al*., 2008). In addition, analysis of the isotherm data is important to develop an equation which accurately represents the results and which could be used for design purposes and to optimize an operating procedure. The Langmuir and Freundlich isotherms are used most frequently to describe the adsorption data and for that reason, they were tested in this work for both textile and petrochemical wastewater.

4.5.1 Textile wastewater

In the present study, the experimental data for removal of direct red dyes from textile wastewater using SB400 and CFA were fitted to the Langmuir model (equation (2.1)) and Freundlich model (equation (2.4)). However, only the experimental data for removal of DR80 by SB400 and CFA were selected and used to illustrate the modeling in Figure 4.18. A linear regression technique was then used to determine

all the isotherm parameters as shown in Figure 4.19 to 4.20 for DR80 and DR81 removal using SB400 and CFA. Similarly, the linear regression analysis for DR23 removal is presented in Figure D1 (Appendix).

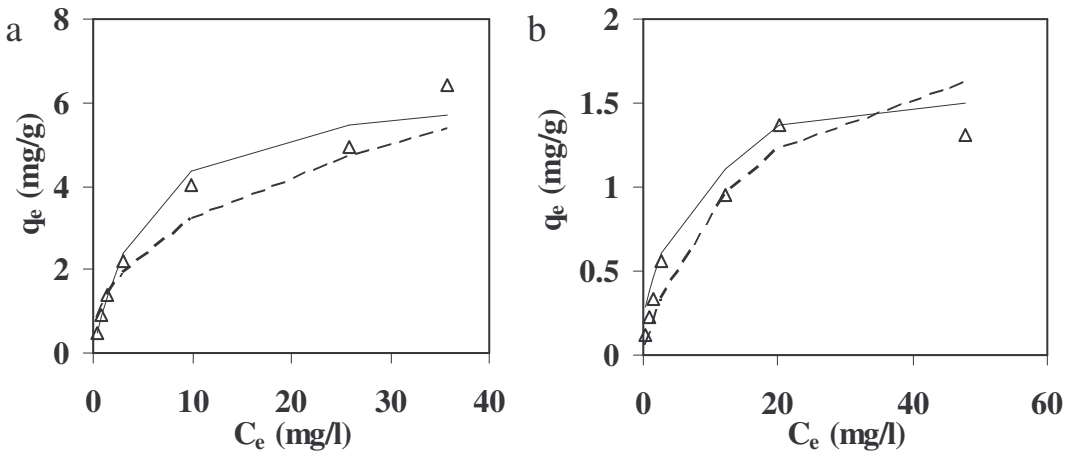

Figure 4.18. Fitting of Langmuir (—) and Freundlich (---) isotherm models to experimental data (Δ) for removal of DR 80 using (a) SB400 and (b) CFA (pH = 6.0, temperature = 25°C, shaking speed = 250 rpm, dose = 40 g/l, volume = 100 ml).

All the isotherm constants (model parameters) are summarized in Table 4.5 together with the R^2 values (goodness of fit criterion) computed by linear regression for the two types of isotherms. It is clear from the R^2 values that the Langmuir isotherm is most appropriate for adsorption of DR80, DR81 and DR23, suggesting a monolayer coverage of dye molecules onto the studied adsorbents. On average, a favourable adsorption tends to have Freundlich constant, n between 1 and 10. Larger value of n (smaller value of $1/n$) implies stronger interaction between the adsorbent and the adsorbate while n equal to 1 indicates linear adsorption leading to identical adsorption energies for all sites (Site, 2001). It can be seen that all the values of n were between 1 and 10 showing favourable adsorption of the dyes onto SB400 and CFA.

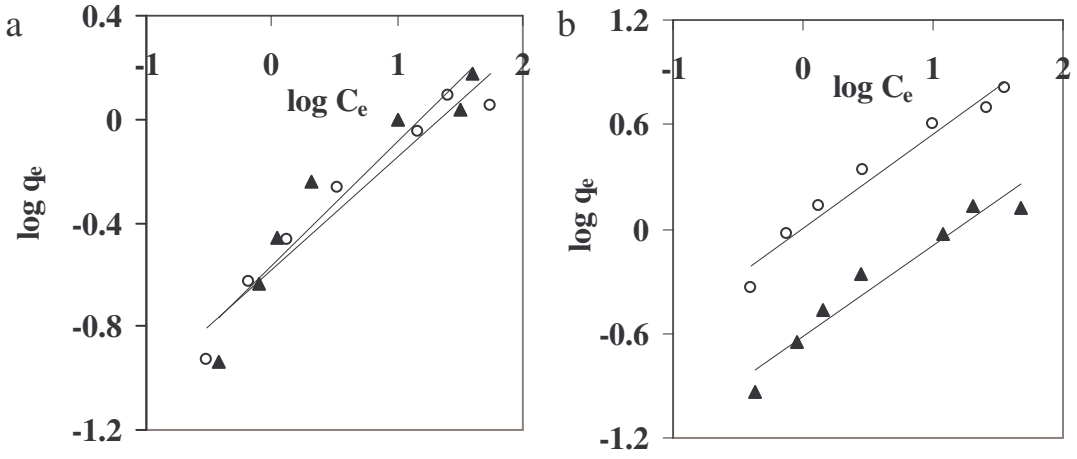

Figure 4.19. Linear regression analysis of (a) DR80 and (b) DR81 removal using CFA (▲) and SB400 (○) for Freundlich isotherm.

Studies by Arami *et al*. (2006) on the adsorption of DR80 and DR81 on soy meal hull, an agricultural by-product, showed that the sorption process was better described by the Langmuir isotherm and the maximum adsorption capacity values for DR80 and DR81 were 178.57 and 120.48 mg/g, respectively. Also, Ardejani *et al*. (2007) studied the sorption of DR23 and DR80 using orange peel and it was found that the equilibrium data were well represented by the Langmuir isotherm with q_{max} values of 10.718 and 21.052 mg/g for DR23 and DR80, respectively. In the present investigation, the maximum monolayer adsorption capacities, q_{max}, of CFA for DR80, DR81 and DR23 are 1.5601, 1.1261 and 1.0471 mg/g, respectively. At the same time, the q_{max} values of SB400 for DR80, DR81 and DR23 are 6.5360, 2.1320 and 1.8248 mg/g, respectively. Thus, it is clear that SB400 is a better adsorbent than CFA in the treatment of textile wastewater. This could be due to the high porosity and surface area of SB400 (160.48 m^2/g) as compared to CFA (1.73 m^2/g), suggesting physical adsorption during dye removal. The low adsorption capacities observed in this study could be due to the fact that the adsorbents were not activated. The coal fly ash was used without any chemical or heat pre-treatment whereas SB400 was only produced from the carbonization of sugarcane bagasse at 400°C (section 3.3.3).

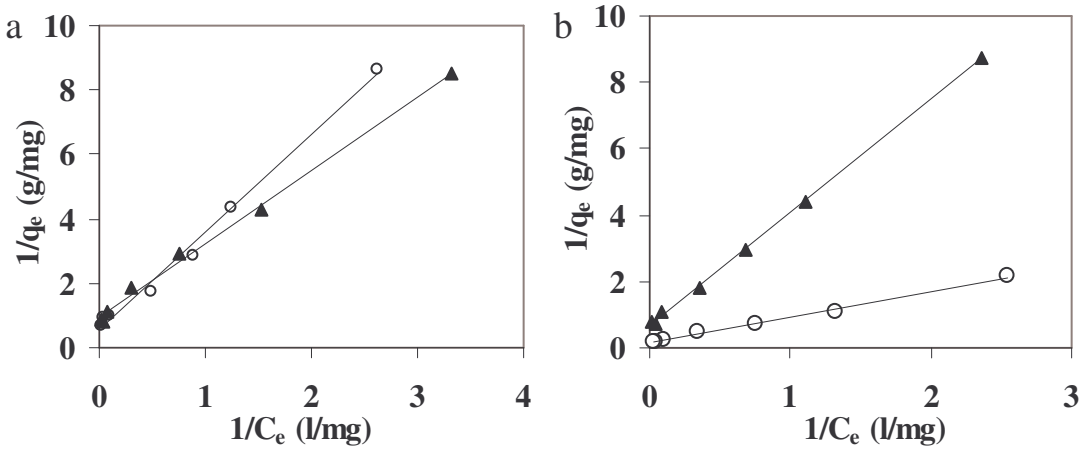

Figure 4.20. Linear regression analysis of (a) DR80 and (b) DR81 removal using CFA (▲) and SB400 (○) for Langmuir isotherm.

For both adsorbents, the q_{max} values followed the order: DR80 > DR81 > DR23. It is apparent that DR80 has more preference than other dyes for adsorption on CFA and SB400. This order is consistent with the maximum percentage removals from section 4.3.1. It may be postulated that due to the presence of large number of sulphonic groups on DR80 in comparison with other dyes, the higher adsorption capacity of SB400 and CFA toward DR80 might be attributed to the increased electrostatic attraction between the surface of the adsorbent and those abundant sulphonic anionic groups at pH 6.0. The other dyes (DR81 and DR23) have the same number of sulphonic groups, however, DR81 has a smaller size than DR23 and also the shape of the DR81 molecule might play a determining factor by enhancing the trapping of dye molecules into pores and cavities of the adsorbent, so increasing its adsorption capacity (Arami *et al*., 2006).

Table 4.5

Freundlich and Langmuir adsorption isotherm constants for textile wastewater

Adsorbent	Adsorbate	Langmuir			Freundlich		
		q_{max} (mg/g)	K_L (l/mg)	R^2	n	K_F (mg/g)	R^2
CFA	DR23	1.0471	0.9694	0.989	2.4390	0.3954	0.943
SB400	DR23	1.8248	0.0962	0.991	1.8349	0.2128	0.915
CFA	DR81	1.1261	0.1974	0.995	1.8222	0.2438	0.964
SB400	DR81	2.1320	0.1873	0.999	1.9268	1.0139	0.936
CFA	DR80	1.5601	0.1804	0.992	2.0921	0.2636	0.909
SB400	DR80	6.5360	0.4190	0.995	2.3042	0.2716	0.945

4.5.2 Petrochemical wastewater

The experimental data for treatment of petrochemical wastewater using SD500, CFA, SAS and CAC were fitted to the Langmuir model (equation (2.1)) and Freundlich model (equation (2.4)). Nevertheless, it must be pointed out that only the experimental data for removal of cobalt by SD500 and CAC were selected and used to illustrate the modeling in Figure 4.21. Additionally, linear regression was used to determine all the isotherm parameters as shown in Figure 4.22. More linear regression analysis of the experimental data for petrochemical wastewater is shown in Figures D2 and D3 (Appendix). It was found that when compared to the Langmuir isotherm, the Freundlich isotherm resulted in a good fit with experimental data as evidenced in Figure 4.22 (a) to (c) (for cobalt, iron and lead) and Figure D2 (a) (for nickel) (Appendix). The empirical parameters for both isotherms were presented in Table 4.6 along with the correlation coefficients, R^2 values.

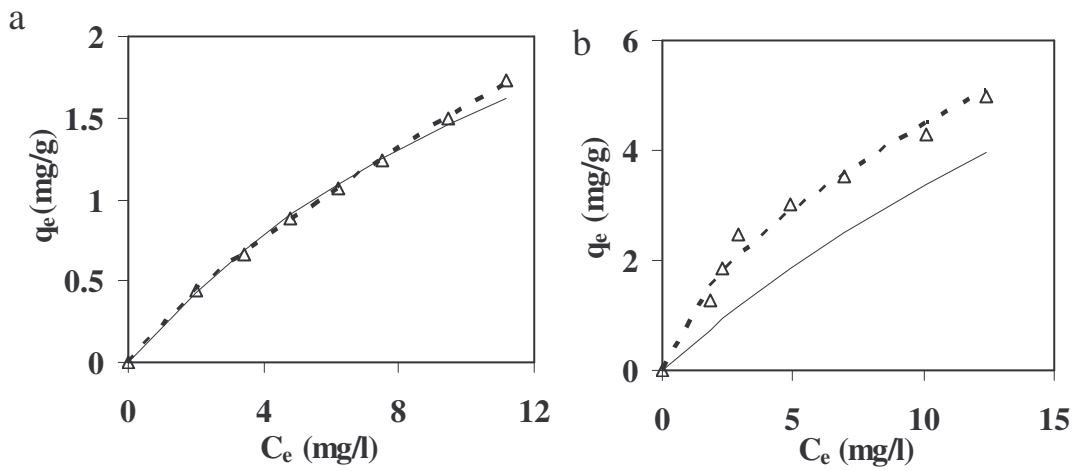

Figure 4.21. Fitting of Langmuir (—) and Freundlich (---) isotherm models to experimental data (Δ) for removal of cobalt using (a) SD500 and (b) CAC (pH = 4.0, temperature = 25°C, shaking speed = 250 rpm, SD500 dose = 40 g/l, CAC dose = 16 g/l, volume = 100 ml).

It has been shown in section 4.1.6 that the specific surface area follows the sequence: CAC > SAS > SD500 > CFA. Thus, it is interesting to note that the maximum monolayer adsorption capacity, q_{max} values shown in Table 4.6 generally follow the same order with a few exceptions. For example, CFA performed better than SD500 in the removal of iron and lead although it has the lowest surface area. Thus, from these observations, one can conclude that surface area plays a very important role in adsorption; however, it is not necessarily the only adsorbent property which determines performance. This better performance of CFA as compared to SD500 towards iron and lead could be attributed to the presence of silica in CFA which is a well-known inorganic cation exchanger (Sen and De, 1987). The sequence of sorption affinity for both SAS and CAC was: Fe > Co > Ni > Pb. This similarity in sequence of sorption affinity can be explained by the fact that both CAC and SAS have almost similar physicochemical properties as is evident from their XRD patterns, FT-IR spectra and SEM images except for surface area. It can be noted from the q_{max} values that the order for cobalt binding affinity was: CAC > SAS >

SD500 > CFA which is in agreement with the q_e values calculated from the pseudo-second order model in section 4.4.

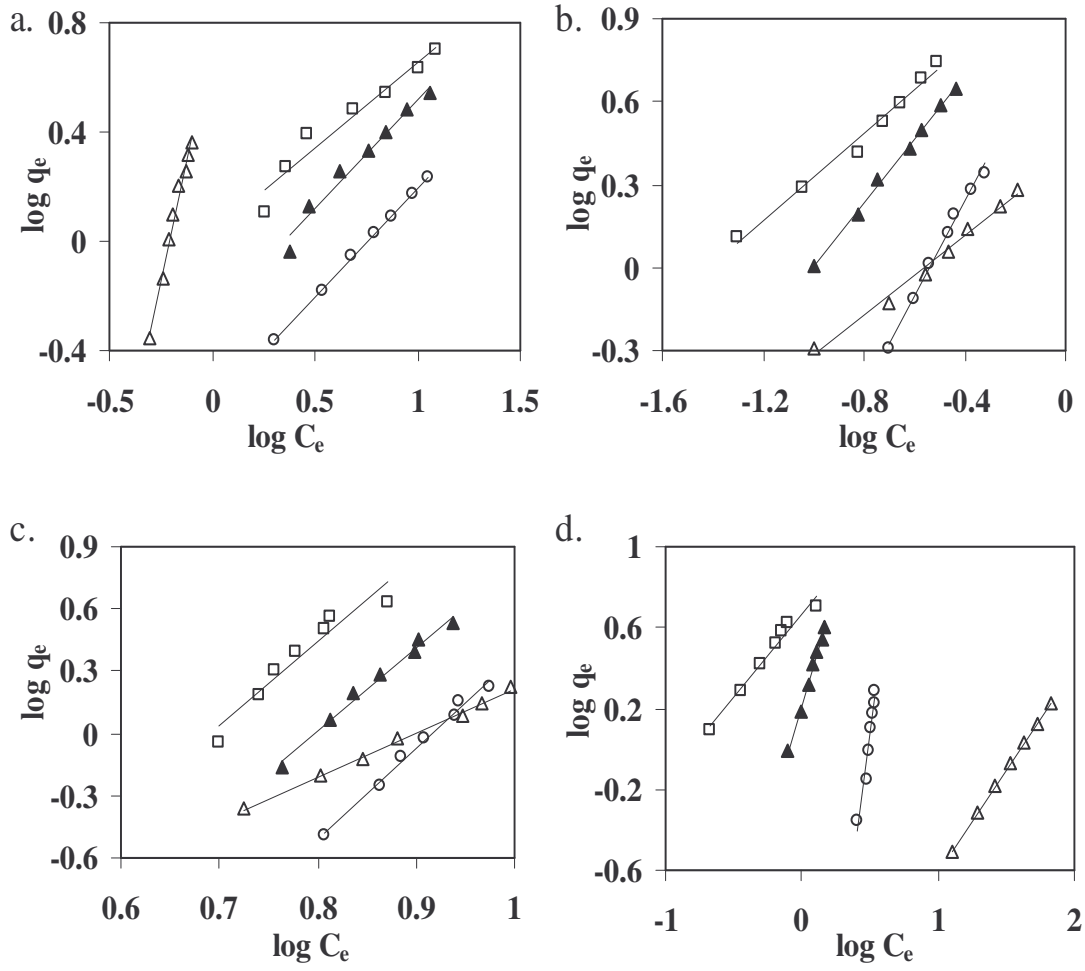

Figure 4.22. Freundlich isotherm for (a) cobalt, (b) iron, (c) lead, (d) phenol removal using CAC (□), SAS (▲), SD500 (○) and CFA (Δ).

The specific surface area and total pore volume of CAC is higher than that of SAS and this could explain why it performed better. However, the performance of SAS was not far from that of CAC in the removal of lead and nickel. The sequence of adsorption affinity for SD500 was: Co > Ni > Fe > Pb and that for CFA was: Fe > Ni > Pb > Co. This difference in sequence of sorption affinity can be attributed to the

difference in the physicochemical characteristics of SD500 and CFA as evidenced by their XRD patterns, FT-IR spectra, SEM images and surface area. In all the cases the sequence of binding affinity cannot be attributed to the different sizes of the metal ions due to the fact that even the hydrated metal ions are small compared to the average pore diameters of the adsorbents (Papandreou *et al*., 2007). From Table 4.6, it is clear that the adsorption capacities of CFA and CAC for Pb were comparable. Thus, given the low cost of CFA, it can then be recommended for Pb removal. Tao and Xiaqin (2008) carried out the adsorption of Pb^{2+} ions from aqueous solution in a batch system using granular active and obtained a maximum adsorption capacity of 2.337 mg/g.

Conversely, the removal of phenol by CAC, SAS, SD500 and CFA was better described by the Langmuir isotherm. It is observed that the experimental data deviate more in the case of the Freundlich (Figure 4.22 (d)) than the Langmuir model (Figure D3 (d)) for all the adsorbents. This is further verified by the regression coefficient values R^2 (Tables 4.6) of the linear plots. It is noted that the sequence of sorption affinity for phenol, i.e. CAC > SAS >SD500 > CFA is in accordance with the increase in surface area of the adsorbents with CAC having the highest and CFA having the lowest surface area. The applicability of the Langmuir isotherm suggests good monolayer coverage of sorbate on the sorbent surface in the concentration range studied. The excellent fitting of the Langmuir isotherm also points to the adsorption sites having equal activity towards phenol. This observation is not consistent with the heterogeneous nature of for example CFA which consists of different groups of surface adsorption sites such as ≡SiOH, ≡AlOH and ≡FeOH. Therefore, an explanation for the above experimental observation could be that phenol molecules have preferable access to a specific group of the surface adsorption sites (Papandreou *et al*., 2007).

Table 4.6

Freundlich and Langmuir isotherm constants for petrochemical wastewater

Adsorbent	Adsorbate	Langmuir			Freundlich		
		q_{max} (mg/g)	K_L (L/mg)	R^2	n	K_F (mg/g)	R^2
CFA	Cobalt	0.401	1.000	0.939	0.276	5.611	0.979
SD500	Cobalt	3.984	0.061	0.996	1.256	0.251	0.999
SAS	Cobalt	9.524	0.096	0.959	1.244	0.520	0.970
CAC	Cobalt	15.39	0.028	0.924	1.603	1.062	0.982
CFA	Nickel	1.078	1.064	0.971	0.575	4.365	0.983
SD500	Nickel	3.677	7.351	0.994	1.177	1.030	0.997
SAS	Nickel	4.016	10.826	0.975	2.439	3.639	0.990
CAC	Nickel	5.435	0.240	0.962	3.378	3.606	0.982
CFA	Iron	3.058	1.912	0.962	1.391	2.518	0.988
SD500	Iron	1.319	1.441	0.977	0.582	8.414	0.991
SAS	Iron	15.385	0.625	0.995	0.885	13.740	0.997
CAC	Iron	28.571	1.000	0.980	1.261	13.090	0.985
CFA	Lead	0.458	0.072	0.994	0.472	0.013	0.995
SD500	Lead	0.203	0.099	0.949	0.231	0.0001	0.990
SAS	Lead	0.464	0.107	0.928	0.249	0.0006	0.986
CAC	Lead	0.591	0.129	0.848	0.193	0.0003	0.990
CFA	Phenol	0.200	0.265	0.999	1.000	0.025	0.998
SD500	Phenol	5.400	0.512	0.984	0.189	0.003	0.954
SAS	Phenol	10.000	0.003	0.990	0.438	1.622	0.988
CAC	Phenol	19.600	0.317	0.995	1.214	4.645	0.974

4.6 Response surface methodology (RSM) and statistical analysis

Response surface methodology (RSM) is a collection of statistical and mathematical techniques useful for developing, improving, and optimizing processes in which a response of interest is influenced by several variables and the objective is to optimize this response. It has important application in the design, development and formulation of new products, as well as in the improvement of existing product design. It defines the effect of the independent variables, alone or in combination, on the processes. In addition to analyzing the effects of the independent variables, this experimental methodology generates a mathematical model which describes the process (Myers and Montgomery, 2002; Bas and Boyaci, 2007). In this study, it was justifiable to apply RSM to the treatment of synthetic petrochemical wastewater using CFA and SAS since no such studies have been reported in literature.

4.6.1 Coal fly ash (CFA)

Fitting of model equations

A 2^3 full-factorial design with four centre points leading to 12 experimental runs was performed using CFA and the results are presented in Table 4.7. It can be seen that the highest adsorption capacities for all the metals were obtained at low dose (20 g/l), high pH (6.0) and high C_o (75.0 mg/l) (i.e run 7) except for lead which had the maximum adsorption capacity at low dose, low pH and high initial concentration (run 5). Under these conditions for run 7, iron had the highest adsorption capacity (3.303 mg/g) followed by nickel (2.918 mg/g) and cobalt (1.118 mg/g) whereas lead had the least maximum q_e value (0.645 mg/g) obtained for run 5. It is interesting to note that this trend is in agreement with the sequence followed by the maximum monolayer adsorption capacity, q_{max} values calculated from the Langmuir isotherm in section 4.5.2. This observation further confirms that the binding affinity of heavy metals towards CFA follows the order: Fe > Ni > Co > Pb as explained in section 4.5.2. Also, this order accords well with the maximum percentage removals given in Table B6 (Appendix) as 100.0, 99.79, 97.44 and 89.85% for Fe, Ni, Co and

Pb, respectively. On the other hand, the highest phenol removal was observed at run 3 at low dose, high pH and low C_o (55.0 mg/l).

Table 4.7

The 2^3 factorial design with centre points for the independent variables for CFA

Run	Coded values			q_e (mg/g)				
	Dose	pH	C_o	Cobalt	Nickel	Iron	Lead	Phenol
1	-1	-1	-1	0.023	0.458	1.345	0.548	0.288
2	1	-1	-1	0.388	0.533	0.449	0.172	0.325
3	-1	1	-1	1.083	1.378	0.993	0.463	1.876
4	1	1	-1	0.361	0.459	0.331	0.136	0.677
5	-1	-1	1	0.060	0.055	1.848	0.645	0.036
6	1	-1	1	1.010	1.465	1.221	0.260	0.155
7	-1	1	1	1.118	2.918	3.303	0.568	0.214
8	1	1	1	1.102	1.520	1.101	0.173	0.817
9	0	0	0	1.085	1.534	1.181	0.150	0.956
10	0	0	0	1.084	1.523	1.171	0.158	0.976
11	0	0	0	1.085	1.541	1.164	0.148	0.977
12	0	0	0	1.083	1.524	1.170	0.146	0.967

The observed data given in Table 4.7 was used to fit a quadratic response surface model and the fitted equations for cobalt, nickel, iron, lead and phenol can be written, respectively, as:

$$q_{Co} = 1.08 + 0.072x_1 + 0.27x_2 + 0.18x_3 - 0.44x_1^2 - 0.26x_1x_2 + 0.16x_1x_3 + 0.015x_2x_3 \quad (4.1)$$

$$q_{Ni} = 1.53 - 0.10x_1 + 0.47x_2 + 0.39x_3 - 0.43x_1^2 - 0.48x_1x_2 + 0.11x_1x_3 + 0.26x_2x_3 \quad (4.2)$$

$$q_{Fe} = 1.17 - 0.55x_1 + 0.11x_2 + 0.54x_3 + 0.15x_1^2 - 0.17x_1x_2 - 0.16x_1x_3 + 0.23x_2x_3 \quad (4.3)$$

$$q_{Pb} = 0.15 - 0.19x_1 - 0.036 + 0.014x_3 + 0.22x_1^2 + 0.005x_1x_2 - 0.01x_1x_3 - 0.005x_2x_3 \quad (4.4)$$

$$q_{Phe} = 0.97 - 0.055x_1 + 0.35x_2 - 0.24x_3 - 0.42x_1^2 - 0.094x_1x_2 + 0.24x_1x_3 - 0.14x_2x_3 \quad (4.5)$$

where q_{Co}, q_{Ni}, q_{Fe}, q_{Pb} and q_{Phe} are the predicted adsorption capacities for cobalt, nickel, iron, lead and phenol, respectively. The variables x_1, x_2, x_3 are the coded values of the test variables, dose (g/l), pH and initial concentration (mg/l), respectively. For testing the fit of the models, the correlation coefficient, R^2 values were evaluated and it was observed that equation (4.5), which is the quadratic response surface model for phenol removal, had the R^2 (0.8754) value which was not close to 1 and the predicted adsorption capacities were not close to the experimental values. Thus, equation (4.5) was upgraded by adding a cross product term (Khuri and Cornell, 1987) and the upgraded model (equation (4.6)) was then fitted and used to describe phenol removal.

$$q_{Phe} = 0.97 - 0.055x_1 + 0.35x_2 - 0.24x_3 - 0.42x_1^2 - 0.094x_1x_2 + 0.24x_1x_3 - 0.14x_2x_3 + 0.21x_1x_2x_3 \quad (4.6)$$

The statistical significance of all the model equations was evaluated by the *F*-test and the analysis of variance (ANOVA). However, the *F*-test and ANOVA for all the adsorbates could not be outlined explicitly in this section. Thus, the response surface model equation for cobalt removal was chosen as an example (as in section 4.4) and its detailed ANOVA is summarized in Table 4.8. The ANOVA for the rest of the adsorbates is presented in Table E6 to E9. In this work, the model acceptance was made on the basis of 95% confidence level. The ANOVA for the cobalt quadratic model (Table 4.8) revealed that this regression model is statistically significant, as is evident from the Fisher's *F*-test with a very low probability value (<0.0001) i.e the associated Prob.> *F* value for the model is lower than 0.05 at 95% confidence level. In order for a term to be significant at this confidence level, the calculated probability should be lower than 0.05 (Bhatia *et al*., 2009). Therefore, the value of Prob. > *F* (i.e., the probability for the *F*-value to be higher than the calculated *F*-value in the

table to accept null hypothesis) for all terms (x_1, x_2 and x_3) as well as the dose-pH (x_1x_2) interaction and the dose-concentration interaction (is less than 0.05 indicating that these model terms are statistically significant. The standard deviation between the measured and the modeled results is only 0.02% and a relatively low coefficient of variation (CV=2.71%) indicates a better precision and reliability of the experiments carried out.

Table 4.8

Analysis of variance (ANOVA) for a quadratic model for cobalt removal

Source of variation	Sum of squares	Degree of freedom	Mean square	*F*-value	Prob.>*F* (p-value)
Model	2.15	7	0.31	670.46	< 0.0001
x_1	0.04	1	0.04	90.82	0.0007
x_2	0.60	1	0.60	1300.00	< 0.0001
x_3	0.26	1	0.26	561.75	< 0.0001
x_1^2	0.52	1	0.52	1132.45	< 0.0001
x_2^2	0	0	-	-	-
x_3^2	0	0	-	-	-
x_1x_2	0.53	1	0.53	1149.78	< 0.0001
x_1x_3	0.21	1	0.21	454.66	< 0.0001
x_2x_3	1.71E-03	1	1.71E-03	3.73	0.1255
Residual	1.83E-03	4	4.58E-04	-	-
Lack of Fit	1.83E-03	1	1.83E-03	28.23	-
Pure Error	2.75E-06	3	9.17E-07	-	-
Total	2.15	11	-	-	-

R^2 = 0.9991; Coefficient of Variance (CV) = 2.71%

For a model to be reliable, the response should be predicted with a reasonable accuracy by the model when compared with the experimental data. In this case, the model presented a high correlation coefficient (R^2 = 0.9991) and since there is a good

agreement between experimental data and predicted values (Figure 4.23), the model equation could be used to directly predict the adsorption capacity under variable conditions with respect to dose, solution pH and initial concentration. The model equations for Ni, Fe, Pb and phenol are all statistically significant since the model Prob. > *F* values are all less than 0.05 and their R^2 values are 0.9360, 0.9338, 0.9988 and 0.9999, respectively (Table E6 to E9 in Appendix).

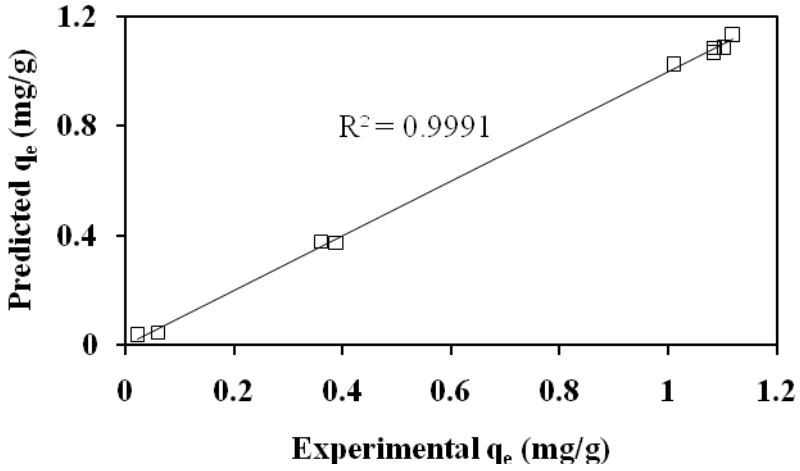

Figure 4.23. Parity plot of the experimental adsorption capacity and adsorption capacity predicted by the quadratic model equation for cobalt removal.

The three-dimensional response surface plots are generally the graphical representations of the regression equation and are presented in Figure 4.24 to 4.26 for cobalt removal from wastewater for which the values of adsorption capacity for different levels of the variables can be predicted. The main goal of response surface is to track efficiently for the optimum values of the variables such that the response is maximized. By analyzing the plots, the best response range can be calculated. Each response plot represents an infinite number of combinations of two test variables with the other maintained constant. It must be noted that the response surfaces for cobalt removal were chosen as an example to represent all the other metals studied (except for lead) since they showed the same trends.

Effects of dose and pH on metal removal

The combined effect of dose and solution pH at constant initial concentration was investigated using response surface methodology. The results are presented in the form of a 3-dimensional plot (Figure 4.24) which reveals that the uptake of cobalt increased with increasing pH and decreasing adsorbent dose, i.e, cobalt exhibited a greater affinity towards coal fly ash particularly at high pH and low dose. This trend predicted by the cobalt response surface model is consistent with the experimental results shown in Table 4.7, in which the highest adsorption capacity for cobalt (1.118 mg/g) was observed at low dose and high pH (run 7). The model equations for the other metals except lead predicted the same trend (response surfaces not shown) which implies that they followed the same sorption mechanism. Furthermore, the

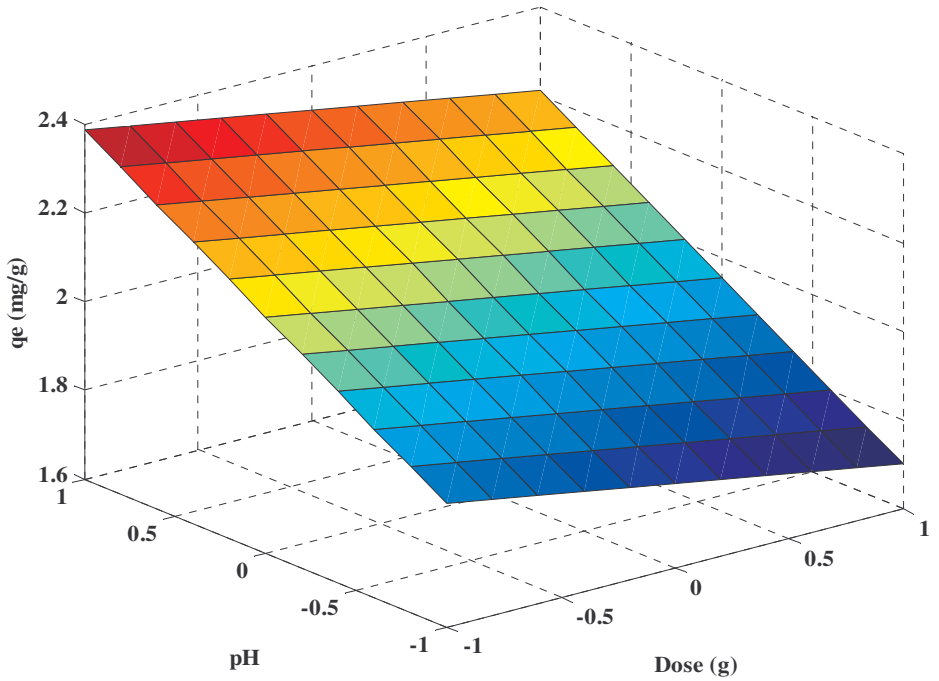

Figure 4.24. Response surface plot showing effects of adsorbent dose and pH on adsorption capacity of cobalt ions at constant initial concentration.

Matlab programs for plotting the response surfaces for Ni, Fe and Pb are presented in Appendix F. It was observed that lead showed an anomalous behaviour of increasing adsorption capacity with decreasing pH. This anomaly could not be explained in the present study.

From Figure 4.24, it is apparent that pH has a significant influence on the system and this is consistent with literature reports (Cho *et al*, 2005). The pH of solution determines surface charge of the adsorbent and the degree of ionization and speciation of the adsorbate. On the surface of the fly ash the functional oxidized groups are present as silica (SiO_2) and hematite (Fe_2O_3) (from characterization). Thus, it will be expected that the metal ions will be mostly adsorbed by silica, hematite or by a combined influence of these oxides (Panday *et al*., 1985) and also unburned carbon present in it (Bhattacharya *et al*., 2007). The surface of silica (SiO_2) has a high affinity towards metal ions (Bayat, 2002). The central ion of silicates (Si^{4+}) has a very strong affinity for electrons; therefore, the oxygen atoms that are bound to the silicon ions have a low basicity, making the silica surface act as a weak acid. The oxygen atoms on the silica surface are free to react with water, forming surface silanol (SiOH) groups. The acidity of the silanol (SiOH) groups determines the dependence of the charge of the silica surface on pH. As a result, at low pH the silica surface is positively charged and at high pH values it is negatively charged (Mohan and Gandhimathi, 2009).

Other solid materials such as Fe_2O_3 also show this same phenomenon of developing positive and negative charges depending on pH (Bayat, 2002). At low pH values (below 2.2, the pH_{pzc} for silica), a positive charge is developed on the surface of the coal fly ash resulting in poor sorption of the metal ions due to repulsion. At pH values above 2.2, the surface of coal fly ash is negatively charged and it becomes more negatively charged as the pH increases and thus the enhanced favorable electrostatic forces resulted in increased removal of the metal ions. Ricou-Hoeffer

et al. (2001) reported that alumina silicate compounds in coal fly ash may also be involved in the adsorption phenomena through a SiO bond with metallic ions.

It is often suggested that the adsorption of metal ions at the solid-solution interface is not governed by the "free" metal concentration, but by the much stronger adsorbed hydroxo, sulfato, carbonato and other metal species (Stumm and Bilinski, 1972):

$$M^{z+}_{(aq)} + nH_2O \Leftrightarrow M(OH)^{(z-n)}_n + nH^+ \quad (4.7)$$

The exact nature and distribution of hydroxo complexes depend on the concentration of the ligands, i.e. solution pH and on the soluble metal concentration. The presence of hydroxide ion (at high pH) seems to be the key reason for the enhanced removal. An alternative interpretation for the coincidence of adsorption and hydrolysis involves surface complex formation between "free" metal ions and deprotonated surface functional groups as (Panday *et al*., 1985):

$$\equiv SiOH + M^{z+} \Leftrightarrow (\equiv SiO)M^{(z-1)} + H^+ \quad (4.8)$$

$$2(\equiv SiOH) + M^{z+} \Leftrightarrow (\equiv SiO)_2 M^{(z-2)} + 2H^+ \quad (4.9)$$

The decrease in adsorption capacity of coal fly ash with an increase in adsorbent dose could be due to the aggregation or overlapping of adsorption sites caused by overcrowding of coal fly ash particles. This results in a decrease in total adsorbent surface available to the metal ions and an increase in diffusional path length. Particle interaction may also desorb some of the sorbate that is only loosely and reversibly bound to the coal fly ash surface (Shukla *et al*., 2002). At high adsorbent dose, some adsorption sites remain unsaturated during the adsorption process because they are not accessible.

Effects of dose and initial concentration

The dependence of adsorption capacity on dose and initial concentration at constant pH is presented in Figure 4.25. It is apparent that the adsorption capacity of coal fly

ash increased with increasing initial concentration and decreasing dose. An increase of cobalt uptake by increasing initial concentration is a result of the increase in the driving force of the concentration gradient between the adsorbate in the bulk solution and the solid phase, rather than increase in the initial cobalt ion concentration (Han *et al*., 2006; Srivastava *et al*., 2006). If the concentration of cobalt ions in the solution were higher, the active sites of coal fly ash would be surrounded by more cobalt ions, and the process of adsorption would be carried out more sufficiently (Han *et al*., 2006). Therefore, the value of q_e increased with increasing initial cobalt ions concentration. These results accord well with the findings of Ghorbani *et al*. (2008). The same trend was followed by all the other metals studied.

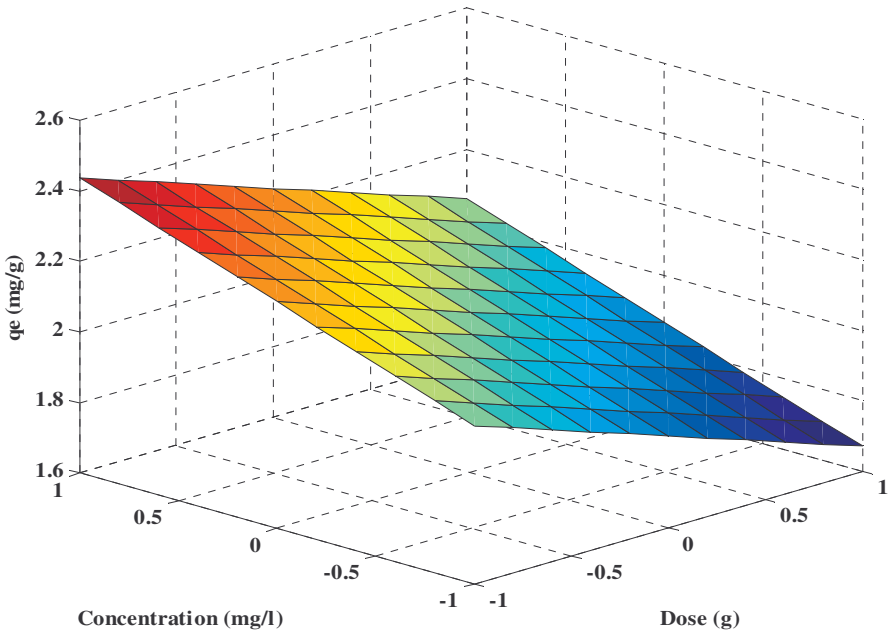

Figure 4.25. Response surface plot showing effects of adsorbent dose and initial concentration on adsorption capacity of cobalt ions at constant pH.

Effects of pH and initial concentration

The combined effect of solution pH and initial cobalt ion concentration at constant dose was investigated. Figure 4.26 reveals that both parameters have an impact on

the adsorption capacity of coal fly ash. It is clear that the cobalt uptake increases with increasing pH and this trend is similar to that observed in Figure 4.24. Also, it can be seen from Figure 4.26 that the predicted q_e values increase with increasing initial concentration of cobalt and this further confirms the trend observed in Figure 4.25. These predictions are consistent with the experimental results shown in Table 4.7, in which the highest cobalt adsorption capacities (1.118 and 1.102 mg/g) were both observed at high pH and high initial concentration (run 7 and 8).

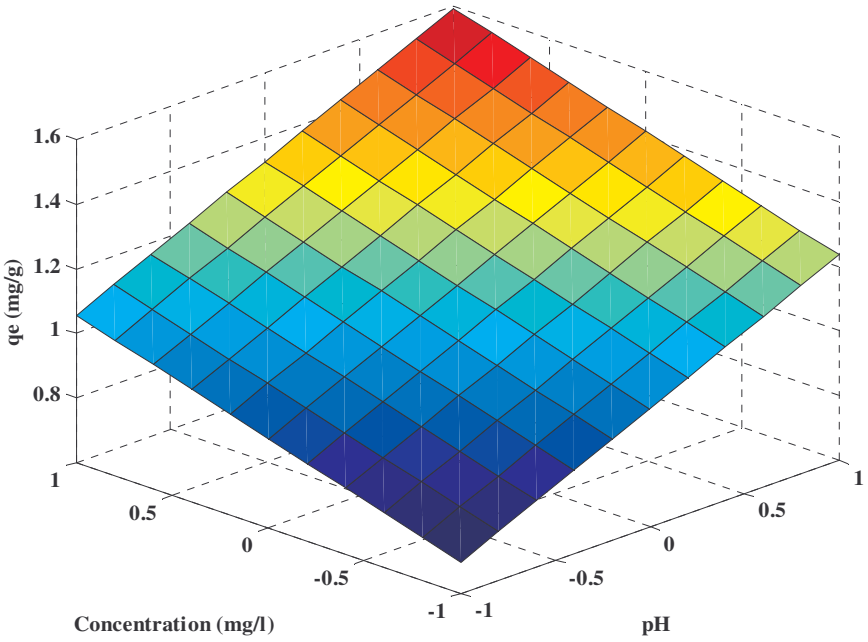

Figure 4.26. Response surface plot showing effects of pH and initial concentration on adsorption capacity of cobalt ions at constant dose.

Determination of optimum conditions for cobalt removal by CFA

The optimum conditions for removal of each adsorbate studied could have been determined separately. However, for simplicity, cobalt removal using CFA was chosen as an example and the method for determining the optimum conditions has been clearly outlined. The predicted optimal conditions were calculated using the

model equation for cobalt removal (equation (4.1)) following the principle that the stationary point (minimum or maximum point) of the second order equation is the point where the first derivative of the function equals to zero (Bas and Boyaci, 2007: Let $y = f(x_1, x_2, x_3)$ such that:

$$y = \beta_o + \beta_1 x_1 + \beta_2 x_2 + \beta_3 x_3 + \beta_{11} x_1^{\,2} + \beta_{22} x_2^{\,2} + \beta_{33} x_3^{\,2} + \beta_{12} x_1 x_2 + \beta_{13} x_1 x_3 + \beta_{23} x_2 x_3 \quad (4.10)$$

where y is the response predicted by the model whilst x_1, x_2, x_3 are the coded forms of dose, pH and initial concentration, respectively. The term β_o is the offset term, β_1, β_2 and β_3 are linear terms, β_{11}, β_{22} and β_{33} are the quadratic terms whilst β_{12}, β_{13} and β_{23} are the interaction terms.

The stationary point is found by computing $\partial y/\partial x_1$, $\partial y/\partial x_2$ and $\partial y/\partial x_3$ and setting them equal to zero:

$$\partial y / \partial x_1 = \beta_1 + 2\beta_{11} x_1 + \beta_{12} x_2 + \beta_{13} x_3 = 0$$

$$\partial y / \partial x_2 = \beta_2 + 2\beta_{22} x_2 + \beta_{12} x_1 + \beta_{23} x_3 = 0 \quad (4.11)$$

$$\partial y / \partial x_3 = \beta_3 + 2\beta_{33} x_3 + \beta_{13} x_1 + \beta_{23} x_2 = 0$$

The system of equations is solved using Matlab software to find the values of x_1, x_2 and x_3. The calculated values of x_1, x_2 and x_3 indicate the coded value of the independent parameters that give the highest or lowest response. To determine whether the stationary point is minimum or maximum, the second order derivative of the model equation is used. If it is a negative value, the optimum point is a maximum, but if it is a positive value, the optimum point is a minimum.

The stationary points were calculated using Matlab in accordance with the method described by Myers and Montgomery (2002) which makes use equation (4.12) as:

$$x_0 = -\frac{\beta^{-1} b}{2} \quad (4.12)$$

where x_o is a (3 x 1) matrix made up of stationary points in coded form (x_1, x_2 and x_3), β is a symmetric (3 x 3) matrix made up of a diagonal of estimated coefficients of the quadratic terms from the model equation and the other elements are the estimated coefficients of the interaction terms divided by 2, b is a (3 x 1) matrix made up of the coefficients of the linear terms of the model equation (Myers and Montgomery, 2002). A Matlab program for calculating the optimum conditions in coded form and the optimum adsorption capacity for cobalt by CFA is given in Appendix F. The conditions in coded form are: x_1 = -1.2703, x_2 = 1.5497 and x_3 = 4.0183 giving a predicted optimum adsorption capacity of 2.1303 mg/g. The optimum point lies outside the experimental region used in this study: $-1 \leq x_i \geq +1$; i = 1, 2, 3; where x_i are the coded variables. This explains why the response surfaces are flat (Figure 4.24 to 4.26). However, the fitted model has been proven to be adequate (Table 4.8 and Figure 4.23) and hence, it can be used to locate areas in the experimental region, or outside the experimental region (Khuri and Cornell, 1987) which is the present case. The coded optimum conditions were converted to the actual variable using equation (4.11) and equation (4.12) which was derived through extrapolation:

$$X_1 = X_{1L} - \frac{(X_{1H} - X_{1L})(x_{1L} - x_1)}{(x_{1H} - x_{1L})} \tag{4.11}$$

$$X_i = \frac{(X_{iH} - X_{iL})(x_i - x_{iL})}{(x_{iH} - x_{iL})} + X_{iL}, \quad i = 2, 3 \tag{4.12}$$

where X_{1H} and X_{1L} are the actual high and low levels of the variable X_1 which is dose (g/l), respectively, x_{1H} and x_{2L} are the coded high and low levels of dose and x_1 is the coded variable being converted. The variables X_{iH} and X_{iL} are the actual high and low levels of X_i (i.e pH or C_o), respectively, x_{iH} and x_{iL} are the coded high and low levels of the variable X_i, respectively, and x_i is the coded variable that is being converted. The optimum conditions in actual variables are: dose = 14.594 g/l, pH = 7.0994 and C_o = 150.4575 mg/l.

Verification of predicted optimum conditions

The estimation capability of the model equation for cobalt removal using CFA was tested by carrying out replicated confirmatory experiments (Table F1 in Appendix) using the optimum conditions as suggested by the model in the presence of phenol and other heavy metals at their respective zero level concentrations. The experimental adsorption capacity for cobalt at optimum condition was found to be 1.9358 mg/g with a percentage error of 9.1%. Thus, the predicted and the experimental adsorption capacity for cobalt (2.1303 mg/g) were close which confirms the validity of the fitted model.

In this study, the optimum conditions for removal of cobalt ions by CFA were determined as an example due to the simplicity of the method. However, it is possible to determine the conditions that will maximize the removal of all the adsorbates once and this method is called multiple response optimization. Multiple response surface optimization is done using the constrained optimization technique (Myers and Montgomery, 2002). These methods are complex and are beyond the scope of the present study.

Effects of operating parameters on phenol removal by CFA

The adsorption of phenol by CFA was found to increase with pH and decreasing dose (Figure 4.27 a). Thus, high adsorption capacities were observed at high pH and low dose. This trend is similar to that observed for the metal ions. Sarkar and Acharya, (2006) tested the sorption of phenol and other organic compounds using fly ash in the pH range of 2 to 11. They observed low adsorption capacities at both low and high pH values with the highest adsorption capacity being recorded in the intermediate region of pH 3.78 to 7.91. However, in the present study, pH above 6.0 could not be tested in order to avoid metal hydroxides precipitation from the synthetic petrochemical wastewater.

The pH dependent behaviour of phenol shown in Figure 4.27 can be well explained considering the pH_{pzc} of silica. At low pH values (below 2.2, the pH_{pzc} of silica) a positive charge is developed at the silica surface in CFA. At the same time at lower pH, the presence of H^+ suppresses the ionization of phenol, hence low adsorption/ uptake results. As pH increases to the region 3.78 to 6, the surface character of CFA finds a suitable condition to accommodate the phenolate ions, thereby improving the uptake. Although pH above 6 was not tested in this study, Sarkar and Acharya (2006) reported that from pH of around 7.91 onwards, phenol completely ionizes forming the phenolate ions and is repelled by the negatively charged surface of the CFA resulting in a decrease in phenol uptake. On the other hand, Figure 4.27 (b) reveals that the adsorption capacity of phenol decreases with increasing initial concentration, however, the cause for this trend was not readily apparent.

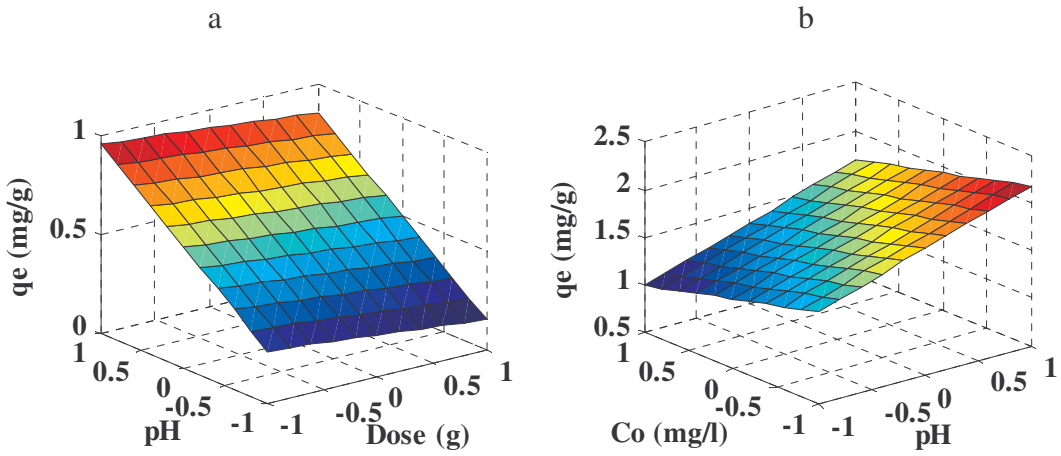

Figure 4.27. Adsorption capacity as a function of: (a) pH and dose at constant initial concentration and (b) initial concentration and pH at constant dose for phenol removal.

4.6.2 Steam activated sawdust (SAS)

Fitting of model equations

A 2^3 full-factorial design with four centre points leading to 12 experimental runs was performed using SAS and the results are presented in Table 4.9. The highest

adsorption capacities of SAS for all the metal ions were observed at a combination of low dose, high pH and high initial concentration i.e run 7 (Table 4.9). This observation was also made for metal removal using CFA. Thus, it can be inferred from these observations and the FT-IR results that the mechanism of heavy metal adsorption in both CFA and SAS could be similar (except for lead) although the active sites in CFA and SAS are different. Comparing the q_e values in Table 4.7 (for CFA) and Table 4.9 (for SAS), it is apparent that SAS performed better than CFA and this could be attributed to the high surface area and pore volume of SAS. Further, SAS also proved to be better than CFA in the removal of phenol. The

Table 4.9

The 2^3 factorial design with centre points for the independent variables for SAS

Run	Coded values			q_e (mg/g)				
	Dose	pH	C_o	Cobalt	Nickel	Iron	Lead	Phenol
1	-1	-1	-1	0.245	0.900	1.845	1.050	6.157
2	1	-1	-1	0.658	0.762	0.910	0.763	2.136
3	-1	1	-1	2.360	2.435	2.540	2.825	10.950
4	1	1	-1	0.797	0.812	0.847	0.983	3.594
5	-1	-1	1	0.575	1.375	4.235	6.335	16.757
6	1	-1	1	1.852	2.738	2.680	2.228	5.639
7	-1	1	1	4.770	8.045	7.660	6.865	22.482
8	1	1	1	2.285	2.987	2.553	2.273	7.506
9	0	0	0	2.260	3.250	2.573	2.233	6.564
10	0	0	0	2.263	3.255	2.568	2.245	6.564
11	0	0	0	2.268	3.245	2.573	2.340	6.556
12	0	0	0	2.255	3.255	2.573	2.323	6.545

highest q_e value for phenol removal using SAS was 22.482 mg/g obtained by a combination of low dose, high pH and high initial concentration i.e run 7. This is in

contrast with the highest q_e value (1.876 mg/g) of CFA which was obtained under similar conditions. These phenol adsorption results are consistent with the q_{max} values discussed in section 4.5.2 which shows that SAS is a better adsorbent than CFA in terms of metal and phenol removal within the operating range tested.

The observed data given in Table 4.9 was used to fit a quadratic response surface model and the fitted equations for cobalt, nickel, iron, lead and phenol can be written, respectively, as:

$$q_{Co} = 2.26 - 0.29x_1 + 0.86x_2 + 0.68x_3 - 0.57x_1^2 - 0.72x_1x_2 - 0.00725x_1x_3 + 0.30x_2x_3 \quad (4.13)$$

$$q_{Ni} = 3.25 - 0.68x_1 + 1.06x_2 + 1.28x_3 - 0.74x_1^2 - 0.99x_1x_2 - 0.24x_1x_3 + 0.67x_2x_3 \quad (4.14)$$

$$q_{Fe} = 2.57 - 1.16x_1 + 0.49x_2 + 1.37x_3 + 0.34x_1^2 - 0.54x_1x_2 - 0.50x_1x_3 + 0.33x_2x_3 \quad (4.15)$$

$$q_{Pb} = 2.29 - 1.35x_1 + 0.32x_2 + 1.51x_3 + 0.63x_1^2 - 0.25x_1x_2 - 0.82x_1x_3 - 0.18x_2x_3 \quad (4.16)$$

$$q_{Phe} = 6.56 - 4.68x_1 + 1.73x_2 + 3.69x_3 + 2.85x_1^2 - 0.90x_1x_2 - 1.84x_1x_3 + 0.17x_2x_3 \quad (4.17)$$

The statistical significance of all the model equations was evaluated by the *F*-test and the ANOVA which is presented in Table E10 to E14 (Appendix). Models found to have a probability value (*p*-value) less than 0.05 are considered to be statistically significant. Thus, it is apparent from the ANOVA that the Prob. > *F* values for all the models were lower than 0.05 at 95 % confident level which means that they were all statistically valid. Additionally, the R^2 values for Co, Ni, Fe, Pb and phenol were 0.9756, 0.9279, 0.9716, 0.9963 and 0.9999, respectively. Thus, these models were used to predict the adsorption capacities of SAS for the heavy metals and phenol presented in Table E1 to E5 (Appendix) along with the experimental adsorption capacity values. Also, the Matlab programmes for plotting the response surfaces are given in Appendix G. Some of the trends observed for the interactive effects of operating parameters were similar to those for CFA discussed in section 4.6.1

especially for cobalt, nickel and iron, the only difference being that higher q_e values were predicted for SAS than CFA in all cases.

Effects of operating parameters on metal removal by SAS

At constant initial concentration, it was found that the adsorption capacity of SAS for heavy metals increased with increasing pH and decreasing dose for all the metals studied. This pH dependence phenomenon can be explained by the surface charge of the adsorbent and the H^+ ions present in the solution. At low pH the cations compete with the H^+ ions in the solution for the active sites and therefore lower adsorption. The surface charge of the biomass materials is a strong function of the pH (Amarasinghe and Williams, 2007). At high pH values, surface of the adsorbent has a higher negative charge which results in higher attraction of cations. It can be assumed from these results and the FT-IR spectra of SAS (Figure 4.9) that the possible adsorption mechanism is probably due to ion exchange. High concentration of H^+ ions at low pH may change the direction of reversible ion exchange equilibrium to give low q_e values (Yu *et al*., 2001). At a high pH, low concentration of H^+ ions means less competition for the adsorption site on SAS particles which result in high q_e values. The FT-IR spectra showed that the —OH and —COOH groups took part in the sorption process. However, the sites responsible for the sorption process might not be exclusively due to the —OH and —COOH groups, other sites on the adsorbent may also contribute to the sorption process and physical adsorption is quite probable (Yu *et al*., 2001). The decrease in adsorption capacity with increasing dose could be due to the aggregation or overlapping of adsorption sites caused by overcrowding of the adsorbent particles as explained in section 4.6.1. The combined effect of dose and initial concentration at constant pH has also been analyzed and the adsorption capacity was found to increase with increasing initial concentration and decreasing dose. An increase in metal uptake by increasing initial concentration is a result of the increase in the driving force of the concentration gradient between the adsorbate in the bulk solution and the solid phase as explained in section 4.6.1.

Effects of operating parameters on phenol removal by SAS

The influence of solution pH and dose at constant initial concentration on the extent of adsorption of phenol is shown in Figure 4.28 (a). It can be seen that adsorption of phenol increases with increase in pH and decrease in dose in the tested region. It has been generally known that the solution pH influences the degree of the ionization of phenolic compounds and surface charge of adsorbents and there by it control the adsorption process. The pH dependence of phenol removal can be explained by the fact that at lower pH values the presence of H^+ ions suppresses the ionization of phenol and hence its uptake on a polar adsorbent is reduced (Rengaraj *et al*.,2002). In this study, the tested pH range was from 2 to 6 to avoid metal hydroxide precipitation from the wastewater, however; in a study by Rengaraj *et al*. (2002) it was found that phenol uptake increased from pH 2 to 5, remained constant from pH 5 to 10 then decreased at higher pH values (above 10). In the higher pH range phenol forms salts which readily ionize leaving a negative charge on the phenolic group. At the same time the presence of OH^- ions on the adsorbent prevents the uptake of phenolate ions.

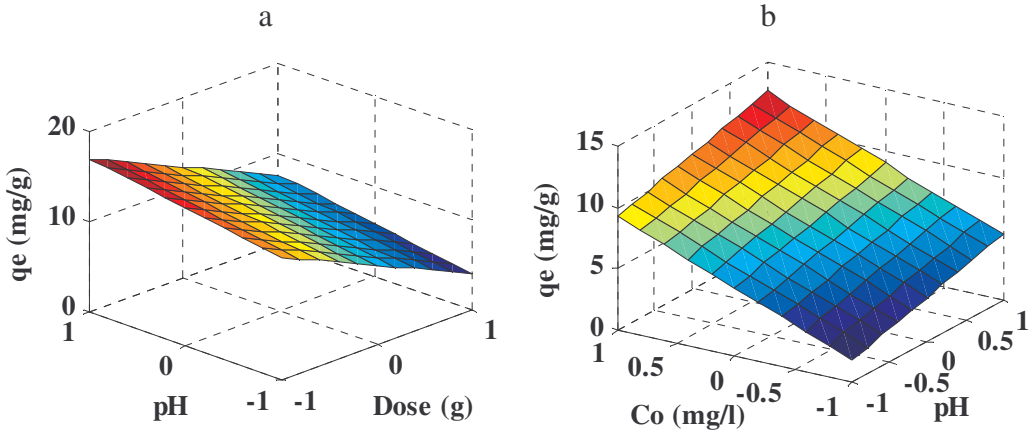

Figure 4.28. Adsorption capacity as a function of: (a) pH and dose at constant initial concentration and (b) initial concentration and pH at constant dose for phenol removal.

The adsorption capacity of SAS for phenol increased with increasing initial concentration and increasing pH at constant dose (Figure 4.28 b). This is in contrast with CFA which had higher adsorption capacities for phenol at low initial concentration. The concentration dependence of phenol removal by SAS can be explained by the fact that the initial concentration provides an important driving force to overcome all mass transfer resistances of phenol between the aqueous and solid phases (Kennedy *et al*., 2007). Hence, higher concentration of phenol enhances the adsorption process.

4.7 Dynamic column studies

Batch equilibrium and kinetic tests are often complemented with dynamic column studies to determine system size requirements, contact time, etc, and these parameters can be obtained from the breakthrough curves (Hamdaoui, 2009). Thus, equilibrium, kinetic and dynamic data are required for a sound engineering design of water treatment plants as the results obtained from the batch studies only may not be directly applied for field applications in the treatment of wastewater (Kumar and Bandyopadhyay, 2006).

Column adsorption tests were carried out using two low cost adsorbents (SD500 and SAS) whereas commercial activated carbon (CAC) was used for comparison purposes. Although SAS performed better in batch experiments as compared to SD500, more column tests were conducted using SD500. This decision was made on the basis of the preparation procedures of these two adsorbents and also the adsorption potential shown by SD500 in batch experiments. The preparation of SAS requires the use of high temperatures (up to 800°C) as compared to SD500 whose preparation method uses relatively low temperatures (up to 500°C). In addition, no gases are involved in the preparation of SD500; hence the method is simple to effect. On the other hand, an attempt was made to test an industrial by-product (CFA) in column adsorption experiments. However, there was severe column clogging which made it difficult to use CFA in an adsorption column. This was due to the fact that

the CFA was transformed into an impermeable solid concrete after a short period of time.

4.7.1 Effect of bed height

Contact time is most important in the design of fixed bed adsorption columns and therefore bed height, *Z* is a major design parameter since it determines contact time. In this study, breakthrough was considered to have occurred when the effluent concentration reached the maximum allowable discharged limits according to the South African Water Quality Guidelines (DWAF, 1996). Further, saturation was assumed to have occurred when the effluent concentration was equal to 95% of the influent concentration (C/C_o= 0.95) (Estevinho *et al*., 2007). The effect of changing bed height (10, 20 and 30 cm) was investigated by carrying out column tests using synthetic petrochemical wastewater consisting of 90 mg/l (Co(II), Ni(II), Fe(II) , Pb(II) and phenol) at pH 2.6 and flow rate of 5ml/min. Furthermore, the breakthrough curves were constructed as C_t/C_o versus time.

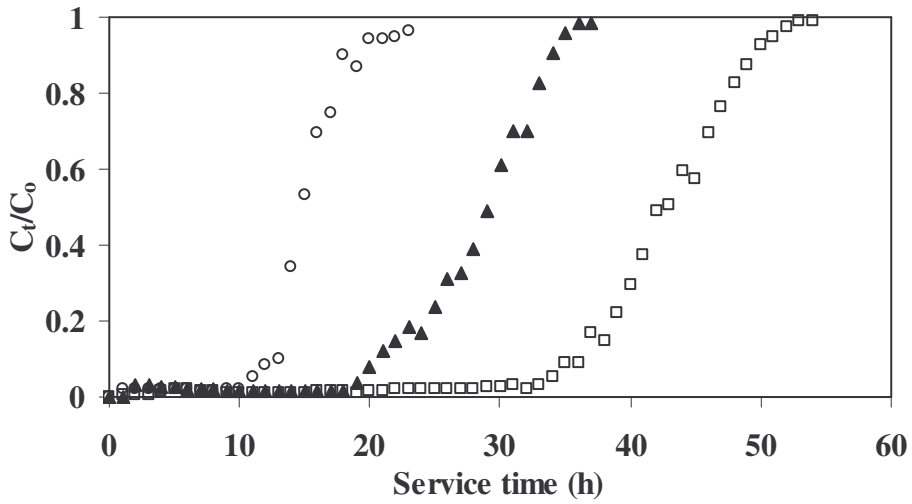

Figure 4.29. Effect of bed height on breakthrough curves of phenol removal by SD500 at 10 cm (○), 20 cm (▲) and 30 cm (□) bed height. (flow rate = 5 ml/min, pH = 2.6, influent phenol and metal concentration = 90 mg/l).

The observed breakthrough curves at three different bed heights (10, 20 and 30 cm) for phenol removal at a constant flow rate, Q_w of 5.0 ml/min are shown in Figure 4.29 (typical S-shaped curves). The time needed to reach the breakthrough point was lower for 10 cm bed depth than the rest. The breakthrough times, t_B and exhaustion times, t_E increased with increasing bed height from 10 to 30 cm. Decreasing the bed height caused the breakthrough curves to become steeper showing faster saturation, which resulted in early exhaustion of the bed. The increase in phenol uptake with increase in bed height was due to the increase in the surface area of the adsorbent, which provided more binding sites for adsorption. Thus, beds of increased height may be required for phenol adsorption since the rate at which the adsorption zone travels through the column decreases with increasing bed height (Walker and Weatherley, 1997). As bed height increased, phenol had more contact time with SD500 that resulted in higher removal efficiency.

Table 4.10

Breakthrough and exhaustion times for different bed heights

Adsorbate	Bed height, Z					
	10 cm		20 cm		30 cm	
	t_B (h)	t_E (h)	t_B (h)	t_E (h)	t_B (h)	t_E (h)
Phenol	11.00	21.30	19.50	34.00	34.20	49.00
Cobalt	0.085	1.500	0.107	1.935	0.256	2.983
Nickel	0.060	1.492	0.073	1.923	0.253	2.500
Iron	0.055	1.052	0.067	1.263	0.240	2.380
Lead	0.047	1.003	0.062	1.168	0.220	2.000

Although an increase in bed height increased the breakthrough time, a very high bed height is not practical for a single column; instead multiple-beds should be designed (Netpradit *et al*., 2004). On the other hand, the breakthrough and exhaustion times corresponding to phenol and the heavy metals at different bed heights and constant flow rate (5.0 ml/min) are shown in Table 4.10. Additionally, the breakthrough

curves at different bed heights for the heavy metals are shown in Figure 4.30 and it can be seen that the breakthrough and saturation times increased with an increase in bed height as shown in Table 4.10. As the value of Z increased, the metal ions had sufficient time to diffuse into whole mass of SD500 that resulted in an increase in t_B.

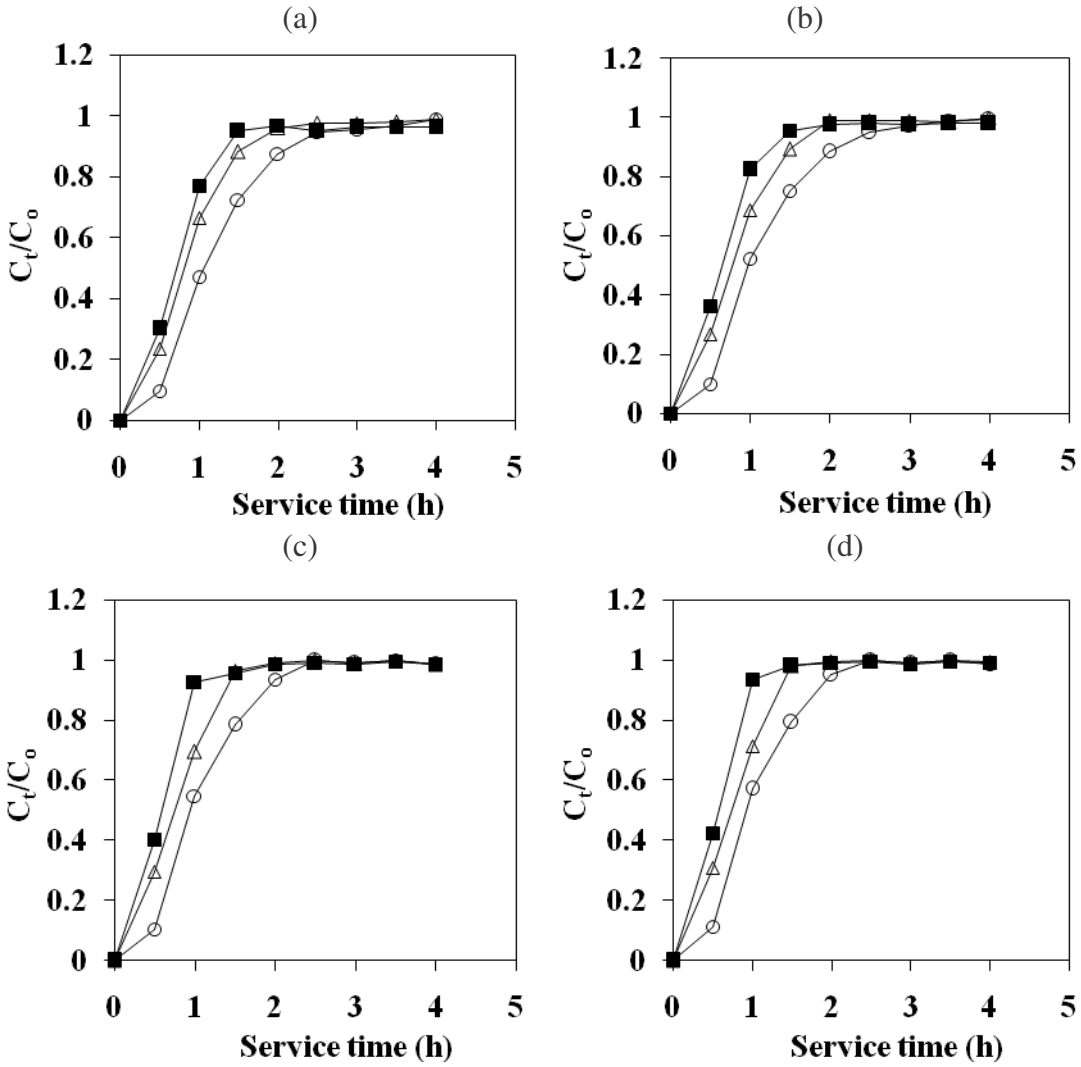

Figure 4.30. Effect of bed height on breakthrough curves of: (a) cobalt, (b) nickel, (c) iron and (d) lead removal by SD500 at 10 cm (■), 20 cm (Δ) and 30 cm (○) bed height. (Flow rate = 5 ml/min, pH = 2.6, column diameter = 2.5 cm, influent phenol and metal concentration = 90 mg/l).

It is evident from the t_B values that the binding affinity for the metals on SD500 follows the order: Co > Ni > Fe > Pb and this order is consistent with the q_{max} values discussed in section 4.5.2. It is apparent from the breakthrough times, t_B (Table 4.10) that SD500 has high binding affinity for phenol than the heavy metal and this is consistent with the batch experimental results (section 4.5.2). The shorter breakthrough times obtained for the heavy metals could be due to the competition from the H^+ ions at pH 2.6.

4.7.2 Effect of aspect ratio

The aspect ratio is defined as the bed depth-to-diameter ratio (Celenza, 2000). Figure 4.31 shows the effect of aspect ratio on breakthrough time, t_B under constant flow rate, pH and initial concentration. Generally, the increase of aspect ratio induces the enhancement of adsorption capacity through increase of contacting probability (Kim *et al*., 2006b). It can be seen from Figure 4.31 that increasing the aspect ratio

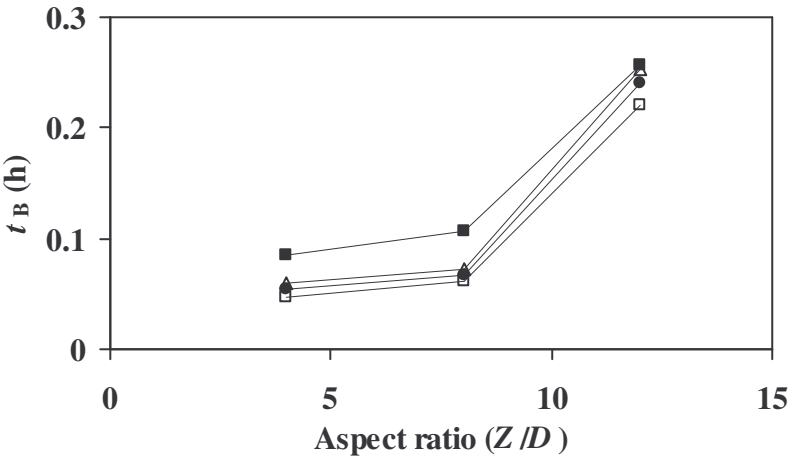

Figure 4.31. Effect of aspect ratio on breakthrough time, t_B in the removal of cobalt (■), nickel (Δ), iron (●) and lead (□) using SD500. (Flow rate = 5 ml/min, pH = 2.6, column diameter = 2.5 cm, influent phenol and metal concentration = 90 mg/l).

results in an increase in breakthrough time. This means that the column will have a longer service time at high aspect ratio. However, a too large aspect ratio is not essential when designing adsorption process in field application (Pan *et al*., 2005).

4.7.3 Effect of initial concentration

Once the breakthrough time was determined, the breakthrough capacity, Q_B, of SD500, i.e the amount adsorbed on SD500 at the breakthrough point expressed in mg of adsorbate adsorbed per gram of adsorbent was calculated as (Goel *et al*., 2005):

$$Q_B = \frac{(t_B \times Q_w \times C_0)}{m} \tag{4.18}$$

where t_B is the breakthrough time (min), Q_w is the flow rate of the influent wastewater (l/min), C_o is the inlet concentration (mg/l) and m is the mass (g) of the dry SD500.

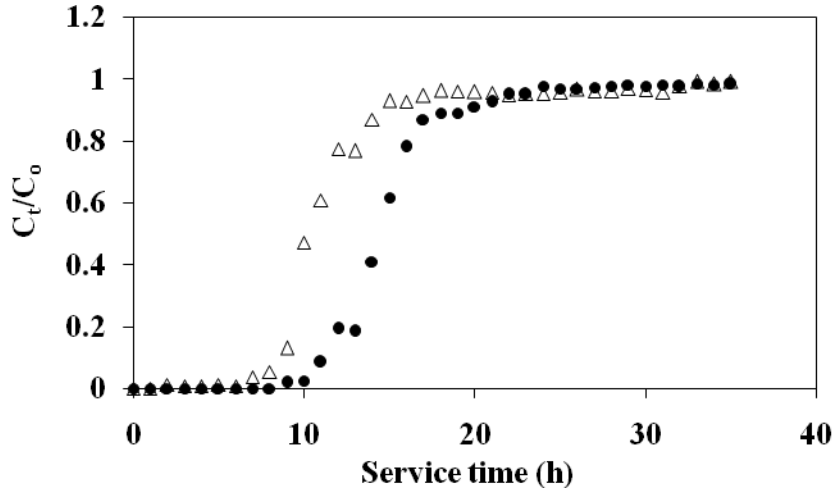

Figure 4.32. Effect of initial concentration on breakthrough curves of phenol removal at 180 mg/l (Δ) and 90 mg/l (●) using SD500 (Flow rate = 5 ml/min, pH = 2.6, column diameter = 2.5 cm, influent metal concentration = 50 mg/l, bed height = 10 cm).

It can be observed from Figure 4.32 that the breakthrough time increased from 8.0 to 10.8 h when the phenol concentration was reduced from 180.0 mg/l to 90.0 mg/l. This means that a higher phenol inlet concentration saturates the SD500 particles more rapidly. As for the heavy metals, cobalt was selected as an example to demonstrate the effect of initial metal ion concentration on the breakthrough curves for metal removal (Figure 4.33). It is clear that an increase in cobalt concentration from 25 mg/l to 50 mg/l resulted in a decrease in breakthrough time from 0.353 to 0.238 h. Thus, the breakthrough capacity of SD500 increased with an increase of initial concentration for both phenol and cobalt (Table 4.11). Similar trends were reported by Goel *et al*. (2005). A high concentration difference between the adsorbate on SD500 and the adsorbate in solution (concentration gradient) provides a high driving force for the adsorption process, which may explain why higher adsorption capacities were achieved at the high concentrations (Vazquez *et al*., 2006).

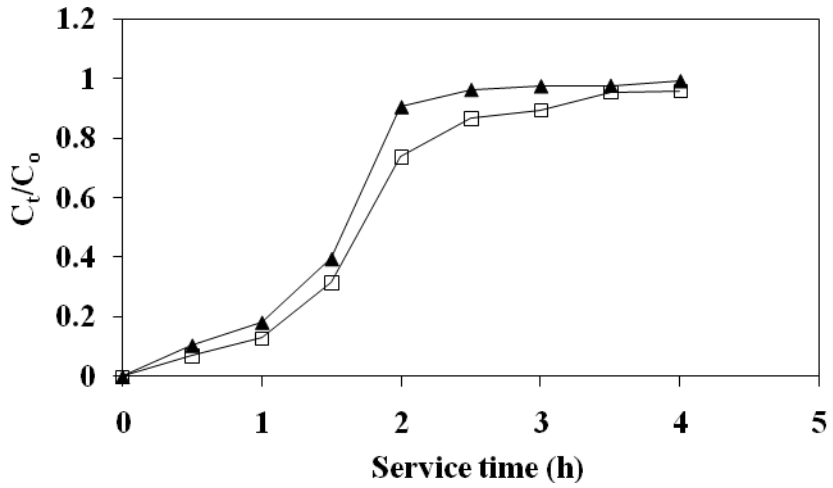

Figure 4.33. Effect of initial concentration on breakthrough curves of cobalt removal at 50 mg/l (▲) and 25 mg/l (□) using SD500 (flow rate = 5 ml/min, pH = 2.6, column diameter = 2.5 cm, influent phenol concentration = 180 mg/l, bed height = 10 cm).

The effects of initial metal ion concentration on the breakthrough curves of phenol and vice versa were investigated at pH 2.6 and the results are presented in

Figure 4.34. It is clear from Figure 4.34 (a) that changing the initial metal concentration from 50 to 90 mg/l did not have a significant effect on the breakthrough curve of phenol (90 mg/l) removal. Thus, the effect of competitive adsorption of the

Table 4.11

Breakthrough capacity at different concentrations

C_o (mg/l)	t_B (h)	t_E (h)	Q_B (mg/g)
Phenol			
90	10.8	21.48	35.65
180	8.0	17.06	52.81
Cobalt			
25	0.353	3.49	0.32
50	0.238	1.99	0.44

metal ions in the multi-component system on the phenol adsorption by SD500 was minimal. In Figure 4.34 (b), cobalt was selected as an example to represent the metal ions and it can be seen that the breakthrough curves for cobalt removal in the presence of 90 and 180 mg/l phenol were almost identical. It can therefore be inferred from these results that the behaviour of metal ions in the SD500-column are not influenced by phenol as the behaviour of phenol is not influenced by the metal ions. This could imply that metal ions and phenol are not adsorbed onto similar active sites. Lee *et al*. (2003) made similar observations in the removal of Pb, Cr, Cd and phenol using activated carbon prepared from coconut shells.

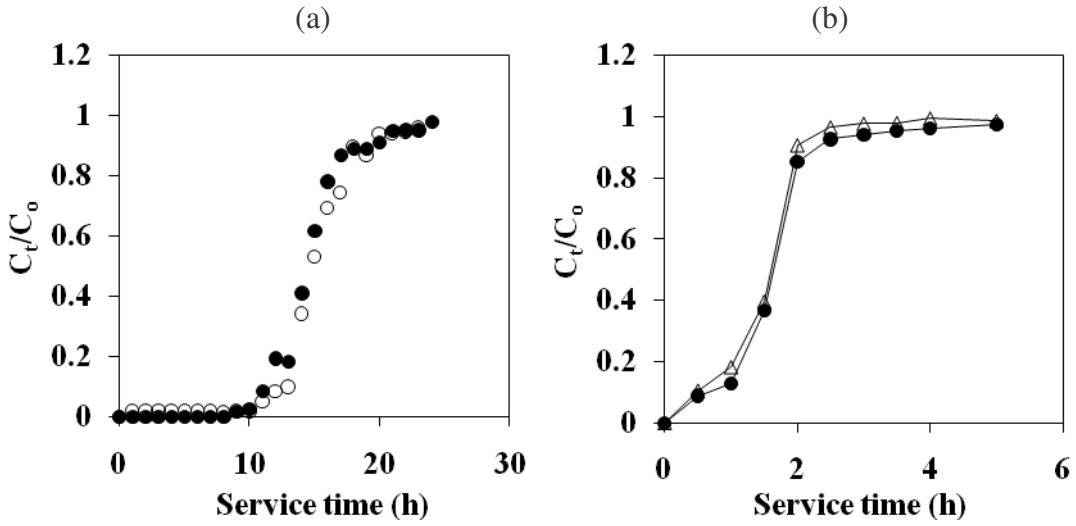

Figure 4.34. Breakthrough curves for removal of: (a) 90 mg/l phenol in the presence of 50 mg/l (●) and 90 mg/l (○) heavy metal ions, (b) 50 mg/l cobalt in the presence of 90 mg/l (●) and 180 mg/l (Δ) phenol at 10 cm bed height. (flow rate = 5 ml/min, pH = 2.6, column diameter = 2.5 cm).

In another study, Faur-Brasquet *et al*. (2002) demonstrated that at high solution pH, the adsorbed phenol is in the phenolate form ($C_6H_5O^-$) and may form some ligands with metal cations and thus, the following reaction may occur which induces an increase in metal ion removal as phenol concentration increase:

$$s - C_6H_5O^- + M^{2+} \rightarrow s - (C_6H_5O - M)^+ \qquad (4.19)$$

where '*s*' is the adsorbent and M^{2+} is the metal ion. However, in the present study a pH of 2.6 was used and at this pH, phenol is in the form C_6H_5OH due to suppression of ionization by H^+ ions and hence there is no ligand formation and this explains why there was no increase in adsorption of metal ions with increase in phenol concentration.

4.7.4 Effect of type of adsorbent

The breakthrough curves obtained for the different adsorbents exhibited almost similar shapes (Figure 4.35). A comparison of the adsorbents in terms of the breakthrough time, at an influent concentration of 90 mg/l for all the adsorbates reveals that CAC exhibited the longest breakthrough time for both phenol and cobalt removal (Table 4.12). Overall, the breakthrough and exhaustion time obtained for the different adsorbents at identical operating conditions exhibited the following descending order: CAC > SAS > SD500. This trend is consistent with the specific surface areas and the total pore volumes of the studied adsorbents discussed in section 4.1.6 (Table 4.2). It is also consistent with the maximum adsorption capacities, q_{max} values from section 4.5.2 (Table 4.6). Nevertheless, the performance of SAS was not very far from that of CAC especially in the removal of phenol and this can be attributed to their physicochemical properties which are comparable.

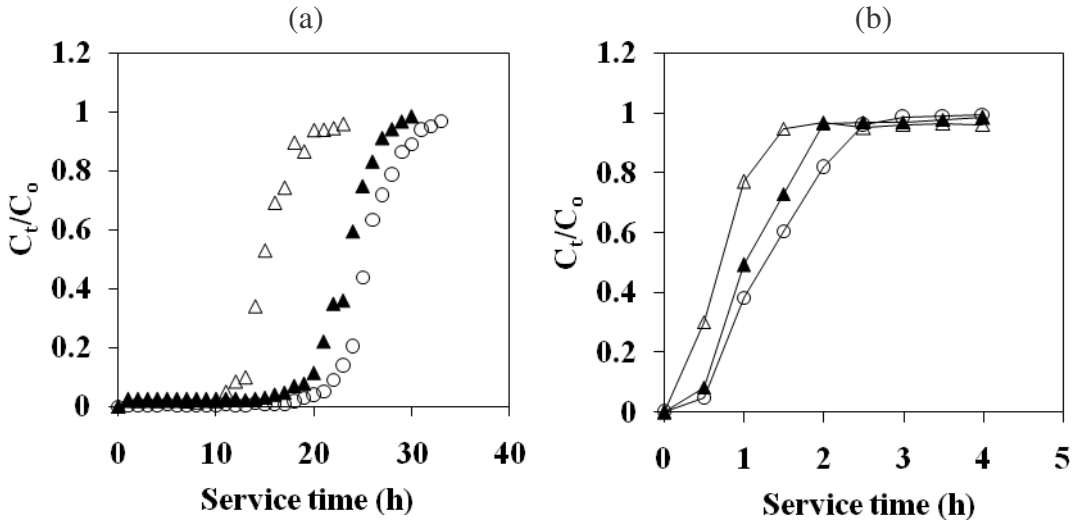

Figure 4.35. Breakthrough curves for removal of: (a) phenol and (b) cobalt using SD500 (Δ), SAS (▲) and CAC (○) at 10 cm bed height. (flow rate = 5 ml/min, pH = 2.6, column diameter = 2.5 cm, C_o of phenol and heavy metal ions = 90 mg/l).

In addition to quantitative data, a qualitative observation was noted when comparing the low cost adsorbents used to treat petrochemical wastewater in this study. All these adsorbents did not emit or release any notable colouring matter into the solution during the experiments. This observation was so encouraging because certainly, the end-user would prefer a clean, non-polluting product. Also, if these adsorbents were to be commercialized, toxicity tests are recommended first. Disposal of the agricultural adsorbents after use can be accomplished by either composting or incineration (Marshall and Johns, 1996) and the metal residues could be recovered by subsequent treatment of the post-combustion ash (Wase and Forster, 1997). On the other hand, coal fly ash after use as an adsorbent can be employed as a filling material in pavement linings, in soil stabilisation, in cement and concrete industries, or can be disposed off in a landfill (Weng and Huang, 1994; Sarkar and Acharya, 2006).

Table 4.12

Breakthrough and exhaustion times for different adsorbents

Adsorbent	Phenol		Cobalt	
	t_B (h)	t_E (h)	t_B (h)	t_E (h)
SD500	11.00	21.30	0.085	1.500
SAS	17.91	28.42	0.304	1.970
CAC	20.69	31.89	0.501	2.477

CHAPTER 5

5 Conclusions and recommendations

5.1 Conclusions

In industry, effluents rarely contain a single component; hence adsorption systems design must be based on multi-component effluents, making multi-component adsorption data a necessity. In this study, low cost adsorbents were successfully prepared from agricultural wastes and industrial solid waste. Further, the co-adsorption of recalcitrant compounds from synthetic wastewater using these locally available low cost adsorbents was studied. Additionally, response surface methodology was used to investigate the interactive effect of the operating parameters namely; adsorbent dose, initial concentration and solution pH. Similarly, the influence of various adsorption process parameters such as initial concentration, bed height and aspect ratio was further investigated in column adsorption studies. Also, the performance of the low cost adsorbents was compared with that of commercial activated carbon (CAC).

Results indicate that low cost adsorbents particularly steam activated sawdust (SAS) could be a promising solution to the removal of heavy metals and phenol from petrochemical wastewater. At the same time, sugarcane bagasse carbonized at 400°C (SB400) appears to be a promising adsorbent for the removal of direct red dyes from textile wastewater. Generally, coal fly ash (CFA) had the lowest adsorption capacity and this may be due to the fact that it was used without any chemical or heat pre-treatment. Thus, there is need to modify the coal fly ash before use in future work. Based on the data from the present investigation, the following conclusions are made:

(a) Low cost adsorbents prepared from agricultural wastes (pine sawdust and sugarcane bagasse) and industrial solid waste (coal fly ash) can be successfully used to treat industrial wastewater.

(b) The surfaces of the adsorbents were complex due to the presence of several functional groups. Some functional groups such as —OH and —COOH which are responsible for cation binding were found on the surfaces of all the adsorbents except coal fly ash. However, coal fly ash managed to adsorb some heavy metals in the absence of these functional groups. Therefore, addition of these groups through chemical modification would greatly improve the performance of coal fly ash in terms of heavy metal removal. The physicochemical properties of commercial activated carbon and steam activated sawdust were almost similar except for specific surface area.

(c) The trend followed by the maximum monolayer adsorption capacities for the four adsorbents used to treat petrochemical wastewater was in agreement with the specific surface area of the adsorbents i.e adsorbents with high specific surface area had high maximum monolayer adsorption capacities with a few exceptions. The highest adsorbed contaminant by steam activated sawdust was Fe (15.385 mg/g) followed by phenol (10.000 mg/g).

(d) Amongst the low cost adsorbent prepared, steam activated sawdust proved to be the best for petrochemical wastewater treatment. Therefore, steam activation is recommended for the other low cost adsorbents to improve their performance. The adsorption capacities of commercial activated carbon (0.591 mg/g) and coal fly ash (0.458 mg/g) were comparable with respect to Pb removal. However, coal fly ash was used without any chemical or thermal pre-treatment. Hence, given the low cost and abundance of coal fly ash, it can be recommended for removal of Pb from aqueous solution. Also, the performance of steam activated sawdust was comparable to that of commercial activated carbon in the removal of Pb and Ni. Thus, considering the low cost of sawdust, it can therefore be used as an alternative adsorbent for removal of Pb and Ni from wastewater. The SB400 was a better adsorbent than CFA with respect to dye removal from textile wastewater due to the high porosity and specific surface area.

(e) Adsorption capacity was found to vary with initial concentration, adsorbent dose and pH. An increase in pH led to a significant increase in heavy metal removal suggesting the involvement of ion exchange mechanism. Response surface methodology was undoubtedly a powerful technique for studying the interactive influence of major process parameters on adsorption capacity. The derived statistical model equations were satisfactory in predicting the adsorption capacities. Hence, they could be used to directly predict the adsorption capacity under variable conditions with respect to dose, pH and initial concentration.

(f) Equilibrium data for metal removal conformed well to the Freundlich isotherm whereas phenol and direct dye removal complied with the Langmuir adsorption isotherm model. Also, the removal of cobalt followed pseudo second order kinetics suggesting chemisorption due to the sharing of electrons between the adsorbent surface and the *d* orbitals of Co^{2+} for all the tested adsorbents. Intraparticle diffusion was not the only step controlling the overall adsorption process of cobalt in all the adsorbents studied.

(g) Dynamic adsorption conditions such as initial concentration (C_o), bed height (Z) and aspect ratio (Z/D) influenced the removal of phenol and heavy metals from synthetic petrochemical wastewater. Although an increase in bed height increased the breakthrough time, a very high bed height is not practical for a single column; instead multiple-beds should be designed.

The behaviour of heavy metal ions in the sawdust adsorption column were not influenced by phenol as the behaviour of phenol was not influenced by the heavy metal ions. Thus, metal ions and phenol are not adsorbed onto similar active sites and hence the adsorption of heavy metals, typical found in petrochemical wastewater can be studied in the absence of phenol. Similarly, that of phenol may be studied in the absence of metals. Some shifts in the Fourier Transform Infrared (FT-IR) spectra bands after adsorption and also a significant increase in heavy metal removal due to

an increase in solution pH confirmed the involvement of ion exchange mechanism (chemisorption) during heavy metal adsorption. At the same time, the increase in performance with increase in specific surface area suggests that physical adsorption also occurred. Therefore, both physisorption and chemisorption were effective in heavy metal removal.

Overall, commercial activated carbon is still the best adsorbent with respect to petrochemical wastewater treatment as compared to the low cost adsorbents prepared in this study. Therefore, more experiments are recommended to improve the performance of the low cost adsorbents in future work. The physicochemical properties of the adsorbents influence their performance. In most cases, both physical and chemical adsorption occurred simultaneously. Although the generation of wastewater by different industries is nearly unavoidable, the results presented here can help to design an appropriate environmental management strategy to minimize the adverse impacts caused by industrial wastewater. Since sugarcane bagasse, sawdust and coal fly ash are abundant in South Africa, regeneration of these low cost adsorbents after use is not required. Instead, the loaded adsorbents can be disposed by incineration or landfilling.

5.2 Recommendations for future work

The approach used in this study has given very promising results; however, there are a number of areas that need further investigation. In order to improve the adsorption capacities of the studied low cost adsorbents, further pretreatment experiments must be carried out to increase the physicochemical properties such as specific surface area, pore volume and active sites. These properties have a significant influence on the performance of the adsorbents. For instance, more carbonization and activation experiments must be carried out on the preparation of activated carbon from sawdust and also sugarcane bagasse in order to come up with optimum preparation conditions which will increase the surface area to that of commercial activated carbon or even higher if possible. On the other hand, some functional groups present on the surfaces

of CFA are not found on SAS, SB400 or SD500, thus the possibility of forming a hybrid adsorbent which could perform better than CFA, SB400, SAS or SD500 alone due to synergic effects must be explored. Although, the experiments were carried out at laboratory scale, the cost of preparing low cost adsorbents needs to be determined in further studies since cost is an important parameter for comparing the sorbent materials.

Further research could be carried out to study the adsorption properties of CFA in the form of pellets rather than dusty ash. The pelletization of fly ash could solve two very important drawbacks related to its utilization as adsorptive material. Dusty fly ash cannot be applied for adsorption in columns due to the fact that after a short period of time it is transformed to solid impermeable concrete. Its application in agitated vessels causes serious problems which are related to the separation of a dusty material from an aqueous solution. The use of fly ash pellets may permit the application of adsorption in columns without problems. Wastewater can percolate easily within a column filled with fly ash pellets without the risk of clogging with time. Additionally, the use of dusty fly ash changes the wastewater pH substantially and creates strong alkaline effluents with higher pH values after wastewater treatment. The use of fly ash pellets may affect slightly the wastewater pH after treatment producing effluents with pH lower than 8 which lies within the allowed limits for discharge in several natural receivers (Papandreou *et al*., 2007). Coal fly ash is an aluminosilicate, thus zeolitization could improve its performance towards metal ions or pretreatment with an acid will improve its surface area and hence its performance.

Studies on the effects of other process parameters such as temperature, particle size and ionic strength can also be an interesting area of future study. It could also be of particular interest to study the adsorption performance of sawdust from different sources. Besides a 2^3 full-factorial design with four centre points in RSM, other design of experiments such as the central composite design (CCD) and the Box–

Behnken design must be explored. In addition, multiple response surface optimization must be done using the constrained optimization technique which allows the optimum condition for removal of all the adsorbates to be determined simultaneously. On the other hand, leaching experiments must be carried out on SD500 to check for the presence of some soluble toxic pesticides (insecticide /fungicide /herbicides) which might be present depending on whether the source of sawdust (in this case pine tree) has been treated before. It is expected that leachability will depend on different factors such as solution pH, contact time, ionic strength, particle size, specimen size, etc (Townsend *et al*., 2004) and this makes it a new avenue of research.

It could be of particular importance to investigate the effects of heavy metal ion interactions on adsorption capacity. Also, the adsorption data could also be fitted to other adsorption isotherm models such as the Sips isotherm, Redlich-Peterson, Tóth, Dubinin-Radushkevitch, etc. Additionally, the kinetics of the removal of other metals besides cobalt must be investigated. At the same time, mathematical models such as the Bohart-Adams, Clark, Wolborska and the Bed Depth Service Time (BDST) models could be used to predict the breakthrough curves and to determine the characteristic parameters of the column useful for process design.

With a view to recover the adsorbed metal ions from SAS, SD500 and CFA, some desorption experiments could be carried out. In addition, desorption studies could be explored as a function of concentration (0.01–0.1 M) of different stripping agents such as hydrochloric and nitric acid. Also, desorption of phenol could be achieved using acetone; and distilled water could be used to strip the direct red dyes from the loaded adsorbents (SB400 and CFA). Finally, in order to widen the applicability of the studied adsorbent, they must be tested using the real textile and petrochemical wastewater.

CHAPTER 6

6 References

Abdelwahab, O., Amin, N.K., El-Ashtoukhy, E.S.Z. (2009). Electrochemical removal of phenol from oil refinery wastewater, *Journal of Hazardous Materials* (163): 711-716.

Alfafara, C.G., Migo, V.P., Amrante, J.A., Dallo, R.F., Matsumara, M. (2000). Ozone treatment of distillery slop waste, *Water Science and Technology* (42): 193-198.

Ali, A.A., El-Bishtawi, R. (1997). Removal of Lead and Nickel ions using zeolite tuff, *Journal of Chemical Technology and Biotechnology* (69): 27-34.

Al-Qodah; Z., Shawabkah, R. (2009). Production and characterization of granular activated carbon from activated sludge, *Brazilian Journal of Chemical Engineering* (26): 127-136.

Alzaydien, A.S. (2009). Adsorption of Methylene Blue from Aqueous Solution onto a Low-Cost Natural Jordanian Tripoli, *American Journal of Environmental Sciences* (5): 197-208.

Amarasinghe, B.M.W.P.K., Williams, R.A. (2007). Tea waste as a low cost adsorbent for the removal of Cu and Pb from wastewater, *Chemical Engineering Journal* (132): 299–309.

Amuda, O.S. and Alade, A. (2006). Coagulation/flocculation process in the treatment of abattoir wastewater, *Desalination* (196): 22-31.

Arami, M., Limaee, N.Y., Mahmoodi, N.M., Tabrizi, N.S. (2006). Equilibrium and kinetics studies for the adsorption of direct and acid dyes from aqueous solution by soy meal hull, *Journal of Hazardous Materials* (135): 171-179.

Ardejani, F.D, Badii, Kh, Limaee, N.Y., Shafaei, S.Z., Mirhabibi, A.R. (2007). Numerical modelling and laboratory studies on the removal of Direct Red 23 and Direct Red 80 dyes from textile effluents using orange peel, a low-cost adsorbent, *Dyes and Pigments* (73): 178-185.

Attia, A.A., Girgis, B.S., Farth, N.A. (2008). Removal of methylene blue by carbons derived from peach stones by H_3PO_4 activation: Batch and column studies, *Dyes and Pigments* (76): 282-289.

Ayyappan, R., Sophia, A.C., Swaminathan, K., Sandhya S. (2005). Removal of Pb(II) from aqueous solution using carbon derived from agricultural wastes. *Process Biochemistry* (40): 1293–1299.

Babel, S., Kurniawan, T.A. (2003). Low-cost adsorbents for heavy metals uptake from contaminated water: a review, *Journal of Hazardous Materials* (97): 219–243.

Bas, D., Bayaci, I.H. (2007). Modeling and optimization I: Usability of response surface methodology, *Journal of Food Engineering* (78): 836–845.

Basha, S., Murphy, Z.V.P., Jha, B. (2008). Sorption of Hg(II) from aqueous solutions onto *Carica papaya*: Application of Isotherms, *Industrial and Engineering Chemistry Research* (47): 980-986.

Basha, S., Murphy, Z.V.P., Jha, B. (2009). Removal of Cu(II) and Ni(II) from Industrial Effluents by Brown Seaweed, *Cystoseira indica*, *Industrial and Engineering Chemistry Research* (48): 961–975.

Basu, A., Mustafiz, S., Islam, M.R., Bjorndalen, N., Rahaman, M.S., Chaalal, O. (2006). A Comprehensive Approach for Modeling Sorption of Lead and Cobalt Ions through Fish Scales as an Adsorbent, *Chemical Engineering Communications* (193): 580–605.

Bayat, B. (2002). Comparative study of adsorption properties of Turkish fly ashes: II. The case of chromium (VI) and cadmium (II), *Journal of Hazardous Materials* (95): 275-290.

Bes-Pia, A., Mendoza-Roca, J.A., Alcaina-Miranda, M.I., Iborra-Clar, A., Iborra, Clar, M.I. (2003). Combination of physico-chemical treatment and nanofiltration to reuse wastewater of printing, dyeing and finishing textile industry, *Desalination* (157): 73-80.

Bhakat, P.B., Gupta, A.K., Ayoob, S. (2007). Feasibility analysis of As(III) removal in a continuous flow fixed bed system by modified calcined bauxite (MCB), *Journal of Hazardous Materials* (B139): 286–292.

Bhatia, S., Wong, C.T., Abdullah, A.Z. (2009). Optimization of air-borne butyl acetate adsorption on dual-function Ag–Y adsorbent-catalyst using response surface methodology, *Journal of Hazardous Materials* (164): 1110-1117.

Bhattacharya, A.K., Naiya, T.K., Mandal, S.N., Das, S.K., (2008). Adsorption, kinetics and equilibrium studies on removal of Cr(VI) from aqueous solutions using different low-cost adsorbents, *Chemical Engineering Journal* (137): 529-541.

Bouchelta, C., Medjram, M.S., Bertrand, O. and Bellat, J.P. (2008). Preparation and characterization of activated carbon from date stones by physical activation with steam, *Journal of Analytical and Applied Pyrolysis* (82): 70–77.

Bouguerra, W., Ali, M.B.S., Hamrouni, B., Dhahbi, M. (2007). Equilibrium and kinetic studies of adsorption of silica onto activated alumina, *Desalination* (206): 141-146.

Bratby, J. (2006). Coagulation and flocculation in water and wastewater treatment, IWA Publishing, London, pp 6-7.

Bulut, Y., Tez, Z. (2007). Removal of heavy metals from aqueous solution by sawdust adsorption, *Journal of Environmental Sciences* (19): 160-166.

Butler, M., Hallowes, D. (2002). Corporate Accountability in South Africa: The petrochemical industry and air pollution, pp 30-38.

Cavaco, S.A., Fernandes, S., Quina, M.M., Ferreira, L.M. (2007). Removal of chromium from electroplating industry effluent by ion exchange resins, *Journal of Hazardous Materials* (144): 634-638.

Carvalho, M.F., Duque, A.F., Gonçalves, I.C., Castro, P.M.L. (2007). Adsorption of fluorobenzene onto granular activated carbon: Isotherm and bioavailability studies, *Bioresource Technology* (98): 3424-3430.

Celenza, G.J. (2000). Industrial waste treatment process engineering: Specialized treatment systems, Volume III, A Technomic Publishing Company, Lancaster, PA.

Chaiko, D.J, Kopasz, J.P., Ellison, J.G. (1998). Use of Sol-Gel system for solid/liquid separation, *Industrial and Engineering Chemistry Research* (37): 1071-1078.

Cheremishinoff N.P., Moressi A.C. (1978). Carbon adsorption applications, in Cheremisinoff NP and F Ellerbusch (EDS.), *Carbon Adsorption Handbook*: 1-53. Ann Arbor: Ann Arbor Science.

Chiarle, S., Ratto, M., Rovatti, M. (2000). Mercury removal from water by ion exchange resins adsorption, *Water Research* (34): 2971-2978.

Cho, H., Oh, D., Kim, K. (2005). A study on removal characteristics of heavy metals from aqueous solution by fly ash, *Journal of Hazardous Materials* (B127): 187-195.

Cooney, D.O. (1980). Activated Charcoal Antidotal and other Medical Uses, Marcel Dekker, New York.

Cooney, D.O. (1998). Adsorption design for wastewater treatment, Lewis Publishers, CRC Press LLC, Florida, pp 66-68.

Crini, G. (2005). Recent developments in polySAScharide-based materials used as adsorbents in wastewater treatment, *Progress in Polymer Science* (30): 38–70.

Dakiky, M., Khamis, M., Manassra, M., Mer'eb, M. (2002). Selective adsorption of Chromium(VI) in industrial wastewater using low cost abundantly available adsorbents, *Advanced Environmental Research* (6): 533–540.

Das, D.D., Mahapatra, R., Pradhan, J., Das, S.N., Thakur, R.S. (2000). Removal of Cr(VI) from aqueous solution using activated cow dung carbon, *Journal of Colloid Interface Science* (232): 235–240.

Dash, R.R., Gaur, A., Balomajumder, C. (2009). Cyanide in industrial wastewaters and its removal: A review on biotreatment, *Journal of Hazardous Materials* (163): 1-11.

Davidson, H.W., Wiggs, P.K., Churchouse, A.H., Maggs, F.A., Bradley, R.S. (1968). Manufactured Carbon, Oxford, UK: Pergamon.

Davis, T.A., Volesky, B., Mucci, A. (2003). A review of the biochemistry of heavy metal biosorption by brown algae, *Water Research* (37): 4311-4330.

Department of Environmental Affairs and Tourism (DEAT), Republic of South Africa (2004). Kwa-Zulu Natal Waste Management Strategy Implementation Project Recycling Workshop report: 9-10.

Department of Water Affairs and Forestry (DWAF) (1996). South African Water Quality Guidelines, Second Edition, Volume 3: Industrial use.

Diaz-Teran, J., Nevskaia, D.M., Lopez-Peinado, A.J., Jerez, A. (2001). Porosity and absorption properties of an activated charcoal, *Colloids and Surfaces A: Physiochemical and Engineering Aspects* (187– 188): 167-175.

Drinan, J.E. (2001). Water and wastewater treatment: A guide for the non-engineering professional, CRC Press, Florida, pp 71.

Du, X., Yuan, Q., Li, Y. (2008). Equilibrium, thermodynamics and breakthrough studies for adsorption of solanesol onto macroporous resins, *Chemical Engineering and Processing* (47): 1420–1427.

Elibol, M. (2002). Response surface methodological approach for inclusion of perfluorocarbon in actinorhodin fermentation medium, *Process Biochemistry* (38): 667-773.

El-Naggar, M.R., El-Kamash, A.M., El-Dessouky, M.I., Ghonaim, A.K. (2008). Two-step method for preparation of NaA-X zeolite blend from fly ash for removal of cesium ions, *Journal of Hazardous Materials* (154): 963-972.

El Qada, E.N., Allen S.J., Walker, G.M. (2007). Adsorption of basic dyes from aqueous solution to activated carbons, *Chemical Engineering Journal* (135): 174-184.

Eskandarpour, A., Onyango, M.S., Aoyi, O., Asai, S. (2008). Removal of fluoride ions from aqueous solution at low pH using schwertmannite, *Journal of Hazardous Materials* (152): 571-579.

Estevinho, B.N., Ribeiro, E., Alves, A., Santos, L. (2007). A preliminary feasibility study for pentachlorophenol column sorption by almond shell residues, *Chemical Engineering Journal* (136): 188-194.

Farooqi, A., Masuda, H., Firdous, N. (2007). Toxic fluoride and arsenic contaminated groundwater in the Lahore and Kasur districts, Punjab, Pakistan and possible contaminant sources, *Environmental Pollution* (145): 839-849.

Febrianto, J., Kosasih, A.N., Sunarso, J., Ju, Y., Indraswati, N., Ismadji S. (2009). Equilibrium and kinetic studies in adsorption of heavy metals using biosorbent: A summary of recent studies, *Journal of Hazardous Materials* (162): 616-645.

Fontanals, N., Marce, R. M., Borrull, F. (2007). New materials in sorptive extraction techniques for polar compounds, *Journal of Chromatography A* (1152): 14-31.

Freundlich, H. (1906). Uber die adsorption in lusungen, *Journal of Physical Chemistry* (57): 385.(in German)

Gambolas, I., Molina, J. M., Jaray, P., Vitai, G., Bekassy-Molnar, E. (2004). High organic content industrial wastewater treatment by membrane separation, *Desalination* (162): 117-120.

Garg, U., Kaur, M.P, Jawa, G.K, Sud, D., Garg, V.K. (2008). Removal of cadmium (II) from aqueous solutions by adsorption on agricultural waste biomass, *Journal of Hazardous Materials* (154): 1149-1157.

Ghorai, S., Pant, K.K. (2005). Equilibrium, kinetics and breakthrough studies for adsorption of fluoride on activated alumina, *Separation and Purification Technology* (42): 265-271.

Ghorbani, F., Younesi H., Seyed, M.G., Ali, A.Z., Amini, M., Danesh, A. (2008). Application of response surface methodology for optimization of cadmium biosorption in an aqueous solution by *Saccharomyces cerevisiae*, *Chemical Engineering Journal* (145): 267-275.

Goel, J., Kadirvelu, K., Rajagopal, C., Garg, V.K. (2005). Removal of lead (II) by adsorption using treated granular activated carbon: Batch and column studies, *Journal of Hazardous Materials* (B125): 211–220.

Goel, J., Kadirvelu, K., Rajagopal, C., Garg, V.K. (2006). Cadmium (II) Uptake from Aqueous Solution by Adsorption onto Carbon Aerogel Using a Response Surface Methodological Approach, *Industrial and Engineering Chemistry Research* (45): 6531-6537.

Gonzalo, V., Alonso, R., Freire, S., Gonza´lez-A´lvarez, J., Antorrena, G. (2006). Uptake of phenol from aqueous solutions by adsorption in a *Pinus pinaster* bark packed bed, *Journal of Hazardous Materials* (B133): 61–67.

Gupta, S., Babu, B.V. (2009). Removal of toxic metal Cr (VI) from aqueous solutions using sawdust as adsorbent: Equilibrium, kinetics and regeneration studies, *Chemical Engineering Journal* (150): 352–365.

Habib-ur-Rehman, Shakirullah, M., Ahmad, I., Shah, S., Hameedullah (2006). Sorption Studies of Nickel Ions onto Sawdust of *Dalbergia sissoo*, *Journal of the Chinese Chemical Society* (53): 1045-1052.

Hamdaoui, O. (2009). Removal of copper (II) from aqueous phase by Purolite C100-MB cation exchange resin in fixed bed columns: Modeling, *Journal of Hazardous Materials* (161): 737-746.

Han, H., Li, Y., Li, J., Zhang, H.X., Shi, J. (2006). Biosorption of copper and lead ions by waste beer yeast, *Journal of Hazardous Materials* (137): 1569–1576.

Hanafiah, M.A.K.M., Zakaria, H., Wan Ngah, W.S. (2009). Preparation, Characterization, and Adsorption Behavior of Cu(II) Ions onto Alkali-Treated Weed (Imperata cylindrica) Leaf Powder, *Water, Air and Soil Pollution* (201): 43-53.

Ho, Y.S. (1995). Adsorption of Heavy Metals from Waste Streams by Peat, PhD Thesis, University of Birmingham, Birmingham,UK.

Ho, Y. (2004). Selection of optimum sorption isotherms, *Carbon* (42): 2113-2130.

Ho, Y.S., John Wase, D.A., Forster, C.F. (1995). Batch nickel removal from aqueous solution by sphagnum moss peat, *Water Research* (29): 1327-1332.

Ho, Y.S., McKay, G. (2000). The kinetics of sorption of divalent metal ions onto sphagnum moss peat, *Water Research* (34):735–42

Hui, K.S., Chao, C.Y.H., Kot, S.C. (2005). Removal of mixed heavy metal ions in wastewater by zeolite 4A and residual products from recycled coal fly ash, *Journal of Hazardous Materials* (127): 89-101.

Innes, R.W., Fryer, J.R., Stoeckli, H.F. (1989). On the correlation between micropore distribution obtained from molecular probes and from high resolution electron microscopy, *Carbon* (27): 71-76.

Isik, M. (2008). Biosorption of Ni (II) from aqueous solutions by living and non-living ureolytic mixed culture, *Colloids and Surfaces* (62): 97-104.

Ismadji, S., Sudaryanto, Y., Hartono, S.B., Setiawan, L.E.K., Ayucitra, A. (2005). Activated carbon from char obtained from vacuum pyrolysis of teak sawdust: pore structure development and characterization, *Bioresource Technology* (96): 1364-1369.

Jain, A.K., Jain, S.S., Bhatnagar, A. (2001). Utilization of industrial wastes for the removal of anionic dyes, *Toxicology Environmental. Chemistry* (84): 41.

Jime´nez, A.F, Palomo, A. (2005). Mid-infrared spectroscopic studies of alkali-activated fly ash structure, *Microporous and Mesoporous Materials* (86): 207-214.

Johnson, R. (2005). Drinking Water Treatment Methods, http://www.cyber-nook.com/water/Solutions.html, Accessed on 18 February 2009.

Kadirvelu, K., Palanival, M., Kalpana, R., Rajeswari, S. (2000). Activated carbon from an agricultural by-product, for the treatment of dyeing industry wastewater, *Bioresource Technology* (74): 263-265.

Karnitz,O. Jr, Gurgel, L.V.A., de Melo, J.C.P., Botaro, V.B., Melo, T.M.S., Gil, R.P.F., Gil, L.F. (2007). Adsorption of heavy metal ion from aqueous single metal solution by chemically modified sugarcane bagasse, *Bioresource Technology* (98): 1291-1297.

Kavitha, D., Namasivayam, C. (2008). Capacity of activated carbon in the removal of acid brilliant blue: Determination of equilibrium and kinetic model parameters, *Chemical Engineering. Journal* (139): 453-461.

Kelleher, B. P., O'Callaghan, M. N., Leahy, M.J., O'Dwyer, T.F., Leahy, J.J. (2002). The use of fly ash from the combustion of poultry litter for the adsorption of chromium (III) from aqueous solution, *Journal of Chemical Technology and Biotechnology* (77): 1212-1218.

Kennedy, L.J., Vijaya, J.J., Kayalvizhi, K., Sekaran, G. (2007). Adsorption of phenol from aqueous solutions using mesoporous carbon prepared by two-stage process, *Chemical Engineering Journal* (132): 279-287.

Khuri, A.I., Cornell, J.A. (1987). Response Surfaces: Designs and Analyses. Marcel Dekker, Inc., New York.

Kim, H., Baek, K., Lee, J., Iqbal, J., Yang, J. (2006). Comparison of separation methods of heavy metal from surfactant micellar solutions for the recovery of surfactant, *Desalination* (191): 186-192.

Kim, K., Kang , C., You, Y., Chung, M., Woo, M., Jeong, W., Park, N., Ahn, H. (2006). Adsorption–desorption characteristics of VOCs over impregnated activated carbons, *Catalysis Today* (111): 223–228.

Ko, D.C.K., Porter, J.F., McKay, G. (2000). Optimised correlations for the fixed-bed adsorption of metal ions on bone char, *Chemical Engineering Science* (55): 5819-5829.

Kumar, B.G.P., Shivakamy, K., Miranda, L.S., Velan, M. (2006). Preparation of steam activated carbons from rubberwood sawdust (*Hevea Brasiliensis*) and its adsorption kinetics, *Journal of Hazardous Materials* (B136): 922-929.

Kumar, P.A., Chakraborty, S. (2009). Fixed-bed column study for hexavalent chromium removal and recovery by short-chain polyaniline synthesized on jute fiber, *Journal of Hazardous Materials* (162): 1086-1098.

Kumar, U. (2006). Agricultural products and by-products as a low cost adsorbent for heavy metal removal from water and wastewater: A review. *Scientific Research and Essay* (1): 033-037.

Kumar, U., Bandyopadhyay, M. (2006). Sorption of cadmium from aqueous solution using pretreated rice husk, *Bioresource Technology* (97): 104-109.

Kurniawan, T.A., Chan, G.Y.S., Lo, W., Babel, S. (2006). Comparisons of low-cost adsorbents for treating wastewaters laden with heavy metals, *Science of the Total Environment* (366): 409-426.

Lagergren, S. (1898). About the theory of so-called adsorption of soluble substances, *Kungliga Svenska Vetenskapsakademiens. Handlingar*, Band (24): 1-39.

Lam, K. F., Yeung, K. L., McKay, G. (2006). An investigation of gold adsorption from a binary mixture with selective mesoporous silica adsorbents, *Journal of Physical Chemistry B* (110): 2187-2194.

Langmuir, I. (1918). The adsorption of gases on plane surfaces of glass, mica and platinum, *Journal of American Chemical Society* (40): 1361-1403.

Lapuente, R., Cases F., Garcés, P., Morallón E., Vázquez, J.L. (1998). A voltammeter and FTIR–ATR study of the electro polymerization of phenol on platinum electrodes in carbonate medium: Influence of sulfide. *Journal of Electroanalytical Chemistry* (451): 163-171.

Laslo, Z., Hodur, C. (2007). Purification of thermal wastewater by membrane separation and ozonation, *Desalination* (206): 333-340.

Lee, J.K., Park, G., Ryu, S.K., Kim, J.H. (2003). Effect of Two-step Surface Modification of Activated Carbon on the Adsorption Characteristics of Metal Ions in Wastewater II. Dynamic Adsorption, *Carbon Science* (4): 14-20.

Lenntech Water Treatment and Air Purification Holdings B.V. (2008). http://www.lenntech.com/petrochemical.htm (Accessed on 25 February 2009).

Liu, Y. and Liu, Y. (2008). Biosorption isotherms, kinetics and thermodynamics, *Separation and Purification Technology* (61): 229-242.

Lu, S.G., Bai, S.Q., Zhu, L. and Shan, H.D. (2009). Removal mechanism of phosphate from aqueous solution by coal fly ash, *Journal of Hazardous Materials*, (161): 95-101.

Madhava, R.M., Reddy, D.H.K.K., Venkateswarlu, P., Seshaiah, K. (2009). Removal of mercury from aqueous solutions using activated carbon prepared from agricultural by-product/waste, *Journal of Environmental Management* (90): 634-643.

Mahmoodi, N.M., Arami, M., Limaee, N.Y., Tabrizi, N.S. (2005). Decolorization and aromatic ring degradation kinetics of Direct Red 80 by UV oxidation in the presence of hydrogen peroxide utilizing TiO_2 as a photocatalyst, *Chemical Engineering Journal* (112): 191-196.

Malik, P.K. (2004). Dye removal from wastewater using activated carbon developed from sawdust: adsorption equilibrium and kinetics, *Journal of Hazardous Materials* (B113): 81–88.

Marshall, W.E., Johns, M.M. (1996) Agricultural by-products as metal adsorbents: sorption properties and resistance to mechanical abrasion. *Journal of Chemical Technology and Biotechnology* (66): 192-198.

Marshall, W.E, Wartelle, L.H., Boler, D.E., Toles, C.A. (2000). Metal ion adsorption by soybean hulls modified with citric acid: A comparative study, *Environmental Technology* (21): 601-607.

McKay, G. (1984). Adsorption of dyestuffs from aqueous solutions using the activated carbon adsorption model to determine breakthrough curves**,** *Chemical Engineering Journal and the Biochemical Engineering Journal* (28): 95-104.

McSweeny, J.D. Rowell, R.M. and Min, S.H. (2006). Effect of Citric Acid Modification of Aspen Wood on Sorption of Copper Ion, *Journal of Natural Fibers* (3): 43-58.

Meena, A.J., Kadirvelu, K., Mishra, G.K., Rajagopal, C., Nagar, P.N. (2008). Adsorptive removal of heavy metals from aqueous solution by treated sawdust (Acacia arabica), *Journal of Hazardous Materials* (150): 604-611.

Mohan, D., Kunwar, P.S. (2002). Single and multi-component adsorption of cadmium and zinc using activated carbon derived from bagasse- an agricultural waste, *Water Research* (36): 2304-2318.

Mohan, S., Gandhimathi, R. (2009). Removal of heavy metal ions from municipal solid waste leachate using coal fly ash as an adsorbent, *Journal of Hazardous Materials* (169): 351-359.

Mohana, S., Acharya, B.K., Madamwar, D. (2009). Distillery spent wash: Treatment technologies and potential applications, *Journal of Hazardous Materials* (163): 12-25.

Mohanty, K., Das, D., Biswas, M.N. (2005). Adsorption of phenol from aqueous solutions using activated carbons prepared from *Tectona grandis* sawdust by $ZnCl_2$ activation, *Chemical Engineering Journal* (115): 121–131.

Mozammel, H.M., Masahiro, O., SC, B. (2002). Activated charcoal from coconut shell using $ZnCl_2$ activation, *Biomass and Bioenergy* (22): 397-400.

Mukherjee S., Kumar, S., Misra, A.K., Fan, M. (2007). Removal of phenols from water environment by activated carbon, bagasse ash and wood charcoal, *Chemical Engineering Journal* (129): 133-142.

Myers, R.H., Montgomery, D.C. (2002). Response surface methodology: Process and product optimization using designed experiments (Second Edition.), John Wiley and Sons, New York.

Naiya, T.K., Chowdhury, P., Bhattacharya, A.K., Das, S.K. (2009). Saw dust and neem bark as low-cost natural biosorbent for adsorptive removal of Zn(II) and Cd(II) ions from aqueous solutions, *Chemical Engineering Journal* (148): 68-79.

Namasivayam, C., Kavitha, D. (2006). IR, XRD and SEM studies on the mechanism of adsorption of dyes and phenols by coir pith carbon from aqueous phase, *Microchemical Journal* (82): 43 – 48.

Netpradit, S., Thiravetyan, P., Towprayoon, S. (2004). Evaluation of metal hydroxide sludge for reactive dye adsorption in a fixed-bed column system, *Water Research* (38): 71–78.

Ngah, W.W.S., Hanafiah, M.A.K.M. (2008), Removal of heavy metal ions from wastewater by chemically modified plant wastes as adsorbents: A review, *Bioresource Technology* (99): 3935-3948.

Norris, G. and Volschenk, J. (2007). Biomass waste-to-electricity: Kwa-Zulu Natal, Renewable Energy, USB Leaders' Lab: 10-11.

Ochieng, A., Ogada, T., Sisenda, W., Wambua, P. (2002). Brewery wastewater treatment in a fluidized-bed bioreactor, *Journal of Hazardous Materials* (90): 311-321.

Onyango, M.S., Kojima, Y., Ochieng A., Bernardo, E.C., Matsuda, H. (2004). Adsorption equilibrium modeling and solution chemistry dependence of fluoride removal from water by trivalent-cation-exchanged zeolite F-9, *Journal of Colloid and Interface Science* (279): 341-350.

Pan, B.C., Meng, F.W., Chen, X.Q., Pan, B.J., Li, X.T., Zhang, W.M., Zhang, X., Chen, J.L., Zhang, Q.X., Sun, Y. (2005). Application of an effective method in predicting breakthrough curves of fixed-bed adsorption onto resin adsorbent, *Journal of Hazardous Materials* (B124): 74–80.

Pan, B., Du, W., Zhang, W., Zhang, X., Zhang, Q., Pan, B., Lv, L., Zhang, Q., Chen, J. (2007). Improved adsorption of 4-Nitrophenol onto a Novel Hyper-Cross linked Polymer, *Environmental Science and Technology* (41): 5057-5062.

Panday, K.K., Prasad, G., Singh, V.N. (1985). Copper (II) removal from aqueous solutions by fly-ash, *Water Research* (19): 869–873.

Papandreou, A., Stournaras, C.J., Panias, D. (2007). Copper and cadmium adsorption on pellets made from fired coal fly ash, *Journal of Hazardous Materials* (148): 538-547.

Patel, H., Madamwar, D. (2002). Effects of temperatures and organic loading rates on bio-methanation of acidic petrochemical wastewater using an anaerobic upflow fixed-film reactor, *Bioresource Technology* (82): 65-71.

Pavia, D.L., Lampman, G.M., Kaiz, G.S. (1987). Introduction to Spectroscopy: A Guide for Students of Organic Chemistry, W.B. Saunders Company, Philadelphia.

Pena, M., Coca, M., Gonzalez, R., Rioja, R., Garcia, M.T. (2003). Chemical oxidation of wastewater from molasses fermentation with ozone, *Chemosphere* (51): 893-900.

Peters, R.W., Young, K., Bhattacharyya, D. (1985). Evaluation of recent treatment techniques for removal of heavy metals from industrial wastewater, *AIChE Symposium Series* (81): 165-203.

Pollard, S.J.T., Fowler, G.D., Sollars, C.J., Perry, R. (1992). Low-cost adsorbents for waste and wastewater treatment: a review, *The Science of the Total Environment* (116): 31-52.

Pollution Prevention and Abatement Handbook (1998). World Bank Group Environmental, Health and Safety General Guidelines, pp 371-376. http://www.ifc.org/ifcext/enviro.nsf/ContentEnvironmentalGuidelines (Accessed on 02 November 2007).

Potgieter, J.H., Bada, S.O., Potgieter-Vermaak, S.S. (2009). Adsorptive removal of various phenols from water by South African coal fly ash, *Water SA* (35): 89-96.

Puziy, A.M., Poddubnaya O.I., Matinez-Alonso, A., Suarez-Garcia, F., Tascon, J.M.D. (2002). Characterization of synthetic carbon activated with phosphoric acid, *Applied surface science* (200): 196-202.

Qiu, W., Zheng, Y. (2007). Arsenate removal from water by an alumina-modified zeolite recovered from fly ash, *Journal of Hazardous Materials* (148): 721-726.

Rangasayatorn, N., Pokethitiyook, P., Upatham, E.S., Lanza, G.R. (2004). Cadmium biosorption by cells of *Spirulina platensis* TISTR 8217 immobilized in alginate and silica gel, *Environmental International* (30): 57-63.

Ravikumar, K., Krishnan, S., Ramalingam, S., Balu, K. (2007). Optimization of process variables by the application of response surface methodology for dye removal using a novel adsorbent, *Dyes and Pigments* (72): 66-74.

Rengaraj, S., Moon, S., Sivabalan, R., Arabindoo, B., Murugesan, V. (2002). Agricultural solid waste for the removal of organics: adsorption of phenol from water and wastewater by palm seed coat activated carbon, *Waste Management* (22): 543–548.

Reynolds, K., Kruger, R., Rethman, N., Truter, W. (2002). The production of an artificial soil from sewage sludge and fly-ash and the subsequent evaluation of growth enhancement, heavy metal translocation and leaching potential, *Water SA Special Edition: WISA Proceedings*: 73-77.

Ricou-Hoeffer, P., Lecuyer, I., Le Cloirec, P. (2001). Experimental design methodology applied to adsorption of metallic ions onto fly ash, *Water Research* (35): 965-976.

Rodriguez-Reinoso, F., Linares-Solano, A. (1989). Chemistry and physics of carbon: a series of advances (P.A.Thrower, Ed.), Marcel Dekker, Inc., New York.

Rowe, D.R., Abdel-Magid, I.M. (1995). Handbook of wastewater reclamation and reuse, Lewis Publishers, New York, pp 194-196.

Ruthven, D. M. (1984). Principles of Adsorption and Adsorption Processes, John Wiley and Sons, New York.

Salamane, I.I., Bandosz, T.J. (2003). Role of surface chemistry in adsorption of phenol on activated carbons, *Journal of Colloid and Interface Science* (264): 307–312.

Sarkar, M., Acharya, P.K. (2006). Use of fly ash for the removal of phenol and its analogues from contaminated water, *Waste Management* (26): 559–570.

Satyawali, Y., Balakrishnan, M. (2008). Wastewater treatment in molasses-based alcohol distilleries for COD and color removal: A review, *Journal of Environmental Management* (86): 481-497.

Sen, A.K., De, A.K. (1987). Adsorption of Mercury (II) by coal fly ash, *Water Research* (21): 885-888.

Shukla, A., Zhang,Y., Dubey, P., Margrave, J.L., Shukla, S.S. (2002). The role of sawdust in the removal of unwanted materials from water, *Journal of Hazardous Materials* (B95): 137–152.

Sing, K.S.W., Everett, D.H., Haul, R.A.W., Moscou, L., Pierotti, R.A., Rouquerol, J., Siemieniewska, T. (1985). Reporting physisorption data for gas/solid systems with special reference to the determination of surface area and porosity, *Pure and Applied Chemistry* (57): 603-619.

Singh, K.P., Malik, A., Sinha, S., Ojha, P. (2008). Liquid-phase adsorption of phenols using activated carbons derived from agricultural waste material, *Journal of Hazardous Materials* (150): 626–641.5

Site, A.D. (2001). Factors affecting sorption of organic compounds in natural sorbent/water systems and sorption coefficients for selected pollutants: A review, *Journal of Physical and Chemical Reference Data* (30): 187-439.

Sonune, A., Ghate, R. (2004). Developments in wastewater treatment methods, *Desalination* (167): 55-63.

Srivastava, V.C., Swamy, M.M., Mall, I.D, Prasad, B., Mishra, I.M. (2006). Adsorptive removal of phenol by bagasse fly ash and activated carbon: Equilibrium, kinetics and thermodynamics, *Colloids and Surfaces A: Physicochemical and Engineering Aspects* (272): 89-104.

Stoeckli, H.F. (1990). Microporous carbons and their characterization: the present state of the art, *Carbon* (28): 1-6.

Stoeckli H.F., Guillot A, Slasli A.M, Hugi-Cleary D. (2002). The comparison of experimental and calculated pore size distributions of activated carbons, *Carbon* (40): 383-388.

Stumm, W., Bilinski, H. (1972). Trace Metals in Natural Waters. *Proceedings of the 6th International Conference on Water Pollution Research*, Pergamon Press, New York.

Sun, J., Hippo, E.J., Marsh, H., O'Brien, W.S., Crelling, J.C. (1997). Activated carbon produced from an Illinois Basin Coal, *Carbon* (35): 341-352.

Sun, Q., Yang, L. (2003). The adsorption of basic dyes from aqueous solution on modified peat–resin particle, *Water Research* (37): 1535-1544.

Tao, X., Xiaoqin, L. (2008). Peanut Shell Activated Carbon: Characterization, Surface Modification and Adsorption of Pb^{2+} from Aqueous Solution, *Chinese Journal of Chemical Engineering* (16): 401-406.

Ting, W., Huang, Y., Lu, M. (2007). Catalytic treatment of petrochemical wastewater by electro-assisted Fenton Technologies, *Reaction Kinetics and Catalysis Letters* (92): 41-48.

Townsend, T., Tolaymat, T., Solo-Gabriele, H., Dubey,B., Stook, K., Wadanambi, L. (2004). Leaching of CCA-treated wood: implications for waste disposal, *Journal of Hazardous Materials* (B114): 75-91.

Tsai, W.T., Chang, C.Y., Lin, M.C., Chien, S.F., Sun, H.F., Hsieh, M.F. (2001). Adsorption acid dye onto activated carbons prepared from agricultural waste bagasse by $ZnCl_2$ activation, *Chemosphere* (45): 51-58.

US EPA (1985). Technical Support Document for Water Quality Based Toxics Control. EPA/440/485032, United States Environmental Protection Agency, Washington, DC.

US EPA (2000). Wastewater Technology Fact Sheet: Chemical precipitation, US. EPA 832-F-00-018, Washington DC.

Valderrama, C., Cortina, J.L., Farran, A., Gamisans, X., de las Heras, F.X. (2008). Kinetic study of acid red ‘‘dye” removal by activated carbon and hyper-cross-linked polymeric sorbents Macronet Hypersol MN200 and MN300, *Reactive & Functional Polymers* (68): 718–731.

Vazquez, G., Alonso, R., Freire, S., Gonzalez-Alvarez, J., Antorrena, G. (2006). Uptake of phenol from aqueous solutions by adsorption in a *Pinus pinaster* bark packed bed, *Journal of Hazardous Materials* (B133): 61–67.

Vijayaraghavan, K., Ahmad, D., Yazid, A.Y.A. (2008). Electrolytic treatment of Standard Malaysian Rubber process wastewater, *Journal of Hazardous Materials* (150): 351-356.

Viraraghava, T., Rao, G.A.K. (1991). Adsorption of cadmium and chromium from wastewater by fly ash, *Journal of Environmental Science and Health, Part A* (26): 721-753.

Wafwoyo, W., Seo, W.S., Marshall, W.E. (1999). Utilisation of peanut shells as adsorbents for selected metals, *Journal of Chemical Technology and Biotechnology* (74): 1117-1121.

Wang, J., Xu, F., Xie, W., Mei, Z., Zhang, Q., Cai, J., Cai, W. (2009). The enhanced adsorption of dibenzothiophene onto cerium/nickel-exchanged zeolite Y, *Journal of Hazardous Materials* (163): 538-543.

Wang, L.K., Hung, Y., Lo, H.H., Yapijakis, C. (2004). Handbook of Industrial and Hazardous Wastes Treatment, Second Edition, Marcel Dekker, New York, pp 71-75.

Wang, L.K., Hung, Y., Lo, H.H., Yapijakis, C. (2006). Waste treatment in the process industries, Taylor and Francis Group, New York, pp 470.

Wang, S., Zhu, Z.H. (2007). Humic acid adsorption on fly ash and its derived unburned carbon, *Journal of Colloids and interface Science* (315): 41–46.

Walker, G.M., Weatherley, L.R. (1997). Adsorption of acid dyes onto granular activated carbon in fixed beds, *Water Research* (31): 2093-2101.

Wase, D.A.J., Forster, C. F. (1997). Biosorbents for metal ions, Taylor and Francis, London.

Weber, W.J., Morris, J.C. (1963). Kinetics of adsorption on carbon from solution, *Journal of Sanitary Engineering Division ASCE* (89): 31-39.

Weller, M.G. (2000). Immunochromatographic techniques-a critical review, *Fresenius Journal of Analytical Chemistry* (366): 635-645.

Weng, C.H., Huang, C.P. (1994). Treatment of metal industrial wastewater by fly ash and cement fixation, *Journal of Environmental Engineering* (120): 1470-1487.

Wong, K.K., Lee, C.K., Low, K.S., Haron, M.J. (2003). Removal of Cu(II) and Pb(II) by tartaric acid modified rice husk from aqueous solutions, *Chemosphere* (50): 23-28.

Woolard, C.D., Petrus, K., Van der Horst, M., (2000). The use of modified fly ash as an adsorbent for lead, *Water SA* (26): 531-536.

Wu, F., Tseng, R., Juang, R. (2009). Initial behavior of intraparticle diffusion model used in the description of adsorption kinetics, *Chemical Engineering Journal* (153): 1-8.

Yang, T., Lua, A. (2003). Characteristics of activated carbons prepared from pistachio-nut shells by physical activation, *Journal of Colloid and Interface Science* (267): 408-417.

Yasemin, B., Zeki, T. (2007). Removal of heavy metals from aqueous solution by sawdust adsorption, *Journal of Environmental Sciences* (19): 160-166.

Yu, B., Zhang, Y., Shukla, A., Shukla, S.S., Dorris, K.L. (2001). The removal of heavy metals from aqueous solutions by sawdust adsorption - removal of lead and comparison of its adsorption with copper, *Journal of Hazardous Materials* (84): 83-94.

Yu, L., Ya-Juan, L. (2008). Biosorption isotherms, kinetics and thermodynamics: A review, *Separation and Purification Technology* (61): 229-242.

Zabkova, M., Otero, M., Minceva, M., Zabka, M., Rodrigues, A.E. (2006). Separation of synthetic vanillin at different pH onto polymeric adsorbent Sephabeads SP206, *Chemical Engineering and Processing* (45): 598-607.

Zhang, W., Chen, J., Pan, B., Zhang, Q. (2006). Cooperative adsorption behaviours of 1-naphthol and 1-naphthylamine onto non-polar macroreticular adsorbents, *Reactive and Functional Polymers* (66): 485-493.

Zhu, Z., Li, A., Yan, L., Liu, F., Zhang,Q. (2007). Preparation and characterization of highly mesoporous spherical activated carbons from divinylbenzene-derived polymer by $ZnCl_2$ activation, *Journal of Colloid and Interface Science* (316): 628–634.

APPENDIX A

Characterization data

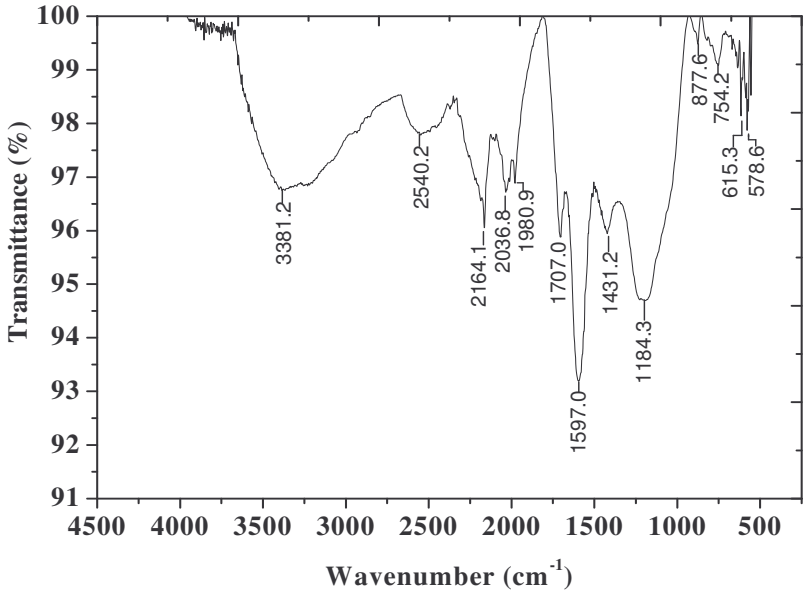

Figure A1. FT-IR spectrum of SD500 before use

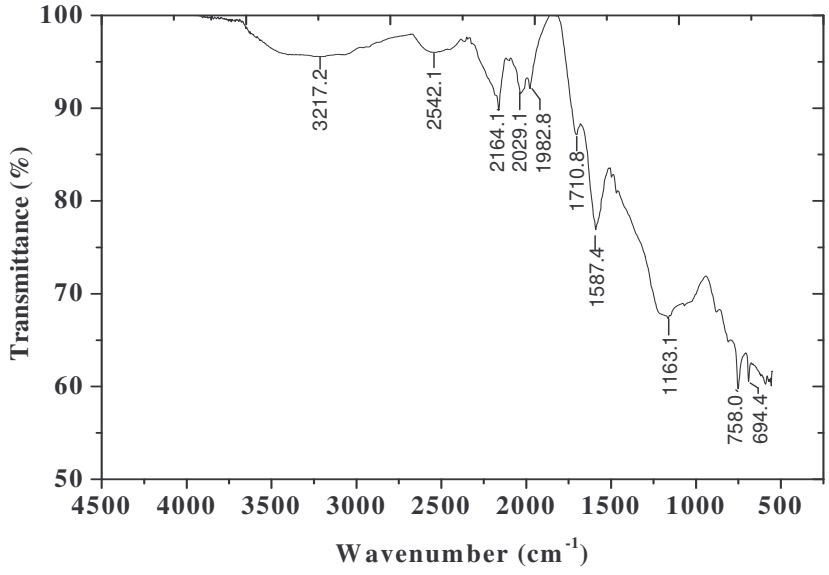

Figure A2. FT-IR spectrum of SD500 after adsorption of metals and phenol

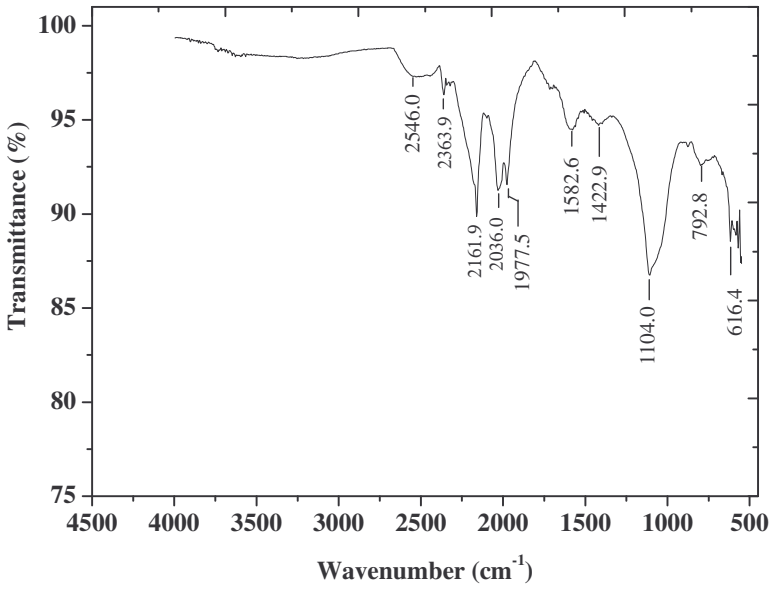

Figure A3. FT-IR spectra of SB400 before use.

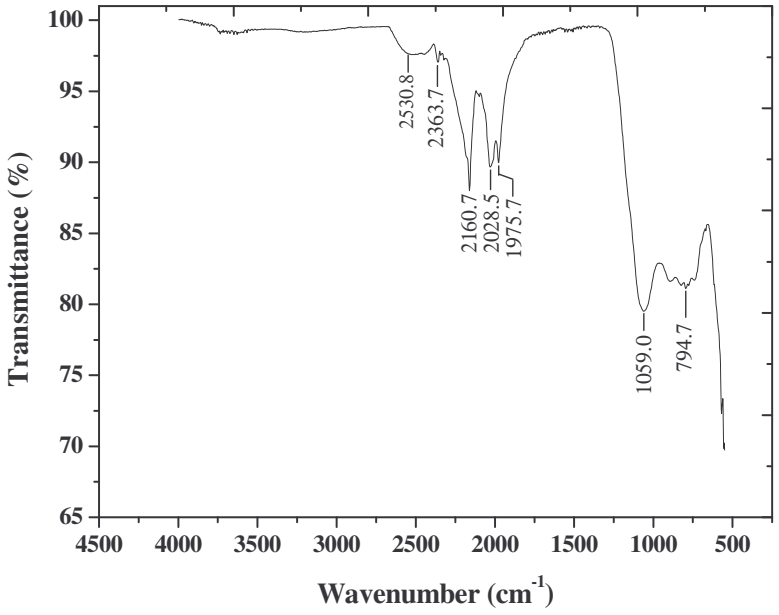

Figure A4. FT-IR spectrum of CFA before use

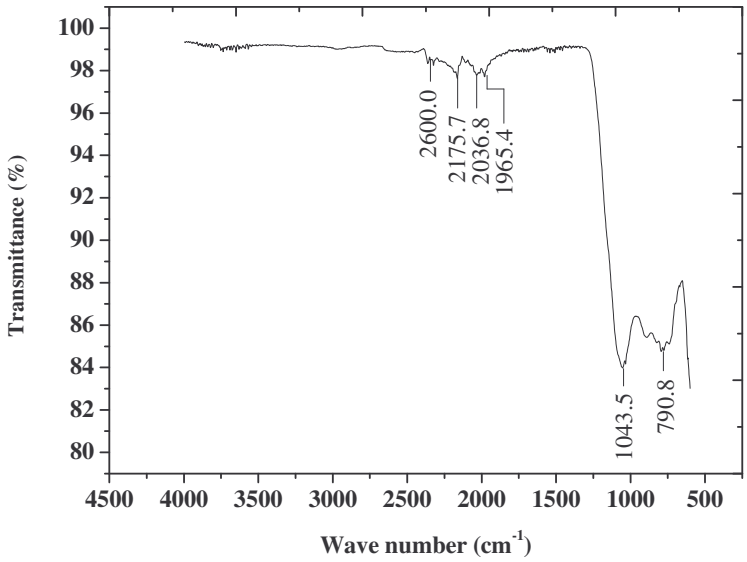

Figure A5. FT-IR spectrum of CFA after adsorption of metals and phenol

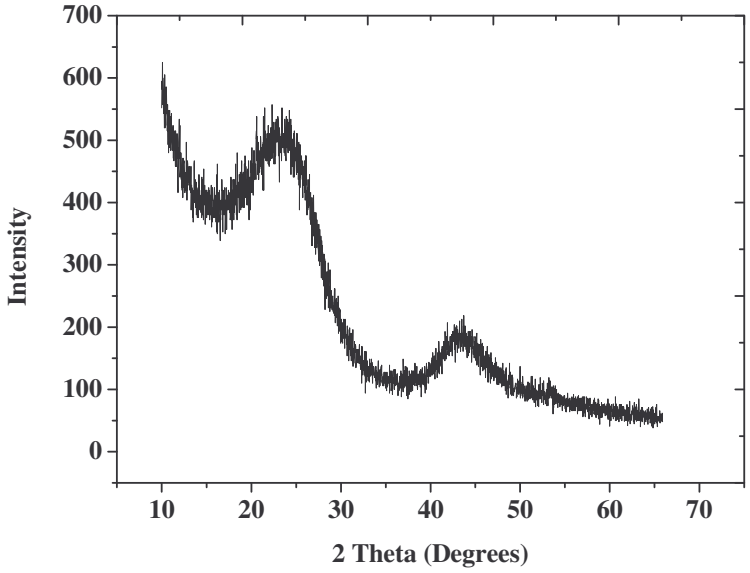

Figure A6. The X-ray diffraction profile (diffractogram) of SAS.

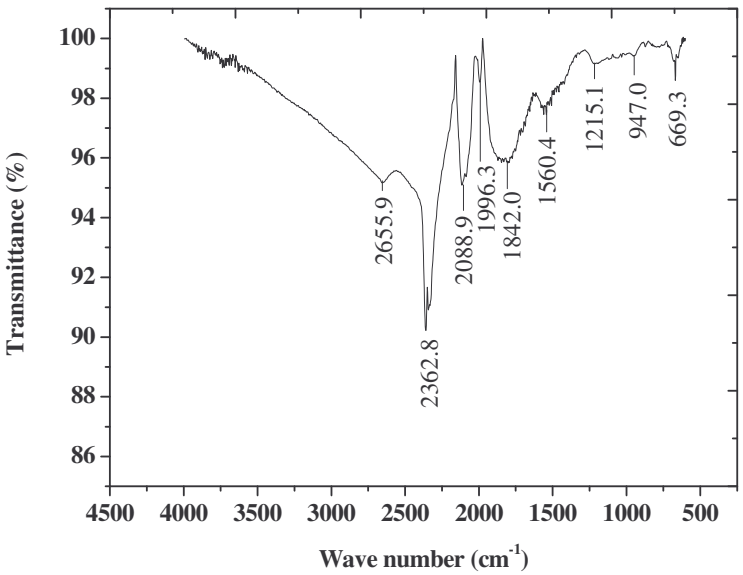

Figure A7. FT-IR spectrum of SAS before use

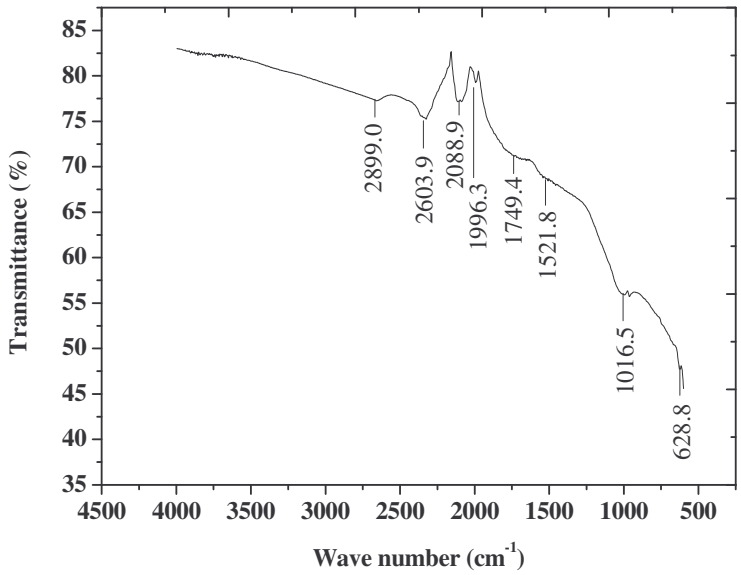

Figure A8. FT-IR spectrum of SAS after adsorption of metals and phenol

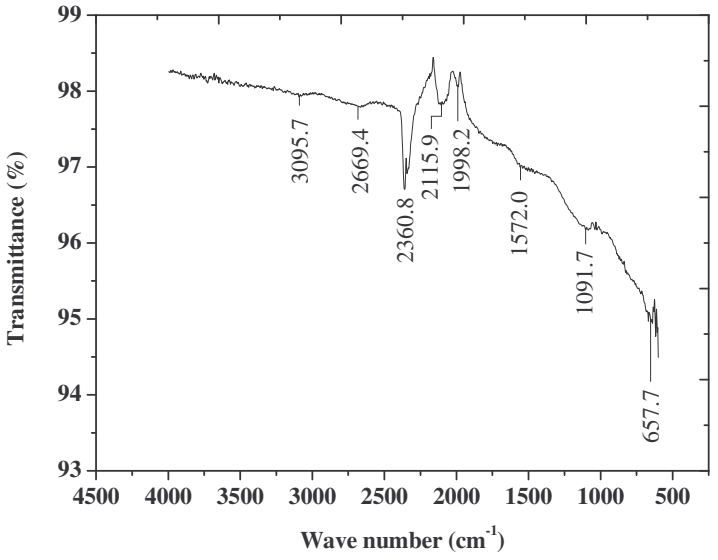

Figure A9. FT-IR spectrum of CAC before use

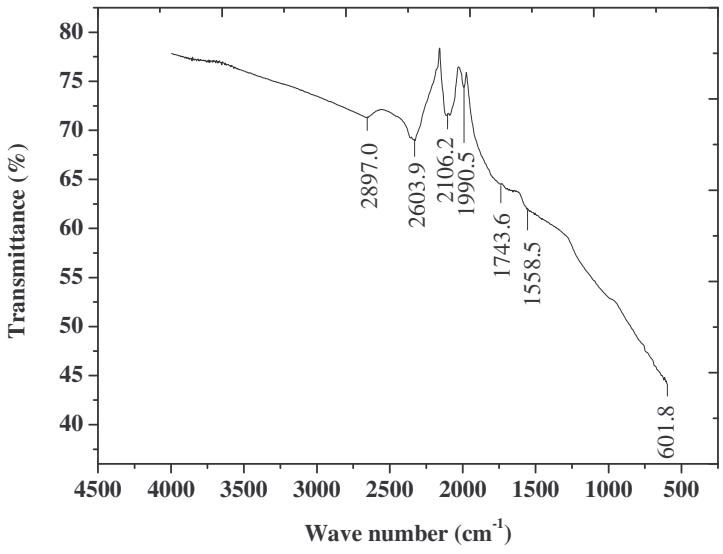

Figure A10. FT-IR spectrum of CAC after adsorption of metals and phenol

APPENDIX B

Data for determining adsorbent optimum mass and contact time

Table B1

Data for determining the optimum CFA mass

Adsorbent mass (g)	Percentage removal (%)				
	Co	Ni	Fe	Pb	Phenol
0	0	0	0	0	0
0.20	2.97	3.61	16.25	16.34	2.66
0.40	5.17	14.91	25.32	52.69	2.47
0.60	6.26	17.71	50.14	75.70	3.50
0.80	10.99	33.76	75.95	86.56	5.19
1.00	22.5	58.72	99.02	85.48	8.37
1.20	35.82	77.21	100.0	85.27	19.86
1.40	41.21	91.31	100.0	86.56	27.19
1.60	50.66	99.16	100.0	86.56	33.49
1.80	58.79	100.0	100.0	86.56	34.07
2.00	72.20	100.0	100.0	85.05	40.56
3.00	88.33	99.89	100.0	86.56	65.22
4.00	100.0	100.0	100.0	86.56	73.01
5.00	99.10	99.92	100.0	86.56	72.81
6.00	99.12	100.0	100.0	86.56	72.81

Optimum mass = 4.0 g

Table B2

Data for determining the optimum SD500 mass

Adsorbent mass (g)	Percentage removal (%)				
	Co	Ni	Fe	Pb	Phenol
0	0	0	0	0	0
0.20	1.62	10.13	18.89	24.25	33.20
0.40	6.20	12.21	42.01	58.12	61.76
0.60	21.59	59.95	70.57	63.50	78.01
0.80	40.41	74.44	78.92	72.87	82.64
1.00	89.07	92.54	84.79	76.69	89.02
1.20	91.79	96.66	96.98	80.13	90.64
1.40	95.23	97.00	97.36	80.87	90.98
1.60	98.09	97.62	98.21	81.37	91.01
1.80	98.57	98.22	98.22	81.75	92.11
2.00	98.66	99.02	98.22	82.47	91.66
3.00	97.00	99.02	98.21	82.59	92.65
4.00	97.82	99.00	98.22	82.59	92.66
5.00	97.82	99.02	98.22	82.59	92.66

Optimum mass = 4.0 g

Table B3

Data for determining the optimum SAS mass

Adsorbent mass (g)	Percentage removal (%)				
	Co	Ni	Fe	Pb	Phenol
0	0	0	0	26.14	0
0.20	2.67	12.42	78.49	80.95	92.90
0.40	6.40	15.26	100.0	84.03	89.76
0.60	23.59	60.95	99.57	84.50	91.01
0.80	42.41	77.44	99.79	84.87	91.64
1.00	90.07	96.02	99.79	84.69	92.90
1.20	91.79	98.96	99.79	84.13	91.64
1.40	95.23	100.0	99.36	84.87	89.76
1.60	98.09	99.62	99.79	84.87	91.01
1.80	98.66	99.81	99.79	83.75	92.10
2.00	100.0	100.0	99.79	83.47	92.27
3.00	99.83	100.0	99.79	84.69	92.27
4.00	99.81	100.0	99.79	84.69	92.27

Optimum mass = 2.0 g

Table B4

Data for determining the optimum CAC mass

Adsorbent mass (g)	Percentage removal (%)				
	Co	Ni	Fe	Pb	Phenol
0	0	0	0	0	0
0.20	15.02	5.27	93.89	66.69	96.48
0.60	46.82	61.13	99.79	81.32	98.69
0.80	65.90	84.82	98.95	81.43	99.0
1.00	82.59	100.0	100.0	81.76	99.02
1.60	98.54	100.0	100.0	82.42	100.0
2.00	98.54	99.84	100.0	82.42	99.93
3.00	98.54	100.0	100.0	82.39	99.25
4.00	98.23	100.0	100.0	82.42	99.33

Optimum mass = 1.6 g

Table B5

Data for determining contact time for the removal of dyes using SB400 and CFA

Time (min)	Percentage removal (%)					
	SB400			CFA		
	DR80	DR81	DR23	DR80	DR81	DR23
0	0	0	0	0	0	0
30.0	35.97	25.38	25.00	22.84	8.67	8.63
60.0	42.77	34.58	34.04	27.89	15.57	15.68
90.0	48.66	43.92	42.10	32.15	20.44	21.29
120.0	48.85	44.41	43.25	34.82	22.89	22.43
180.0	54.14	47.39	46.92	35.99	28.99	27.18
240.0	56.29	49.74	50.67	39.10	33.02	32.05
300.0	59.04	53.92	54.71	43.32	38.14	36.02
360.0	62.00	58.62	57.71	46.66	42.89	41.49
420.0	67.10	63.35	61.75	51.90	49.41	48.42
480.0	69.36	65.63	64.25	54.15	51.01	50.14
540.0	69.87	67.18	66.27	55.30	52.24	50.52
600.0	70.09	67.80	66.54	55.30	52.24	50.52
660.0	70.10	67.80	66.54			

Table B6

Data for determining contact time using CFA to treat petrochemical wastewater

Time (min)	Percentage removal (%)				
	Co	Fe	Ni	Pb	Phenol
0	0	0	0	0	0
5.0	20.22	8.61	60.23	43.67	3.12
10.0	31.09	11.02	82.98	69.11	7.43
15.0	46.72	15.90	94.45	83.65	11.78
30.0	59.74	34.84	99.79	84.21	25.58
45.0	65.45	48.68	99.79	84.21	24.70
60.0	67.42	50.15	99.47	85.34	27.73
75.0	72.10	65.16	99.79	86.47	27.50
90.0	76.50	69.77	99.36	87.78	31.34
120.0	78.46	96.47	99.79	87.78	32.14
150.0	86.70	94.11	99.79	88.35	33.39
180.0	94.82	98.82	99.79	88.72	33.58
210.0	95.10	99.02	99.57	89.47	37.59
240.0	97.35	100.0	99.79	89.85	39.49
300.0	97.44	100.0	99.79	89.04	41.46
360.0	97.44	100.0	99.68	89.85	42.02
1140.0	97.43	99.80	99.79	89.04	43.86
1380.0	97.44	100.0	99.36	89.85	44.67
1500.0	97.44	100.0	99.79	89.66	44.67
1620.0	97.25	99.81	99.57	89.85	44.67
1740.0	97.44	100.0	99.79	89.85	44.67
1980.0	97.44	100.0	99.79	89.66	44.98

Table B7

Data for determining contact time using SAS to treat petrochemical wastewater

Time (min)	Percentage removal (%)				
	Co	Ni	Fe	Pb	Phenol
0	0	0	0	0	0
5.0	55.78	63.10	71.94	22.89	44.92
10.0	81.65	86.76	96.58	39.45	89.65
15.0	92.08	99.62	99.36	52.88	94.34
30.0	92.96	99.81	99.58	57.52	97.01
60.0	94.72	100.0	99.79	57.74	99.05
90.0	95.60	100.0	99.79	59.07	99.17
120.0	96.04	99.81	99.79	59.51	99.19
180.0	96.04	100.0	99.79	67.04	99.45
240.0	96.04	100.0	99.79	67.04	99.45

Table B8

Data for determining contact time using CAC to treat petrochemical wastewater

Time (min)	Percentage removal (%)				
	Co	Ni	Fe	Pb	Phenol
0	0	0	0	0	0
5.0	64.27	71.99	70.82	23.87	55.94
10.0	88.69	94.79	93.48	40.99	89.71
15.0	93.20	99.74	99.42	55.29	95.20
30.0	94.01	99.92	99.58	62.78	97.06
60.0	94.92	100.0	99.82	68.14	99.98
90.0	95.87	100.0	99.98	72.8	100.0
120.0	98.10	99.89	100.0	73.92	100.0
180.0	98.26	100.0	100.0	73.93	99.89
240.0	98.26	100.0	100.0	73.92	100.0

Table B9

Data for determining contact time using SD500 to treat petrochemical wastewater

Time (min)	Percentage removal (%)				
	Fe	Co	Ni	Pb	Phenol
0	0	0	0	0	0
5.0	14.85	9.04	56.34	33.55	6.92
10.0	28.67	12.87	72.96	54.64	13.88
15.0	45.82	16.91	93.25	72.25	29.89
30.0	58.84	34.84	95.29	83.2	48.67
45.0	66.49	48.68	96.48	84.53	62.00
60.0	69.24	50.19	98.37	85.34	67.10
75.0	73.80	65.19	99.11	86.47	69.36
90.0	77.51	69.78	99.36	86.99	69.87
120.0	79.48	96.49	99.40	87.78	74.09
150.0	86.70	94.22	99.44	88.35	76.10
180.0	96.82	98.89	99.60	88.72	80.65
210.0	97.10	99.02	99.77	89.47	86.72
240.0	99.35	99.90	99.89	90.40	90.98
300.0	99.61	100.0	99.89	90.40	97.92
360.0	99.62	100.0	99.80	90.50	100.0
420.0	99.61	100.0	99.88	90.40	100.0

APPENDIX C

Adsorption kinetics data

Table C1

Data for Lagergren pseudo-first-order kinetic model for cobalt

Time	log (q_e-q_t)			
(min)	SD500	CFA	SAS	CAC
0	0	0.12385	0.35536	0.49837
5.0	0.01431	0.02531	-0.02226	0.03736
10.0	-0.00437	-0.03858	-0.46910	-0.43053
15.0	-0.02498	-0.15104	-1.02939	-0.58767
30.0	-0.13055	-0.27368	-1.13854	-0.86561
45.0	-0.23424	-0.34080	-1.50651	-0.97026
60.0	-0.24721	-0.36653	-1.98364	-1.11561
75.0	-0.40282	-0.43474		-2.28988
90.0	-0.46423	-0.51039		
120.0	-1.39922	-0.54898		
150.0	-1.18260	-0.76321		
180.0	-1.89920	-1.20412		
210.0	-1.95330	-1.23099		
240.0	-2.94453	-1.54136		

Table C2

Data for pseudo-second-order kinetic model for cobalt removal

Time	t/q_t			
(min)	SD500	CFA	SAS	CAC
0	0	0	0	0
5.0	48.6618	18.5185	3.7980	2.4265
10.0	68.3761	24.0964	5.1894	3.5979
15.0	78.0681	24.0481	6.9026	5.1867
30.0	75.7826	37.6176	13.6746	9.9529
45.0	81.3557	51.5022	20.3611	14.9007
60.0	105.2108	66.6667	26.8409	19.7150
75.0	101.2526	77.9221	33.4656	21.1149
90.0	113.5109	88.1273	39.8908	29.2794
120.0	109.4523	114.5585	52.9440	38.1517
150.0	140.1117	129.5896	66.1802	47.6644
180.0	160.1940	142.0118	79.4160	57.1345
210.0	186.6476	165.1917	92.6521	66.6569
240.0	211.4326	184.4380	105.8881	76.1793
300.0	264.0264	230.3263	132.3601	95.2242
360.0	316.8317	276.3916	158.8321	114.2690
420.0	369.6370	322.4568	185.3041	133.3138

Table C3

Data for the intraparticle diffusion model for cobalt adsorption

$t^{1/2}$ ($min^{1/2}$)	q_t (mg/g)			
	SD500	CFA	SAS	CAC
0	0	0	0	0
2.23607	0.10275	0.27000	1.31650	2.06063
3.16228	0.14625	0.41500	1.92700	2.77938
3.87298	0.19214	0.62375	2.17309	2.89204
5.47723	0.39587	0.79750	2.19386	3.01420
6.70820	0.55313	0.87375	2.23539	3.04337
7.74597	0.57028	0.90000	2.25616	3.07383
8.66025	0.74072	0.96250	2.26654	3.14533
9.48683	0.79288	1.02125	2.26654	3.15046
10.95445	1.09637	1.04750	2.26654	3.15046
12.24745	1.07058	1.15750	2.26654	3.15046
13.41641	1.12364	1.26750	2.26654	3.15046
14.49138	1.12512	1.27125	2.26654	3.15046
15.49193	1.13511	1.30125	2.26654	3.15046
17.32051	1.13625	1.30250	2.26654	3.15046
18.97367	1.13625	1.30250	2.26654	3.15046
20.49390	1.13625	1.30250	2.26654	3.15046

APPENDIX D

Adsorption isotherm data

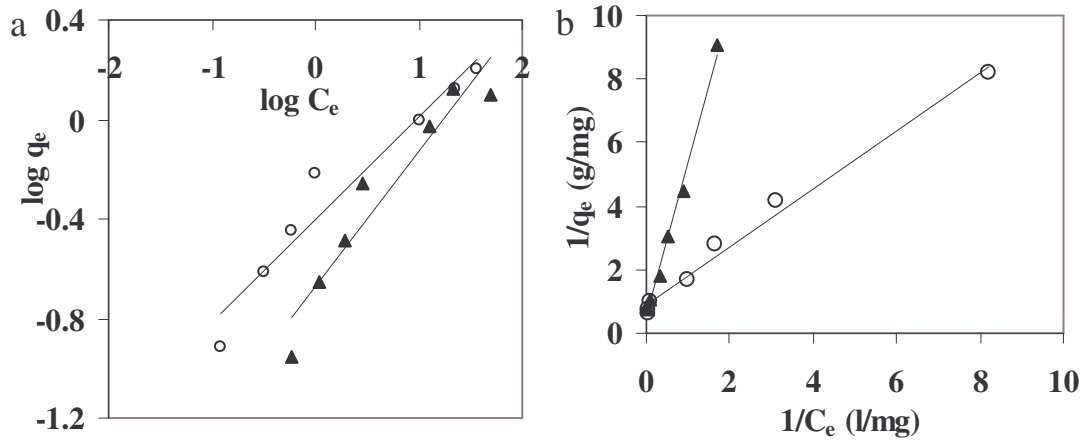

Figure D1. Linear regression analysis of DR23 removal using CFA (▲) and SD500 (○) for (a) Freundlich and (b) Langmuir isotherm.

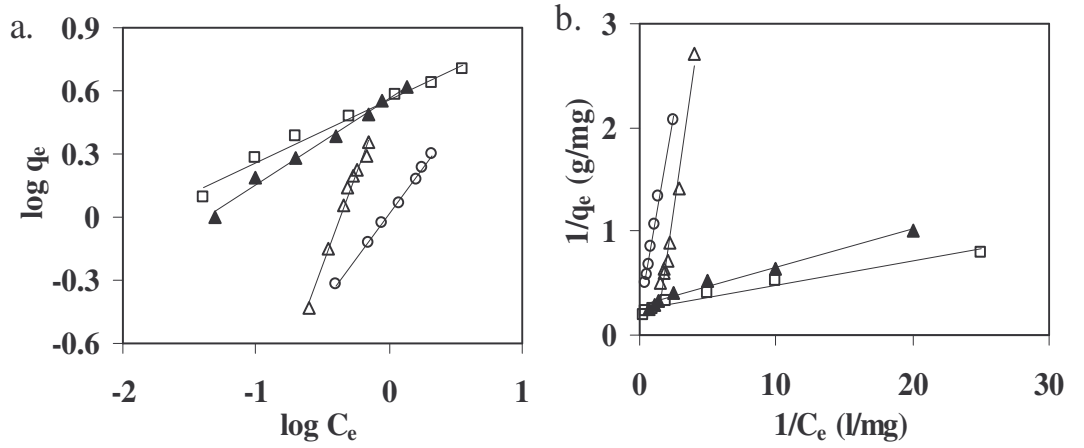

Figure D2. Linear regression analysis of nickel removal using CAC (□), SAS (▲), SD500 (○) and CFA (Δ) for (a) Freundlich and (b) Langmuir isotherm.

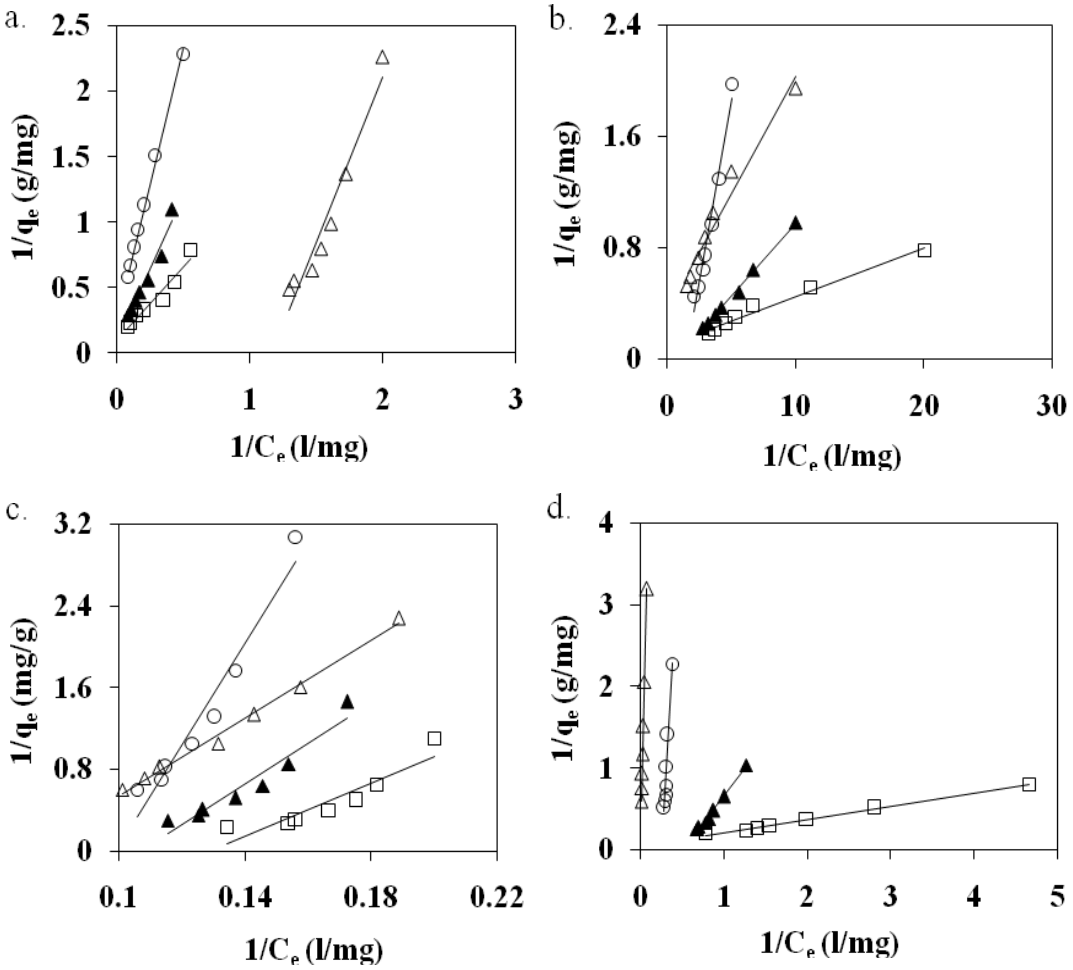

Figure D3. Linear regression analysis of (a) cobalt, (b) iron, (c) lead and (d) phenol removal using CAC (□), SAS (▲), SD500 (○) and CFA (Δ) for Langmuir isotherm.

Table D1

Freundlich and Langmuir adsorption isotherm data for DR80 removal using SB400

C_o (mg/l)	C_e (mg/l)	q_e (mg/g)	log C_e	log q_e	$1/C_e$ (l/mg)	$1/q_e$ (g/mg)
5.06	0.30	0.1175	-0.5212	-0.9301	3.3207	8.5127
10.10	0.66	0.2336	-0.1819	-0.6316	1.5201	4.2817
15.02	1.33	0.3417	0.1249	-0.4664	0.7501	2.9268
25.60	3.38	0.5405	0.5290	-0.2672	0.2958	1.8502
50.34	14.45	0.8888	1.1600	-0.0512	0.0692	1.1252
75.44	25.35	1.2414	1.4039	0.0939	0.0395	0.8056
99.68	55.27	1.1183	1.7425	0.0486	0.0181	0.8942

Table D2

Freundlich and Langmuir adsorption isotherm data for DR80 removal using CFA

C_o (mg/l)	C_e (mg/l)	q_e (mg/g)	log C_e	log q_e	$1/C_e$ (l/mg)	$1/q_e$ (g/mg)
5.08	0.38	0.1154	-0.4176	-0.9376	2.6155	8.6624
10.11	0.80	0.2300	-0.0969	-0.6383	1.2498	4.3479
15.27	1.12	0.3470	0.0491	-0.4597	0.8932	2.8818
25.00	2.06	0.5735	0.3138	-0.2415	0.4856	1.7436
50.10	10.27	0.9934	1.0114	-0.0029	0.0974	1.0067
74.89	31.77	1.0809	1.5020	0.0338	0.0315	0.9252
100.0	39.90	1.5025	1.6010	0.1768	0.0251	0.6656

Table D3

Freundlich and Langmuir adsorption isotherm data for DR81 removal using SB400

C_o (mg/l)	C_e (mg/l)	q_e (mg/g)	log C_e	log q_e	$1/C_e$ (l/mg)	$1/q_e$ (g/mg)
5.00	0.42	0.1144	-0.37239	-0.9416	2.3572	8.7417
9.89	0.91	0.2274	-0.04354	-0.6432	1.1055	4.3978
15.00	1.45	0.3387	0.161438	-0.4701	0.6895	2.9521
24.95	2.80	0.5550	0.447014	-0.2557	0.3573	1.8017
50.00	12.11	0.9473	1.083036	-0.0235	0.0826	1.0556
75.02	20.31	1.3673	1.307678	0.1359	0.0492	0.7314
100.40	47.78	1.3055	1.679245	0.1158	0.0209	0.7660

Table D4

Freundlich and Langmuir adsorption isotherm data for DR81 removal using CFA

C_o (mg/l)	C_e (mg/l)	q_e (mg/g)	log C_e	log q_e	$1/C_e$ (l/mg)	$1/q_e$ (g/mg)
5.22	0.39	0.4607	-0.4052	-0.3366	2.5424	2.1708
10.00	0.76	0.9242	-0.1203	-0.0342	1.3191	1.0820
15.02	1.33	1.3673	0.1229	0.1359	0.7536	0.7314
24.85	2.94	2.2061	0.4681	0.3436	0.3403	0.4533
50.04	9.98	4.0017	0.9993	0.6023	0.1002	0.2499
75.30	25.78	4.9219	1.4113	0.6921	0.0388	0.2032
99.69	35.72	6.4282	1.5529	0.8081	0.0280	0.1556

Table D5

Freundlich and Langmuir adsorption isotherm data for DR23 removal using SB400

C_o (mg/l)	C_e (mg/l)	q_e (mg/g)	log C_e	log q_e	$1/C_e$ (l/mg)	$1/q_e$ (g/mg)
4.99	0.56	0.1104	-0.2322	-0.9572	1.7068	9.0619
10.32	1.10	0.2225	0.0420	-0.6527	0.9079	4.4951
14.92	1.89	0.3277	0.2772	-0.4846	0.5282	3.0519
25.0	2.83	0.5542	0.4522	-0.2564	0.3530	1.8045
49.80	12.59	0.9354	1.0999	-0.0290	0.0795	1.0691
75.01	21.78	1.3305	1.3381	0.1240	0.0459	0.7516
100.20	49.72	1.2569	1.6966	0.0993	0.0201	0.7956

Table D6

Freundlich and Langmuir adsorption isotherm data for DR23 removal using CFA

C_o (mg/l)	C_e (mg/l)	q_e (mg/g)	log C_e	log q_e	$1/C_e$ (l/mg)	$1/q_e$ (g/mg)
5.09	0.12	0.121955	-0.9144	-0.9138	8.2102	8.1998
10.21	0.32	0.241918	-0.4904	-0.6163	3.0931	4.1336
14.29	0.60	0.359966	-0.2209	-0.4437	1.6629	2.7780
25.09	1.00	0.600102	-0.0018	-0.2218	1.0041	1.6664
49.20	10.22	0.994483	1.0095	-0.0024	0.0978	1.0056
74.99	22.35	1.316287	1.3493	0.1194	0.0448	0.7597
100.06	36.69	1.582662	1.5646	0.1994	0.0273	0.6319

Table D7

Freundlich and Langmuir adsorption isotherm data for cobalt removal using SAS

C_o (mg/l)	C_e (mg/l)	q_e (mg/g)	log C_e	log q_e	$1/C_e$ (l/mg)	$1/q_e$ (g/mg)
20.65	2.40	0.9125	0.3802	-0.0398	0.4167	1.0959
30.05	2.95	1.3550	0.4698	0.1319	0.3390	0.7380
40.20	4.20	1.8000	0.6233	0.2553	0.2381	0.5556
49.10	5.80	2.1650	0.7634	0.3355	0.1724	0.4619
57.20	6.99	2.5105	0.8445	0.3998	0.1430	0.3983
69.80	8.95	3.0425	0.9518	0.4832	0.1117	0.3287
81.05	11.45	3.4800	1.0588	0.5416	0.0873	0.2874

Table D8

Freundlich and Langmuir adsorption isotherm data for nickel removal using SAS

C_o (mg/l)	C_e (mg/l)	q_e (mg/g)	log C_e	log q_e	$1/C_e$ (l/mg)	$1/q_e$ (g/mg)
20.0	0.05	0.9975	-1.3010	-0.0011	20.000	1.0025
31.0	0.10	1.5450	-1.0000	0.1890	10.000	0.6473
38.8	0.20	1.9300	-0.6990	0.2856	5.0000	0.5181
48.7	0.40	2.4150	-0.3979	0.3829	2.5000	0.4141
62.5	0.70	3.0900	-0.1549	0.4900	1.4286	0.3236
71.8	0.90	3.5450	-0.0458	0.5496	1.1111	0.2821
83.6	1.35	4.1125	0.1303	0.6141	0.7407	0.2432

Table D9

Freundlich and Langmuir adsorption isotherm data for iron removal using SAS

C_o (mg/l)	C_e (mg/l)	q_e (mg/g)	log C_e	log q_e	$1/C_e$ (l/mg)	$1/q_e$ (g/mg)
20.50	0.10	1.0200	-1.0000	0.0086	10.000	0.9804
31.30	0.15	1.5575	-0.8239	0.1924	6.6667	0.6421
41.70	0.18	2.0760	-0.7447	0.3172	5.5556	0.4817
53.95	0.24	2.6855	-0.6198	0.4290	4.1667	0.3724
62.75	0.27	3.1240	-0.5686	0.4947	3.7037	0.3201
77.41	0.32	3.8545	-0.4949	0.5860	3.1250	0.2594
88.85	0.37	4.4240	-0.4318	0.6458	2.7027	0.2260

Table D10

Freundlich and Langmuir adsorption isotherm data for lead removal using SAS

C_o (mg/l)	C_e (mg/l)	q_e (mg/g)	log C_e	log q_e	$1/C_e$ (l/mg)	$1/q_e$ (g/mg)
19.50	5.80	0.6850	0.7634	-0.1643	0.1724	1.4599
30.00	6.50	1.1750	0.8129	0.0700	0.1539	0.8511
38.10	6.86	1.5620	0.8363	0.1937	0.1458	0.6402
46.00	7.30	1.9350	0.8633	0.2867	0.1370	0.5168
57.30	7.90	2.4700	0.8976	0.3927	0.1266	0.4049
65.10	7.99	2.8555	0.9026	0.4557	0.1252	0.3502
76.20	8.65	3.3775	0.9370	0.5286	0.1156	0.2961

Table D11

Freundlich and Langmuir adsorption isotherm data for phenol removal using SAS

C_o (mg/l)	C_e (mg/l)	q_e (mg/g)	log C_e	log q_e	$1/C_e$ (l/mg)	$1/q_e$ (g/mg)
20.16	0.79	0.9686	-0.1047	-0.0139	1.2727	1.0325
31.69	1.00	1.5346	9.643E-17	0.1860	1.0000	0.6516
42.55	1.14	2.0704	0.0580	0.3161	0.8750	0.4830
54.26	1.21	2.6525	0.0843	0.4237	0.8235	0.3770
62.39	1.29	3.0554	0.1092	0.4851	0.7778	0.3273
71.28	1.43	3.4925	0.1549	0.5431	0.7000	0.2863
81.35	1.46	3.9943	0.1656	0.6014	0.6829	0.2504

Table D12

Freundlich and Langmuir adsorption isotherm data for cobalt removal using SD500

C_o (mg/l)	C_e (mg/l)	q_e (mg/g)	log C_e	log q_e	$1/C_e$ (l/mg)	$1/q_e$ (g/mg)
19.50	2.00	0.4375	0.3010	-0.3590	0.5000	2.2857
29.90	3.44	0.6615	0.5366	-0.1795	0.2907	1.5117
40.10	4.80	0.8825	0.6812	-0.0543	0.2083	1.1332
48.80	6.20	1.0650	0.7924	0.0274	0.1613	0.9390
57.00	7.50	1.2375	0.8751	0.0926	0.1333	0.8081
69.50	9.48	1.5005	0.9768	0.1762	0.1055	0.6665
80.20	11.20	1.7250	1.0492	0.2368	0.0893	0.5797

Table D13

Freundlich and Langmuir adsorption isotherm data for nickel removal using SD500

C_o (mg/l)	C_e (mg/l)	q_e (mg/g)	log C_e	log q_e	1/C_e (l/mg)	1/q_e (g/mg)
19.80	0.40	0.4850	-0.3979	-0.3143	2.5000	2.0619
30.75	0.70	0.7513	-0.1549	-0.1242	1.4286	1.3311
38.20	0.90	0.9325	-0.0458	-0.0304	1.1111	1.0724
47.98	1.20	1.1695	0.0792	0.0680	0.8333	0.8551
61.50	1.60	1.4975	0.2041	0.1754	0.6250	0.6678
70.62	1.80	1.7205	0.2553	0.2357	0.5556	0.5812
82.58	2.10	2.0120	0.3222	0.3036	0.4762	0.4970

Table D14

Freundlich and Langmuir adsorption isotherm data for iron removal using SD500

C_o (mg/l)	C_e (mg/l)	q_e (mg/g)	log C_e	log q_e	1/C_e (l/mg)	1/q_e (g/mg)
20.50	0.20	0.5075	-0.6990	-0.2946	5.0000	1.9704
31.20	0.25	0.7738	-0.6021	-0.1114	4.0000	1.2924
41.60	0.29	1.0328	-0.5376	0.0140	3.4483	0.9683
53.80	0.34	1.3365	-0.4685	0.1260	2.9412	0.7482
62.70	0.36	1.5585	-0.4437	0.1927	2.7778	0.6416
77.39	0.42	1.9243	-0.3768	0.2843	2.3810	0.5197
88.80	0.48	2.2080	-0.3188	0.3440	2.0833	0.4529

Table D15

Freundlich and Langmuir adsorption isotherm data for lead removal using SD500

C_o (mg/l)	C_e (mg/l)	q_e (mg/g)	log C_e	log q_e	1/C_e (l/mg)	1/q_e (g/mg)
19.40	6.40	0.3250	0.8062	-0.4881	0.1563	3.0769
29.90	7.30	0.5650	0.8633	-0.2480	0.1370	1.7699
38.20	7.66	0.7635	0.8842	-0.1172	0.1306	1.3098
46.10	8.10	0.9500	0.9085	-0.0223	0.1235	1.0526
57.40	8.70	1.2175	0.9395	0.0855	0.1149	0.8214
66.00	8.79	1.4303	0.9440	0.1554	0.1138	0.6992
76.40	9.45	1.6738	0.9754	0.2237	0.1058	0.5975

Table D16

Freundlich and Langmuir adsorption isotherm data for phenol removal using SD500

C_o (mg/l)	C_e (mg/l)	q_e (mg/g)	log C_e	log q_e	$1/C_e$ (l/mg)	$1/q_e$ (g/mg)
20.20	2.59	0.4403	0.4133	-0.3563	0.3861	2.2714
31.50	3.00	0.7125	0.4771	-0.1472	0.3333	1.4035
42.45	3.15	0.9825	0.4983	-0.0077	0.3175	1.0178
54.25	3.20	1.2763	0.5052	0.1059	0.3125	0.7836
62.40	3.28	1.4780	0.5159	0.1697	0.3049	0.6766
71.30	3.40	1.6975	0.5315	0.2298	0.2941	0.5891
81.25	3.45	1.9450	0.5378	0.2889	0.2899	0.5141

Table D17

Freundlich and Langmuir adsorption isotherm data for cobalt removal using CFA

C_o (mg/l)	C_e (mg/l)	q_e (mg/g)	log C_e	log q_e	$1/C_e$ (l/mg)	$1/q_e$ (g/mg)
18.15	0.50	0.4413	-0.3010	-0.3553	2.0000	2.2663
29.80	0.58	0.7305	-0.2366	-0.1364	1.7241	1.3689
41.15	0.62	1.0133	-0.2076	0.0057	1.6129	0.9869
50.95	0.65	1.2575	-0.1871	0.0995	1.5385	0.7952
64.20	0.68	1.5880	-0.1675	0.2009	1.4706	0.6297
73.50	0.75	1.8188	-0.1249	0.2598	1.3333	0.5498
83.75	0.77	2.0745	-0.1135	0.3169	1.2987	0.4820

Table D18

Freundlich and Langmuir adsorption isotherm data for nickel removal using CFA

C_o (mg/l)	C_e (mg/l)	q_e (mg/g)	log C_e	log q_e	$1/C_e$ (l/mg)	$1/q_e$ (g/mg)
15.00	0.25	0.3688	-0.6021	-0.4333	4.0000	2.7119
28.80	0.35	0.7113	-0.4559	-0.1480	2.8571	1.4060
45.85	0.46	1.1348	-0.3372	0.0549	2.1739	0.8813
56.35	0.49	1.3965	-0.3098	0.1450	2.0408	0.7161
63.25	0.54	1.5678	-0.2676	0.1953	1.8519	0.6379
67.50	0.57	1.6733	-0.2441	0.2236	1.7544	0.5976
79.10	0.68	1.9605	-0.1675	0.2924	1.4706	0.5101

Table D19

Freundlich and Langmuir adsorption isotherm data for iron removal using CFA

C_o (mg/l)	C_e (mg/l)	q_e (mg/g)	log C_e	log q_e	$1/C_e$ (l/mg)	$1/q_e$ (g/mg)
20.65	0.10	0.5138	-1.0000	-0.2893	10.000	1.9465
29.85	0.20	0.7413	-0.6990	-0.1300	5.0000	1.3491
38.30	0.28	0.9505	-0.5528	-0.0221	3.5714	1.0521
45.85	0.34	1.1378	-0.4685	0.0561	2.9412	0.8789
55.20	0.41	1.3698	-0.3872	0.1366	2.4390	0.7301
67.65	0.55	1.6775	-0.2596	0.2247	1.8182	0.5961
76.50	0.65	1.8963	-0.1871	0.2779	1.5385	0.5274

Table D20

Freundlich and Langmuir adsorption isotherm data for lead removal using CFA

C_o (mg/l)	C_e (mg/l)	q_e (mg/g)	log C_e	log q_e	$1/C_e$ (l/mg)	$1/q_e$ (g/mg)
22.85	5.30	0.4388	0.7243	-0.3578	0.1887	2.2792
31.25	6.35	0.6225	0.8028	-0.2059	0.1575	1.6064
36.90	7.00	0.7475	0.8451	-0.1264	0.1429	1.3378
45.65	7.60	0.9513	0.8808	-0.0217	0.1316	1.0513
57.70	8.85	1.2213	0.9469	0.0868	0.1130	0.8188
65.25	9.25	1.4000	0.9661	0.1461	0.1081	0.7143
76.60	9.90	1.6675	0.9956	0.2221	0.1010	0.5997

Table D21

Freundlich and Langmuir adsorption isotherm data for phenol removal using CFA

C_o (mg/l)	C_e (mg/l)	q_e (mg/g)	log C_e	log q_e	$1/C_e$ (l/mg)	$1/q_e$ (g/mg)
20.55	12.52	0.3130	1.0977	-0.5044	0.0799	3.1945
34.41	19.43	0.4857	1.2884	-0.3136	0.0515	2.0588
35.62	26.36	0.6589	1.4209	-0.1812	0.0379	1.5176
51.55	34.19	0.8548	1.5339	-0.0681	0.0293	1.1698
63.36	42.64	1.0661	1.6299	0.0278	0.0235	0.9380
83.41	53.00	1.3250	1.7243	0.1222	0.0189	0.7547
84.29	67.59	1.6898	1.8299	0.2278	0.0148	0.5918

Table D22

Freundlich and Langmuir adsorption isotherm data for cobalt removal using CAC

C_o (mg/l)	C_e (mg/l)	q_e (mg/g)	log C_e	log q_e	$1/C_e$ (l/mg)	$1/q_e$ (g/mg)
20.65	1.80	1.2747	0.2553	0.1054	0.5556	0.7845
30.05	2.30	1.8555	0.3617	0.2685	0.4348	0.5389
40.20	2.90	2.4836	0.4624	0.3951	0.3448	0.4026
49.10	4.90	3.0256	0.6902	0.4808	0.2041	0.3305
57.20	7.00	3.5222	0.8451	0.5468	0.1429	0.2839
69.80	10.10	4.2997	1.0043	0.6334	0.0990	0.2326
81.05	12.40	4.9973	1.0934	0.6987	0.0807	0.2001

Table D23

Freundlich and Langmuir adsorption isotherm data for nickel removal using CAC

C_o (mg/l)	C_e (mg/l)	q_e (mg/g)	log C_e	log q_e	$1/C_e$ (l/mg)	$1/q_e$ (g/mg)
20.00	0.04	1.2475	-1.3979	0.0960	25.000	0.8016
31.00	0.10	1.9313	-1.0000	0.2858	10.000	0.5178
38.80	0.20	2.4125	-0.6990	0.3825	5.0000	0.4145
48.70	0.50	3.0125	-0.3010	0.4789	2.0000	0.3320
62.50	1.10	3.8375	0.0414	0.5841	0.9091	0.2606
71.80	2.10	4.3563	0.3222	0.6391	0.4762	0.2296
83.60	3.55	5.0031	0.5502	0.6992	0.2817	0.1999

Table D24

Freundlich and Langmuir adsorption isotherm data for iron removal using CAC

C_o (mg/l)	C_e (mg/l)	q_e (mg/g)	log C_e	log q_e	$1/C_e$ (l/mg)	$1/q_e$ (g/mg)
20.50	0.05	1.2781	-1.3010	0.1066	20.000	0.7824
31.30	0.09	1.9506	-1.0458	0.2902	11.1111	0.5127
41.70	0.15	2.5969	-0.8239	0.4145	6.6667	0.3851
53.95	0.19	3.3600	-0.7213	0.5263	5.2632	0.2976
62.75	0.22	3.9081	-0.6576	0.5920	4.5455	0.2559
77.41	0.27	4.8213	-0.5686	0.6832	3.7030	0.2074
88.85	0.31	5.5338	-0.5086	0.7430	3.2258	0.1807

Table D25

Freundlich and Langmuir adsorption isotherm data for lead removal using CAC

C_o (mg/l)	C_e (mg/l)	q_e (mg/g)	log C_e	log q_e	$1/C_e$ (l/mg)	$1/q_e$ (g/mg)
19.50	5.00	0.9063	0.6990	-0.0428	0.2000	1.1035
30.00	5.50	1.5313	0.7404	0.1851	0.1818	0.6531
38.10	5.71	2.0244	0.7566	0.3063	0.1751	0.4940
46.00	6.00	2.5000	0.7782	0.3979	0.1667	0.4000
57.30	6.40	3.1813	0.8062	0.5026	0.1563	0.3143
65.10	6.50	3.6625	0.8129	0.5638	0.1539	0.2730
76.20	7.45	4.2969	0.8722	0.6332	0.1342	0.2327

Table D26

Freundlich and Langmuir adsorption isotherm data for phenol removal using CAC

C_o (mg/l)	C_e (mg/l)	q_e (mg/g)	log C_e	log q_e	$1/C_e$ (l/mg)	$1/q_e$ (g/mg)
20.1	0.21	1.2429	-0.6690	0.0944	4.6667	0.8046
31.64	0.36	1.9549	-0.4472	0.2911	2.8000	0.5115
42.49	0.50	2.6246	-0.3010	0.4191	2.0000	0.3810
54.21	0.64	3.3478	-0.1919	0.5248	1.5556	0.2987
61.29	0.71	3.7859	-0.1461	0.5782	1.4000	0.2641
67.68	0.79	4.1810	-0.1047	0.6213	1.2727	0.2392
81.45	1.29	5.0101	0.1092	0.6999	0.7778	0.1996

APPENDIX E

Response surface methodology data

Table E1

Experimental and predicted adsorption capacities for cobalt using CFA and SAS

Run	Coded values			CFA		SAS	
	Dose	pH	C_o	Exp. q_e (mg/g)	Pred. q_e (mg/g)	Exp. q_e (mg/g)	Pred. q_e (mg/g)
1	-1	-1	-1	0.023	0.038	0.245	0.022
2	1	-1	-1	0.388	0.373	0.658	0.881
3	-1	1	-1	1.083	1.068	2.360	2.583
4	1	1	-1	0.361	0.376	0.797	0.574
5	-1	-1	1	0.060	0.045	0.575	0.799
6	1	-1	1	1.010	1.025	1.852	1.629
7	-1	1	1	1.118	1.133	4.770	4.547
8	1	1	1	1.102	1.087	2.285	2.508
9	0	0	0	1.085	1.084	2.260	2.262
10	0	0	0	1.084	1.084	2.263	2.262
11	0	0	0	1.085	1.084	2.268	2.262
12	0	0	0	1.083	1.084	2.255	2.262

Table E2

Experimental and predicted adsorption capacities for nickel using CFA and SAS

Run	Coded values			CFA		SAS	
	Dose	pH	C_o	Exp. q_e (mg/g)	Pred. q_e (mg/g)	Exp. q_e (mg/g)	Pred. q_e (mg/g)
1	-1	-1	-1	0.458	0.231	0.900	0.283
2	1	-1	-1	0.533	0.760	0.762	1.379
3	-1	1	-1	1.378	1.605	2.435	3.052
4	1	1	-1	0.459	0.232	0.812	0.195
5	-1	-1	1	0.055	0.282	1.375	1.992
6	1	-1	1	1.465	1.238	2.738	2.121
7	-1	1	1	2.918	2.691	8.045	7.428
8	1	1	1	1.520	1.747	2.987	3.604
9	0	0	0	1.534	1.531	3.25	3.251
10	0	0	0	1.523	1.531	3.255	3.251
11	0	0	0	1.541	1.531	3.245	3.251
12	0	0	0	1.524	1.531	3.255	3.251

Table E3

Experimental and predicted adsorption capacities for iron using CFA and SAS

Run	Coded values			CFA		SAS	
	Dose	pH	C_o	Exp. q_e (mg/g)	Pred. q_e (mg/g)	Exp. q_e (mg/g)	Pred. q_e (mg/g)
1	-1	-1	-1	1.345	1.119	1.845	1.496
2	1	-1	-1	0.449	0.675	0.910	1.259
3	-1	1	-1	0.993	1.219	2.540	2.889
4	1	1	-1	0.331	0.105	0.847	0.498
5	-1	-1	1	1.848	2.074	4.235	4.584
6	1	-1	1	1.221	0.995	2.680	2.331
7	-1	1	1	3.303	3.077	7.660	7.311
8	1	1	1	1.101	1.327	2.553	2.902
9	0	0	0	1.169	1.169	2.573	2.572
10	0	0	0	1.171	1.169	2.568	2.572
11	0	0	0	1.164	1.169	2.573	2.572
12	0	0	0	1.170	1.169	2.573	2.572

Table E4

Experimental and predicted adsorption capacities for lead using CFA and SAS

Run	Coded values			CFA		SAS	
	Dose	pH	C_o	Exp. q_e (mg/g)	Pred. q_e (mg/g)	Exp. q_e (mg/g)	Pred. q_e (mg/g)
1	-1	-1	-1	0.548	0.541	1.050	1.184
2	1	-1	-1	0.172	0.179	0.763	0.629
3	-1	1	-1	0.463	0.470	2.825	2.691
4	1	1	-1	0.136	0.129	0.983	1.117
5	-1	-1	1	0.645	0.652	6.335	6.201
6	1	-1	1	0.260	0.253	2.228	2.362
7	-1	1	1	0.568	0.561	6.865	7.000
8	1	1	1	0.173	0.180	2.273	2.139
9	0	0	0	0.150	0.151	2.233	2.285
10	0	0	0	0.158	0.151	2.245	2.285
11	0	0	0	0.148	0.151	2.340	2.285
12	0	0	0	0.146	0.151	2.323	2.285

Table E5

Experimental and predicted adsorption capacities for phenol using CFA and SAS

Run	Coded values			CFA		SAS	
	Dose	pH	C_o	Exp. q_e (mg/g)	Pred. q_e (mg/g)	Exp. q_e (mg/g)	Pred. q_e (mg/g)
1	-1	-1	-1	0.288	0.288	6.157	6.092
2	1	-1	-1	0.325	0.325	2.136	2.201
3	-1	1	-1	1.876	1.876	10.95	11.015
4	1	1	-1	0.677	0.677	3.594	3.529
5	-1	-1	1	0.036	0.036	16.757	16.822
6	1	-1	1	0.155	0.155	5.639	5.574
7	-1	1	1	0.214	0.214	22.482	22.417
8	1	1	1	0.817	0.817	7.506	7.571
9	0	0	0	0.956	0.969	6.564	6.557
10	0	0	0	0.976	0.969	6.564	6.557
11	0	0	0	0.978	0.969	6.556	6.557
12	0	0	0	0.967	0.969	6.545	6.557

Table E6

ANOVA for a quadratic model for nickel removal using CFA

Source of variation	Sum of squares	Degree of freedom	Mean square	*F*-value	Prob.>*F* (*p*-value)
Model	6.01548	7	0.85935	8.35246	0.0290
Residual	0.41155	4	0.10289	-	-
Lack of Fit	0.41132	1	0.41132	83.5900	-
Pure Error	0.00022	3	7.4E-05	-	-
Total	6.42703	11	-	-	-

R^2 = 0.9360, Coefficient of variance = 25.8%

Table E7

ANOVA for a quadratic model for iron removal using CFA

Source of variation	Sum of squares	Degree of freedom	Mean square	*F*-value	Prob.>*F* (*p*-value)
Model	5.76835	7	0.82405	8.05741	0.0309
Residual	0.40909	4	0.10227	-	-
Lack of Fit	0.40906	1	0.40906	16.61800	-
Pure Error	2.9E-05	3	9.7E-06	-	-
Total	6.17744	11	-	-	-

R^2 = 0.9338, Coefficient of variance = 25.1%

Table E8

ANOVA for a quadratic model for lead removal using CFA

Source of variation	Sum of squares	Degree of freedom	Mean square	*F*-value	Prob.>*F* (*p*-value)
Model	0.42881	7	0.06126	472.921	< 0.0001
Residual	0.00052	4	0.00013	-	-
Lack of Fit	0.00044	1	0.00044	15.7274	0.5286
Pure Error	8.3E-05	3	2.8E-05	-	-
Total	0.42932	11	-	-	-

R^2 = 0.9988, Coefficient of variance = 3.8%

Table E9

ANOVA for a quadratic model for phenol removal using CFA

Source of variation	Sum of squares	Degree of freedom	Mean square	*F*-value	Prob.>*F* (*p*-value)
Model	2.97014	8	0.37127	3678.96	< 0.0001
Pure Error	0.0003	3	0.0001	-	-
Total	2.97045	11	-	-	-

R^2 = 0.9999, Coefficient of variance = 1.5%

Table E10

ANOVA for a quadratic model for cobalt removal using SAS

Source of variation	Sum of squares	Degree of freedom	Mean square	*F*-value	Prob.>*F* (*p*-value)
Model	15.9731	7	2.28187	22.8866	0.0045
Residual	0.39881	4	0.09970	-	-
Lack of Fit	0.39872	1	0.39872	40.2	< 0.0531
Pure Error	8.9E-05	3	3.0E-05	-	-
Total	16.3719	11	-	-	-

R^2 = 0.9756, Coefficient of variance = 16.8%

Table E11

ANOVA for a quadratic model for nickel removal using SAS

Source of variation	Sum of squares	Degree of freedom	Mean square	*F*-value	Prob.>*F* (*p*-value)
Model	39.1729	7	5.59613	7.34983	0.0363
Residual	3.04558	4	0.7614	-	-
Lack of Fit	3.04551	1	3.04551	-	-
Pure Error	6.9E-05	3	2.3E-05	-	-
Total	42.2185	11	-	-	-

R^2 = 0.9279, Coefficient of variance = 31.7%

Table E12

ANOVA for a quadratic model for iron removal using SAS

Source of variation	Sum of squares	Degree of freedom	Mean square	*F*-value	Prob.>*F* (*p*-value)
Model	33.3526	7	4.76466	19.5308	0.0061
Residual	0.97582	4	0.24396	-	-
Lack of Fit	0.9758	1	0.9758	-	-
Pure Error	1.9E-05	3	6.2E-06	-	-
Total	34.3284	11	-	-	-

R^2 = 0.9716, Coefficient of variance = 17.7%

Table E13

ANOVA for a quadratic model for lead removal using SAS

Source of variation	Sum of squares	Degree of freedom	Mean square	*F*-value	Prob.>*F* (*p*-value)
Model	40.9484	7	5.84977	154.058	0.0001
Residual	0.15189	4	0.03797	-	-
Lack of Fit	0.14311	1	0.14311	48.9399	0.0600
Pure Error	0.00877	3	0.00292	-	-
Total	41.1003	11	-	-	-

R^2 = 0.9963, Coefficient of variance = 7.2%

Table E14

ANOVA for a quadratic model for phenol removal using SAS

Source of variation	Sum of squares	Degree of freedom	Mean square	*F*-value	Prob.>*F* (*p*-value)
Model	363.947	7	51.9924	6039.68	< 0.0001
Residual	0.03443	4	0.00861	-	-
Lack of Fit	0.03419	1	0.03419	22.547	0.0530
Pure Error	0.00024	3	8.1E-05	-	-
Total	363.981	11	-	-	-

R^2 = 0.9999, Coefficient of variance = 1.1%

APPENDIX F

Matlab programs for plotting response surfaces for coal fly ash

(a) Cobalt

Response surface and contour plot at constant initial concentration

```
[X,Y]=meshgrid(-1:0.2:1, -1:0.2:1);
Z=0.9+0.072*X+0.27*Y+0.44*X^2+0.26*X*Y-0.16*X-0.015*Y
figure (1), surface
mesh(X,Y,Z)
xlabel('Dose'), ylabel('pH')
figure (2), contour(X,Y,Z)
xlabel('Dose'), ylabel('pH')
```

Response surface and contour plot at constant pH

```
[X,Y]=meshgrid(-1:0.2:1, -1:0.2:1);
Z=1.35+0.072*X+0.18*Y+0.44*X^2-0.26*X+0.16*X*Y+0.015*Y
figure (1), surface
mesh(X,Y,Z)
xlabel('Dose'), ylabel('Concentration')
figure (2), contour(X,Y,Z)
xlabel('Dose'), ylabel('Concentration')
```

Response surface and contour plot at constant dose

```
[X,Y]=meshgrid(-1:0.2:1, -1:0.2:1);
Z=1.08+0.27*X+0.18*Y+0.015*X*Y
```

figure (1), surface

mesh(X,Y,Z)

xlabel('pH'), ylabel('Concentration')

figure (2), contour(X,Y,Z)

xlabel('pH'), ylabel('Concentration')

(b) Nickel

Response surface and contour plot at constant initial concentration

[X,Y]=meshgrid(-1:0.2:1, -1:0.2:1);

Z=1.53-0.10*X+0.47*Y-0.43*X^2+0.48*X*Y

figure (1)

mesh(X,Y,Z)

xlabel('Dose'), ylabel('pH')

figure (2), contour(X,Y,Z)

xlabel('Dose'), ylabel('pH')

Response surface and contour plot at constant pH

[X,Y]=meshgrid(-1:0.2:1, -1:0.2:1);

Z=1.53-0.10*X+0.39*Y-0.43*X^2+0.11*X*Y

figure (1)

mesh(X,Y,Z)

xlabel('Dose'), ylabel('Concentration')

figure (2), contour(X,Y,Z)

xlabel('Dose'), ylabel('Concentration')

Response surface and contour plot at constant dose

```
[X,Y]=meshgrid(-1:0.2:1, -1:0.2:1);
Z=1.53+0.47*X+0.39*Y+0.26*X*Y
figure (1)
mesh(X,Y,Z)
xlabel('pH'), ylabel('Concentration')
figure (2), contour(X,Y,Z)
xlabel('pH'), ylabel('Concentration')
```

(c) Iron

Response surface and contour plot at constant initial concentration

```
[X,Y]=meshgrid(-1:0.2:1, -1:0.2:1);
Z=1.17-0.55*X+0.11*Y+0.15*X^2-0.17*X*Y
figure (1)
mesh(X,Y,Z)
xlabel('Dose'), ylabel('pH')
figure (2), contour(X,Y,Z)
xlabel('Dose'), ylabel('pH')
```

Response surface and contour plot at constant pH

```
[X,Y]=meshgrid(-1:0.2:1, -1:0.2:1);
Z=1.17-0.55*X+0.54*Y+0.15*X^2+0.16*X*Y
figure (1)
mesh(X,Y,Z)
```

```
xlabel('Dose'), ylabel('Concentration')
figure (2), contour(X,Y,Z)
xlabel('Dose'), ylabel('Concentration')
```

Response surface and contour plot at constant dose

```
[X,Y]=meshgrid(-1:0.2:1, -1:0.2:1);
Z=1.17+0.11*X+0.54*Y+0.23*X*Y
figure (1)
mesh(X,Y,Z)
xlabel('pH'), ylabel('Concentration')
figure (2), contour(X,Y,Z)
xlabel('pH'), ylabel('Concentration')
```

(d) Lead

Response surface and contour plot at constant initial concentration

```
[X,Y]=meshgrid(-1:0.2:1, -1:0.2:1);
Z=0.15-0.19*X-0.036*Y+0.22*X^2+0.00488*X*Y
figure (1)
mesh(X,Y,Z)
xlabel('Dose'), ylabel('pH')
figure (2), contour(X,Y,Z)
xlabel('Dose'), ylabel('pH')
```

Response surface and contour plot at constant pH

```
[X,Y]=meshgrid(-1:0.2:1, -1:0.2:1);
Z=0.15-0.19*X+0.041*Y+0.22*X^2+0.00963*X*Y
figure (1)
mesh(X,Y,Z)
xlabel('Dose'), ylabel('Concentration')
figure (2), contour(X,Y,Z)
xlabel('Dose'), ylabel('Concentration')
```

Response surface and contour plot at constant dose

```
[X,Y]=meshgrid(-1:0.2:1, -1:0.2:1);
Z=0.15-0.036*X+0.041*Y-0.00538*X*Y
figure (1)
mesh(X,Y,Z)
xlabel('pH'), ylabel('Concentration')
figure (2), contour(X,Y,Z)
xlabel('pH'), ylabel('Concentration')
```

(e) Phenol

Response surface and contour plot at constant initial concentration

```
[X,Y]=meshgrid(-1:0.2:1, -1:0.2:1);
Z=0.97-0.055*X+0.35*Y-0.42*X^2-0.094*X*Y
figure (1)
mesh(X,Y,Z)
```

```
xlabel('Dose'), ylabel('pH')
figure (2), contour(X,Y,Z)
xlabel('Dose'), ylabel('pH')
```

Response surface and contour plot at constant pH

```
[X,Y]=meshgrid(-1:0.2:1, -1:0.2:1);
Z=0.97-.055*X-0.24*Y-0.42*X^2+0.24*X*Y
figure (1)
mesh(X,Y,Z)
xlabel('Dose'), ylabel('Concentration')
figure (2), contour(X,Y,Z)
xlabel('Dose'), ylabel('Concentration')
```

Response surface and contour plot at constant dose

```
[X,Y]=meshgrid(-1:0.2:1, -1:0.2:1);
Z=0.97+0.35*X-0.24*Y+0.14*X*Y
figure (1)
mesh(X,Y,Z)
xlabel('pH'), ylabel('Concentration')
figure (2), contour(X,Y,Z)
xlabel('pH'), ylabel('Concentration')
```

Program for determining optimum conditions for cobalt

```
b=[0.072; 0.27; 0.18];
B=[0.44 0.26/2 0.16/2; 0.26/2 0 0.015/2; 0.16/2 0.015/2 0];
```

x_o=-0.5*inv(B)*b;

a=1.08

q_{Co}=a+x_o'*b

Table F1

Confirmatory experiments for cobalt removal using CFA

Run	C_o (mg/l)	C_e (mg/l)	C_o-C_e (mg/l)	Dose (g/l)	q_e (mg/g)
1	151.25	122.60	28.65	14.6	1.9621
2	151.25	122.33	28.93	14.6	1.9812
3	151.25	124.03	27.22	14.6	1.8641

Average q_e = 1.9358 mg/g

APPENDIX G

Matlab programs for plotting response surfaces for SAS

(a) Cobalt

Response surface and contour plot at constant initial concentration

```
[X,Y]=meshgrid(-1:0.2:1, -1:0.2:1);
Z=2.26-0.29*X+0.86*Y-0.57*X^2+0.72*X*Y
figure (1)
mesh(X,Y,Z)
xlabel('Dose'), ylabel('pH')
figure (2), contour(X,Y,Z)
xlabel('Dose'), ylabel('pH')
```

Response surface and contour plot at constant pH

```
[X,Y]=meshgrid(-1:0.2:1, -1:0.2:1);
Z=2.26-0.29*X+0.68*Y-0.57*X^2-0.00725*X*Y
figure (1)
mesh(X,Y,Z)
xlabel('Dose'), ylabel('Concentration')
figure (2), contour(X,Y,Z)
xlabel('Dose'), ylabel('Concentration')
```

Response surface and contour plot at constant dose

```
[X,Y]=meshgrid(-1:0.2:1, -1:0.2:1);
Z=2.26+0.86*X+0.68*Y+0.3*X*Y
```

```
figure (1)
mesh(X,Y,Z)
xlabel('pH'), ylabel('Concentration')
figure (2), contour(X,Y,Z)
xlabel('pH'), ylabel('Concentration')
```

(b) Nickel

Response surface and contour plot at constant initial concentration

```
[X,Y]=meshgrid(-1:0.2:1, -1:0.2:1);
Z=3.25-0.68*X+1.06*Y-0.74*X^2+0.99*X*Y
figure (1)
mesh(X,Y,Z)
xlabel('Dose'), ylabel('pH')
figure (2), contour(X,Y,Z)
xlabel('Dose'), ylabel('pH')
```

Response surface and contour plot at constant pH

```
[X,Y]=meshgrid(-1:0.2:1, -1:0.2:1);
Z=3.25-0.68*X+1.28*Y-0.74*X^2-0.24*X*Y
figure (1)
mesh(X,Y,Z)
xlabel('Dose'), ylabel('Concentration')
figure (2), contour(X,Y,Z)
xlabel('Dose'), ylabel('Concentration')
```

Response surface and contour plot at constant dose

```
[X,Y]=meshgrid(-1:0.2:1, -1:0.2:1);
Z=3.25+1.06*X+1.28*Y+0.67*X*Y
figure (1)
mesh(X,Y,Z)
xlabel('pH'), ylabel('Concentration')
figure (2), contour(X,Y,Z)
xlabel('pH'), ylabel('Concentration')
```

(c) Iron

Response surface and contour plot at constant initial concentration

```
[X,Y]=meshgrid(-1:0.2:1, -1:0.2:1);
Z=2.57-1.16*X+0.49*Y+0.34*X^2+0.54*X*Y
figure (1)
mesh(X,Y,Z)
xlabel('Dose'), ylabel('pH')
figure (2), contour(X,Y,Z)
xlabel('Dose'), ylabel('pH')
```

Response surface and contour plot at constant pH

```
[X,Y]=meshgrid(-1:0.2:1, -1:0.2:1);
Z=2.57-1.16*X+1.37*Y+0.34*X^2+0.50*X*Y
figure (1)
mesh(X,Y,Z)
```

```
xlabel('Dose'), ylabel('Concentration')
figure (2), contour(X,Y,Z)
xlabel('Dose'), ylabel('Concentration')
```

Response surface and contour plot at constant dose

```
[X,Y]=meshgrid(-1:0.2:1, -1:0.2:1);
Z=2.57+0.49*X+1.37*Y+0.33*X*Y
figure (1)
mesh(X,Y,Z)
xlabel('pH'), ylabel('Concentration')
figure (2), contour(X,Y,Z)
xlabel('pH'), ylabel('Concentration')
```

(d) Lead

Response surface and contour plot at constant initial concentration

```
[X,Y]=meshgrid(-1:0.2:1, -1:0.2:1);
Z=2.29-1.35*X+0.32*Y+0.63*X^2+0.25*X*Y
figure (1)
mesh(X,Y,Z)
xlabel('Dose'), ylabel('pH')
figure (2), contour(X,Y,Z)
xlabel('Dose'), ylabel('pH')
```

Response surface and contour plot at constant pH

```
[X,Y]=meshgrid(-1:0.2:1, -1:0.2:1);
Z=2.29-1.35*X+1.51*Y+0.63*X^2+0.82*X*Y
figure (1)
mesh(X,Y,Z)
xlabel('Dose'), ylabel('Concentration')
figure (2), contour(X,Y,Z)
xlabel('Dose'), ylabel('Concentration')
```

Response surface and contour plot at constant dose

```
[X,Y]=meshgrid(-1:0.2:1, -1:0.2:1);
Z=2.29+0.32*X+1.51*Y+0.18*X*Y
figure (1)
mesh(X,Y,Z)
xlabel('pH'), ylabel('Concentration')
figure (2), contour(X,Y,Z)
xlabel('pH'), ylabel('Concentration')
```

(e) Phenol

Response surface and contour plot at constant initial concentration

```
[X,Y]=meshgrid(-1:0.2:1, -1:0.2:1);
Z=6.56-4.68*X+1.73*Y+2.85*X^2+0.9*X*Y
figure (1)
mesh(X,Y,Z)
```

```
xlabel('Dose'), ylabel('pH')
figure (2), contour(X,Y,Z)
xlabel('Dose'), ylabel('pH')
```

Response surface and contour plot at constant pH

```
[X,Y]=meshgrid(-1:0.2:1, -1:0.2:1);
Z=6.56-4.68*X+3.69*Y+2.85*X^2+1.84*X*Y
figure (1)
mesh(X,Y,Z)
xlabel('Dose'), ylabel('Concentration')
figure (2), contour(X,Y,Z)
xlabel('Dose'), ylabel('Concentration')
```

Response surface and contour plot at constant dose

```
[X,Y]=meshgrid(-1:0.2:1, -1:0.2:1);
Z=6.56+1.73*X+3.69*Y+0.17*X*Y
figure (1)
mesh(X,Y,Z)
xlabel('pH'), ylabel('Concentration')
figure (2), contour(X,Y,Z)
xlabel('pH'), ylabel('Concentration')
```

APPENDIX H

Data for column studies

Table H1

Data for design calculation using SD500 as the adsorbent

Parameters		Value
BET specific surface area (m^2/g)		592.97
Total pore volume (cm^3/g)		0.279
Wastewater composition: phenol (mg/l)		90/180
	cobalt (II) (mg/l)	25/50/90
	nickel (II) (mg/l)	25/50/90
	iron (II) (mg/l)	25/50/90
	lead (II) (mg/l)	25/50/90
Solution pH		2.6
Volumetric flow rate (ml/min)		5.0
Bed height (cm)		10/20/30
Bed diameter (cm)		2.5
Dry adsorbent mass (g)		8.18/16.36/24.54
Temperature (°C)		25.0

Table H2

Data for metal (90 mg/l) breakthrough curves using SD500 at 10 cm bed height

Time (h)	C_t/C_o			
	Cobalt	Nickel	Iron	Lead
0	0	0	0	0
0.5	0.30064	0.36247	0.40156	0.42518
1.0	0.76994	0.82335	0.92713	0.93540
1.5	0.94904	0.95522	0.95784	0.98146
2.0	0.96930	0.97527	0.98784	0.99256
2.5	0.94989	0.97953	0.99055	0.99669
3.0	0.96162	0.97516	0.98618	0.98618
3.5	0.96375	0.97964	0.99457	0.99587
4.0	0.96162	0.97793	0.98618	0.99091

Table H3

Data for metal (90 mg/l) breakthrough curves using SD500 at 20 cm bed height

Time (h)	C_t/C_o			
	Cobalt	Nickel	Iron	Lead
0	0	0	0	0
0.5	0.234871	0.267167	0.296380	0.309955
1.0	0.665129	0.688090	0.694570	0.715271
1.5	0.883047	0.891631	0.964932	0.981109
2.0	0.961373	0.988197	0.991742	0.992873
2.5	0.974249	0.987124	0.997738	0.998077
3.0	0.978004	0.988734	0.988575	0.989706
3.5	0.979614	0.985944	0.999095	0.999095
4.0	0.988734	0.998927	0.984163	0.995475

Table H4

Data for metal (90 mg/l) breakthrough curves using SD500 at 30 cm bed height

Time (h)	C_t/C_o			
	Cobalt	Nickel	Iron	Lead
0	0	0	0	0
0.5	0.097639	0.099031	0.104072	0.113462
1.0	0.471245	0.523143	0.547511	0.570588
1.5	0.724249	0.752422	0.783937	0.793326
2.0	0.875536	0.882885	0.935181	0.950000
2.5	0.945279	0.948439	0.997738	0.997964
3.0	0.955472	0.970398	0.988575	0.989706
3.5	0.968884	0.989128	0.999095	0.998416
4.0	0.972739	0.991389	0.994166	0.987557

Table H5

Data for phenol (90 mg/l) breakthrough curves using SD500 at varying bed height

Time (h)	Bed height, *Z*		
	10 cm	20 cm	30 cm
0	0	0	0
1.0	0.019914	0.002034	0.003359
2.0	0.019501	0.033220	0.004031
3.0	0.020139	0.033220	0.003359
4.0	0.019463	0.027797	0.013437
5.0	0.020290	0.025085	0.020156
6.0	0.020290	0.020339	0.019484
7.0	0.018035	0.020339	0.014781
8.0	0.014654	0.021017	0.015453
9.0	0.020666	0.017627	0.011422
10.0	0.018787	0.018305	0.010750
11.0	0.050349	0.016271	0.009406
12.0	0.085292	0.016271	0.012094
13.0	0.100111	0.016271	0.008062
14.0	0.341334	0.014915	0.009406
15.0	0.531081	0.013559	0.009406
16.0	0.693399	0.015593	0.014109
17.0	0.744875	0.015593	0.014109
18.0	0.898175	0.017627	0.014781
19.0	0.868117	0.035932	0.012765
20.0	0.940634	0.076610	0.014109
21.0	0.942137	0.119322	0.018140
22.0	0.946871	0.145085	0.020156
23.0	0.961299	0.181695	0.020828
24.0		0.168814	0.020828
25.0		0.236610	0.022843
26.0		0.311186	0.020828
27.0		0.326780	0.022171
28.0		0.389153	0.022171
29.0		0.490170	0.024859

30.0	0.610170	0.026203
31.0	0.697627	0.029562
32.0	0.699661	0.023515
33.0	0.828475	0.030906
34.0	0.903051	0.051062
35.0	0.959322	0.087342
36.0	0.982373	0.090030
37.0	0.982102	0.166622
38.0		0.149421
39.0		0.219967
40.0		0.293631
41.0		0.375167
42.0		0.487368
43.0		0.504837
44.0		0.593523
45.0		0.575382
46.0		0.694974
47.0		0.760817
48.0		0.823906
49.0		0.876184
50.0		0.928111
51.0		0.948938
52.0		0.975813
53.0		0.989250
54.0		0.989250